ELECTRIC FIELD AND TEMPERATURE DEPENDENCE OF POSITRON ANNIHILATION IN ARGON GAS

by

GREGORY FRANK LEE

B.Sc., University of British Columbia, 1966

M.Sc., University of British Columbia, 1969

A THESIS SUBMITTED IN PARTIAL FULFILMENT OF
THE REQUIREMENTS FOR THE DEGREE OF
DOCTOR OF PHILOSOPHY

in the Department
of
PHYSICS

We accept this thesis as conforming to the
required standard

THE UNIVERSITY OF BRITISH COLUMBIA

December, 1971

In presenting this thesis in partial fulfilment of the requirements for an advanced degree at the University of British Columbia, I agree that the Library shall make it freely available for reference and study. I further agree that permission for extensive copying of this thesis for scholarly purposes may be granted by the Head of my Department or by his representatives. It is understood that copying or publication of this thesis for financial gain shall not be allowed without my written permission.

Department of PHYSICS

The University of British Columbia
Vancouver 8, Canada

Date MARCH 8, 1972

ABSTRACT

The annihilation rate of positrons in argon has been measured over the temperature range of 135 K to 573 K with applied d.c. electric fields up to 35 V cm^{-1} $amagat^{-1}$. Analysis of this data was carried out assuming that the annihilation rate and the momentum-transfer rate can be approximated by a function of the form Av^B over this velocity range. Results of this analysis indicate a strong velocity dependence in both the annihilation rate and the momentum-transfer rate. For velocities in atomic units ($e^2/\hbar$) corresponding to positron wave number from .03 to .065 a_o^{-1} the annihilation rate was found to be adequately represented by $\nu_a(v) = (1.195 \times 10^6)v^{-.480}$ sec^{-1} $amagat^{-1}$. The momentum-transfer rate was similarly determined as $\nu_d(v) = (2.11 \times 10^{11})v^{-.49}$ sec^{-1} $amagat^{-1}$. The errors in these results are velocity dependent. The largest error is 16%.

This velocity dependence at low energies is not reproduced satisfactorily by any current theoretical models. A modified effective range parameterization of the momentum-transfer cross-section gives a scattering length of $A_0 = -4.4 \pm .5$ a_o for positron-argon collisions.

No evidence of a velocity dependence in the orthopositronium quenching rate at room temperature was detected. The orthopositronium quenching rate was measured at $.255 \pm .009$ μsec^{-1} $amagat^{-1}$, in good agreement with previous results.

TABLE OF CONTENTS

LIST OF TABLES

LIST OF FIGURES

ACKNOWLEDGMENTS

I wish to express my sincere appreciation to Dr. Garth Jones for his help over the past five years. He displayed keen interest in the progress of this work and was always readily available for consultation. Dr. Jones' ability and willingness to communicate his extensive knowledge, physical insight, and exacting standards made the completion of this project immeasurably easier.

At the completion of a Ph.D thesis I would be remiss if I did not thank my parents for their encouragement over the many years leading to this degree.

Most importantly, I wish to thank my wife, Fiona. Words are not sufficient to describe the importance of her contribution and I dedicate this thesis to her.

CHAPTER ONE

POSITRON ANNIHILATION IN THE NOBLE GASES

1.1 Introduction

Despite the fact that the positive particle predicted by Dirac's relativistic quantum theory of the electron, the positron, was discovered some 39 years ago (Anderson (1932)) the detailed nature of its interaction with gas atoms is still not well understood. One of the main reasons is that the experimental data concerning such interactions has been by necessity ambiguous. This ambiguity arises because, until mono-energetic positron beams are developed, the only experimental information available is obtained from swarm experiments using the decay of a nucleus, usually Na^{22}, as a positron source. The experimental results so obtained are necessarily the averaged value over the positron velocity distribution and therefore the velocity dependence of either the annihilation rate or the momentum-transfer rate, the quantities which can be predicted by theory, is not easily determined.

The theoretical understanding of positron-atom interactions is difficult because of the many-body nature of the problem. It might be expected, at first glance, that those theoretical models which have explained electron-atom scattering should also work for positrons, but experimental data has shown this to be untrue for many electron atoms such as argon (Orth and Jones (1969b), Montgomery and LaBahn (1970)). Helium, because of its simpler structure, is a more tractable problem and the results of theory and experiment are much closer (Lee et al. (1969)) but still not completely in agreement. This disagreement for

the case of positrons arises because the annihilation rate depends upon the positron-electron wavefunction overlap and therefore severely tests the validity of the approximate wavefunctions chosen.

For many years the study of positron-atom interactions was concerned principally with the study of positronium formation. The suggestion of a bound positron-electron system was made by Mohorovicic (1934) and named by Ruark (1945). Deutsch (1951) established its existence while investigating the time dependence of the annihilation of positrons in gases. This technique of obtaining the time distribution of annihilation events has been the standard method used to investigate the positron-atom interaction (Tao et al. (1964), Paul (1964), Falk and Jones (1964)).

The lifetime of thermalized free positrons in a noble gas at a particular temperature can be related, as will be demonstrated, to the velocity dependent annihilation rate. If a d.c. electric field is applied a dependence of the lifetime on the momentum-transfer rate is obtained. The experimental investigation of the lifetime of free positrons as a function of electric field and temperature and the determination of momentum-transfer and annihilation cross-sections from this data forms the basis of this thesis.

1.2 Positron-Atom Interactions

1.2.1 Elastic Scattering

A positron with an energy below that of the first excited state of the atoms of the host gas can undergo elastic collisions, annihilation, positronium formation, or formation of a molecular-like complex with the host atoms if such exist. From the practical point of view the determination of momentum-transfer cross-sections for elastic collisions

and the annihilation rate are of importance since these parameters, integrated over the positron velocity distribution, determine the measured lifetime of the free positron when subjected to electric fields.

1.2.1.1 Existing Theoretical Situation

In gases most of the theoretical effort has been directed toward the calculation of elastic scattering cross-sections and annihilation rates in atomic hydrogen, helium, and argon. Such calculations are of interest because of the comparisons that may be made with electron-atom collisions. The most obvious difference is that the positron is a distinguishable particle from the atomic electrons whereas for electron-atom scattering the indistinguishability must be taken into account. The average interaction of the undisturbed atom, the static atomic field, is repulsive for the positron and attractive for the electron. The polarization effects, on the other hand, are attractive in both cases. Hence these two potentials cancel in the case of positron-atom collisions and add for electron-atom collisions. It is therefore possible to obtain new information about the applicability of atomic collision theory by applying it to positrons.

In general a theoretical model with simplifying assumptions must be used because of the complexity of the many-body problem. The calculation of the annihilation rate is a particularly good test of the validity of the approximated wavefunctions of a particular model since this parameter is a direct measure of the positron-electron wavefunction overlap.

Of the noble gases helium is the one which offers the most hope of an "exact" solution. With the exception of atomic hydrogen, which

is experimentally impractical, helium has received the most careful study. A review article by Fraser (1968) outlines the various approximations used in the calculations. Of the current theoretical models the results of Drachman (1966, 1968) appear to be most consistent with experiment (Lee et al. (1969)).

Theoretical calculations in argon are very dependent upon the approximations employed. Early calculations took the polarization effect into account using the Holtzmark polarization potential in a manner similar to that used successfully in electron-argon scattering (Orth and Jones (1966), Massey (1967)). Such calculations failed, however, to yield results consistent with experimental annihilation rates, presumably because of their neglect of positron-electron correlation effects within the atom. More recent calculations have used a polarized orbital method which approximates the distortion interaction with a dipole approximation (Montgomery and LaBahn (1970)) and which has been used successfully for electron scattering from the noble gases (LaBahn and Callaway (1964), Thompson (1966)). This method was also unsuccessful in reproducing the experimental results.

The theoretical model which best fits existing experimental data is that of Hewson et al. (to be published) which takes into account the enhancement of the electron density at the positron position. The theoretical-experimental agreement is good for room temperature electric field results but does not agree with the experimental determination of temperature dependence.

One can in principle parameterize the positron-atom momentum-transfer cross-section at low energy using the modified effective range theory

(E.R.T.) of O'Malley et al. (1962). This theory describes the scattering of a charged particle by a neutral polarizable system which thus contains an attractive $1/r^4$ polarization potential explicitly. For the case of single channel elastic scattering the modified E.R.T. yields a momentum-transfer cross-section that contains a term linear in k (the positron wave number in units a_o^{-1}) and higher order terms, the lowest of which is proportional to $k^2 \ln(k)$. For the case of a bound positron-atom system the normal effective range theory does not require modification (O'Malley et al. (1961)) and the cross-section expansion retains terms only in k^2.

The modified E.R.T. has been used for the case of electron-atom scattering to extrapolate total and momentum-transfer cross-sections to zero energy with only moderate success. The measured values of the momentum-transfer cross-sections from diffusion experiments are inconsistent with the cross-sections obtained by extrapolating the total cross-section to zero energy (O'Malley (1963), Golden (1966)). Several suggestions have been offered to explain such inconsistencies including a pressure effect on the long range polarization (O'Malley (1963)) or the difficulty of extracting diffusion cross-sections from swarm experiments (Golden (1966)).

To date the modified effective range theory has not been applied to the case of positrons in the noble gases since the velocity dependent annihilation rate has not been available and consequently comparison with experiment impossible.

1.2.1.2 Existing Experimental Situation

Experimental estimates of the momentum-transfer cross-section

for positrons in gases have been obtained in two ways each of which is applicable to a different velocity range. By measurement of positronium formation at high electric fields the momentum-transfer cross-section in the neighbourhood of the positronium formation threshold of the host gas can be obtained (Teutsch and Hughes (1956)). The reliability of published values (Teutsch and Hughes (1956)) based upon this method is now questioned since the original measurements in helium (Marder et al. (1956)) have been found to be in error (Lee et al. (1969), Leung and Paul (1969), Albrecht and Jones (private communication - 1971)) and there is also disagreement in the rate of positronium formation increase in argon (Orth (1966)).

A second method of obtaining an estimate for the momentum-transfer cross-section was described by Orth and Jones (1969b). By assuming a constant momentum-transfer rate and using the results of both temperature and electric field measurements they obtained a rough estimate for the momentum-transfer cross-section in argon at thermal velocities.

1.2.2 Non-Elastic Processes

1.2.2.1 Inelastic Scattering

Positrons with energy greater than 500 eV almost exclusively undergo inelastic scattering (ionizing collisions) and consequential rapid energy loss. Between this energy and the first excited state of the gas atom the probability of inelastic and elastic collisions is comparable. Below the first excited state elastic collisions are, excluding positronium formation, the only type possible (Green and Lee (1964)).

1.2.2.2 Direct Annihilation

During any collision with a gas atom the positron may annihilate with an atomic electron. Such processes are also therefore non-elastic events.

The collision of a positron and an electron occurs in the 3S (triplet) spin state three quarters of the time and in the 1S (singlet) state one quarter of the time. Dirac (1931) calculated the annihilation cross-section for annihilation from the singlet state. In the non-relativistic limit this "plane wave" approximation for the decay into two photons is $$\sigma_s = 4\pi r_o^2 \frac{c}{v}$$

where r_o is classical electron radius

v is relative velocity.

The spin-averaged two-photon annihilation rate for a gas of atomic number Z is then $$\lambda = Z\pi r_o^2 c/\text{atom}.$$

Since the Dirac rate is calculated for plane waves the actual rate, taking into account Coulomb distortion, is usually significantly larger. It is convenient to express the true annihilation rate in the same form as that of the Dirac rate, with the Coulomb enhancement included in a Z_{eff} term. Thus

$$\lambda_s = Z_{eff}\pi r_o^2 c/\text{atom}$$

where Z_{eff} depends on the positron velocity.

The triplet state is prevented by selection rules from decaying via two photons. The probability for two-photon decay compared to three-photon decay is 1115:1 (Ore and Powell (1949)). Hence the ratio of the cross-sections for two and three photon decays (spin averaged) is 372:1. Thus for free positron annihilation three-photon decays are negligible.

1.2.2.3 Positronium Formation

An alternate non-elastic process is the formation of positronium. The energetics of positronium formation limits the energy range in which it can be produced. As the binding energy of positronium is 6.78 eV, the minimum energy required by a positron in order to remove an electron from an atom with ionization energy E_{ion} is

$$E_{thr} = E_{ion} - 6.8 \text{ eV}.$$

For energies above the ionization energy of the atom, E_{ion}, inelastic collisions will predominate because of phase space considerations. For energies between E_{ion} and the first excited state, E_{exc}, excitation collisions compete strongly with positronium formation and therefore most positronium formation occurs between E_{thr} and E_{exc} (Green and Lee (1964)). This region is known as the "Ore gap" (Ore and Powell (1949)).

Positronium in its ground state occurs in one of two spin configurations; parapositronium, in which the spins of the positron and electron couple to give total spin equal to zero, and orthopositronium in which total spin is one. Formation of positronium in its ground state appears to follow the statistical weighting expected; the ratio of orthopositronium:parapositronium is 3:1. Formation in an excited state is unlikely (Deutsch (1953)) and has not been observed (Brock and Streib (1958), Bennett et al. (1961), Duff and Heymann (1963)).

Since, as mentioned previously, free orthopositronium can only annihilate by three photons its mean lifetime is 1115 times larger than that of parapositronium. Ore and Powell (1949) calculated the values to be 1.39×10^{-7} and 1.25×10^{-10} seconds respectively. The most recent measurement of the free orthopositronium lifetime is that of Beers and

Hughes (1968) in which they obtained $(1.37 \pm .01) \times 10^{-7}$ seconds.

In addition to the free three-photon decay, orthopositronium can decay via two-photons if it is quenched by interaction with a gas atom. There are several quenching mechanisms possible and these are well summarized by Fraser (1968). The most important of these in the noble gases is "pick-off quenching". The positron of orthopositronium may, during a collision, annihilate if it finds itself at the location of an atomic electron with which it can form a singlet state. This effect depends both on the density of scatterers and also the energy of the collision since the degree of penetration of the orthopositronium and the atom determines the annihilation probability.

1.2.2.4 Positron-Atom Complexes

Measurement of the annihilation rates in hydrocarbon gases and diatomic molecules (Paul and Saint-Pierre (1963), Osmon (1965)) have yielded values of Z_{eff} up to several hundred times the Dirac value. The interpretation of results of this magnitude in terms of free positron annihilation is unreasonable. A tentative explanation is that a positron-molecule complex is formed which greatly enhances the probability of annihilation (Paul and Saint-Pierre (1963), Green and Tao (1963), Massey (1967)) or that a resonant state exists (Paul and Smith (1970)). The lifetime of such a system would be of the same order of parapositronium, that is 10^{-10} seconds. One could expect such complexes, if formed, to be formed at energies below the parapositronium formation threshold since at any higher energies positronium formation would likely dominate.

1.3 Generalized Features of Positron Swarm Experiments

1.3.1 Slowing of Positrons

From the discussions of Section 1.2 it is evident that a positron emitted into a gas with several hundred keV of energy will very rapidly lose energy by inelastic collisions and therefore the probability of annihilating in this time is small. The energy of emission from a Na^{22} source, the positron source used for the work described in this thesis, is up to 542 keV with a maximum in the modified Fermi distribution at about 170 keV. Falk (1965) estimated the time taken for a positron to reach 10 keV in argon at 10 amagats as less than 0.7 nsec. From 10 keV to the last inelastic level is less well defined. Orth (1966) estimated 0.5 nsec as an upper limit under similar conditions. The elastic slowing down of positrons to thermal energies takes a longer time and is comparable to the free annihilation lifetime (Tao et al. (1963)). Thus a significant probability for annihilation prior to attaining thermal equilibrium results. These events in contrast to the annihilations occurring during the rapid inelastic energy loss are experimentally detectable and in fact give rise to a shoulder in the annihilation lifetime spectrum as first observed in argon in 1964 (Tao et al. (1964), Paul (1964), Falk and Jones (1964)). The existence of the shoulder is evidence of the velocity dependence of the direct annihilation rate for positrons in the energy range 0.1 to 11 eV.

During the time in which the positron is in the energy range of the "Ore gap" positronium can, of course, be formed. The positronium formation threshold in argon is 8.9 eV, only 2.7 eV below the last inelastic level, and therefore all positronium is formed within a short time, certainly

well within the shoulder width. (Tao et al. (1963) estimated the formation time to be approximately 1.5 nsec.) The decay of parapositronium then would be experimentally indistinguishable from prompt annihilations in the source and walls for an experimental resolution of several nanoseconds. The orthopositronium decay on the other hand will obviously contribute to the annihilation time spectrum (Section 1.2.2.3).

Once the positrons have slowed to energies below the positronium formation threshold they can conceivably form positron-atom complexes if such exist. The lifetime of such complexes is such that they annihilate well within the experimental resolution time by two-photon decay. This depopulation of the positron distribution would therefore be equal to the complex formation rate which would be linearly density dependent. These events would therefore be indistinguishable from direct annihilations.

Those positrons which reach thermal equilibrium without annihilating or forming positronium or a positron-atom complex have a velocity distribution characterized by the temperature of the host gas, the magnitude of an applied electric field, and the velocity dependences of the momentum-transfer and annihilation rates. It is the annihilations from this distribution that comprise the measured direct annihilation rate in positron swarm experiments.

1.3.2 Positron Velocity Distribution

1.3.2.1 Interpretation of Time Spectrum

The time spectrum which one attains in a positron annihilation experiment is built up of individually measured events. It is, however, convenient to think of all the positrons as having been emitted at one time and existing simultaneously in the positron velocity distribution

from which they annihilation. It is customary to assume that these two approaches are equivalent. In the first case one can define the probability at any time, t, of a positron having a velocity between v and v + dv. In the second case one can define the fraction of positrons that, at time t, have a velocity between v and v + dv. Properly normalized these definitions are equivalent. The one difference which arises is that in describing the positron velocity distribution positron-positron interactions can be neglected. For a weak source this is an obvious assumption in the first case but only holds in the second description if the density of positrons is very much less than the density of the host gas (Lorentz Gas).

1.3.2.2 Diffusion Equation

For elastic scattering collisions the differential equation which describes the positron velocity distribution at time t has been shown to be (Falk (1965))

$$\frac{\partial f(v,t)}{\partial t} = \frac{1}{v^2}\frac{\partial}{\partial v}\left(\left(\frac{a^2v^2}{3\nu_d(v)} + \frac{\mu v^2 \nu_d(v) kT}{m}\right)\frac{\partial f(v,t)}{\partial v} + \mu v^3 \nu_d(v) f(v,t)\right) - (\nu_a(v) + \nu_f(v)) f(v,t). \quad 1\text{-}1$$

where $f(v,t)$ = probability density in velocity space

$a = \frac{eE}{m}$ = acceleration of positron due to electric field

e = positron charge

E = applied electric field

m = mass of positron

$\nu_d(v)$ = momentum-transfer rate for positron-atom collisions

$\nu_a(v)$ = velocity dependent annihilation rate

$\nu_f(v)$ = positronium formation rate

$\mu = \frac{m}{M}$

M = mass of scattering atoms

T = temperature of host gas in K

k = Boltzmann's constant.

The velocity distribution of positrons is then proportional to $v^2 f(v,t)$ and the velocity averaged annihilation rate at time t, $\lambda(t)$, is given by

$$\lambda(t) = \frac{\int_0^\infty \nu_a(v) v^2 f(v,t) dv}{\int_0^\infty v^2 f(v,t) dv}. \qquad 1\text{-}2$$

The time independent or steady state equation has been derived from 1-1 by Orth (1966). The resulting equation is, neglecting positronium formation,

$$\left(\frac{a^2}{3\nu_d(v)} \quad \frac{\mu \nu_d(v) kT}{m} \right) \frac{\partial f(v)}{\partial v} + \mu v \nu_d(v) f(v) = \int_0^v (\nu_a(v') - \lambda) v'^2 f(v') dv'. \qquad 1\text{-}3$$

This equation can then be solved for f(v) either numerically (Orth (1966), Montgomery and LaBahn (1970)) or analytically for special cases. The velocity averaged, time independent, annihilation rate is given as before by 1-2.

For the case of a velocity independent annihilation rate $\nu_a(v) = \lambda$ and the right hand side of 1-3 vanishes. In this case 1-3 can be solved by integration

$$f(v) = C \exp\left(- \int_0^v \frac{v'}{\left(\frac{a^2}{3\mu\nu_d(v')^2} + \frac{kT}{m} \right)} dv' \right). \qquad 1\text{-}4$$

This result is also approximately correct if the integral on the right hand side of 1-3 is much smaller than the terms on the left hand side in which case the effect of removing positrons from the distribution does not appreciably affect the shape of the distribution. Numerical solutions of 1-3 for low electric fields support this approximation and this will be discussed further in Section 4.5. This approximate solution will be used extensively throughout this work.

If the applied electric field is zero it is readily seen from 1-4 that the positron velocity distribution, and hence the average annihilation rate as given by 1-2, does not depend on the momentum-transfer cross-section but only on temperature. That is

$$\lambda(T) = \frac{\int_0^\infty \nu_a(v) v^2 e^{-\frac{mv^2}{2kT}} dv}{\int_0^\infty v^2 e^{-\frac{mv^2}{2kT}} dv}. \qquad 1\text{-}5$$

This equation can therefore be solved for $\nu_a(v)$ if a functional dependence of λ on T can be obtained.

For the case of a constant momentum-transfer cross-section, that is no dependence of ν_d on velocity, 1-4 can be solved again to get

$$f(v) = C\exp\left(-\frac{v^2}{\left(\frac{2a^2}{3\mu\nu_d^2} + \frac{2kT}{m}\right)}\right) \qquad 1\text{-}6$$

which can be written as

$$f(v) = C\exp\left(-\frac{mv^2}{2kT_{eff}}\right) \qquad 1\text{-}7$$

where

$$T_{eff} = \left(\frac{ma^2}{3\mu\nu_d^2 k} + T\right)$$

is the effective temperature of the steady state Boltzmann distribution.

Thus for constant momentum-transfer cross-sections the effect of an applied d.c. electric field is to raise the effective temperature of the positron velocity distribution.

The exact solution of 1-3 that does not neglect the effect of annihilations must be obtained by numerical integration. For such an integration the values of $\nu_d(v)$ and $\nu_a(v)$, assuming no positronium formation, must be supplied either by theory or experiment. The techniques involved in such numerical solutions are further described in Section 4.5.

It is because the experimentally determined value, λ, cannot be obtained from $\nu_d(v)$ and $\nu_a(v)$ without solving 1-3 and subsequently 1-2 that the comparison between theory and experiment is difficult. In order to obtain estimates of $\nu_d(v)$ and $\nu_a(v)$ from experimental data it is convenient to neglect the effect of annihilations on the shape of the positron velocity distribution. This assumption is made extensively throughout this work. The validity of this approximation will be tested in Section 4.5.

1.3.3 Existing Experimental Situation

Many swarm experiments in the noble gases have been performed in the last seven or eight years but until the temperature dependence of the annihilation rate in argon was measured by Miller et al. (1968) there was no method of extracting an unambiguous $\nu_d(v)$ or $\nu_a(v)$ from the results. Early workers could only test the prediction of theoretical models and perhaps give an averaged annihilation rate over the thermalized positron velocity distribution. Although d.c. electric fields could change this distribution, unless the $\nu_d(v)$ were known the resulting

shape of the distribution was unknown. The temperature measurements of Miller et al. (1968) used the approximate solution 1-5 to obtain the functional dependence of $\nu_a(v)$. Following this result Orth and Jones (1969b) obtained an estimate of the momentum-transfer cross-section in argon at thermal velocities by using the approximation inherent in 1-7. They assumed that a small electric field had the equivalent effect of a small temperature increase and by comparing temperature and electric field measurements obtained a value for $\nu_d(v)$. With the exception of the value near E_{thr}, inferred by Marder et al. (1956) from measurements of positronium formation enhancement (Section 1.2.2.1), no other experimental values of the momentum-transfer cross-section are available.

1.4 Summary of Thesis Content

In terms of the current experimental tests of theory (Section 1.3.3) it is possible for two widely differing theoretical models to both fit the experimental data. This could occur because the measured annihilation lifetime is averaged over the velocity distribution and therefore in principle two differing models could give two different values of $\nu_d(v)$ which result in the same averaged annihilation rate.

This thesis describes a research program in which the combined electric field and temperature dependence of the annihilation of positrons in argon was measured. Based upon these results, the velocity dependences of the momentum-transfer cross-section and annihilation cross-section in the region of thermal velocities are separately determined. The determination of these cross-sections provides criteria upon which the correctness of any theoretical model may be judged.

CHAPTER TWO

EXPERIMENTAL PROCEDURE AND RESULTS

2.1 Outline of Experimental Techniques

2.1.1 Experimental Determination of Lifetime Spectrum

The experimental determination of the lifetime of positrons is generally performed by measuring the time interval between a suitable "birth" signal, indicating the generation of a positron, and a "death" signal, indicating annihilation of the positron. The beta decay of Na^{22} to the first excited state of Ne^{22} is followed within 10^{-11} seconds by a 1.28 MeV nuclear gamma ray. This signal is used to indicate the birth of a positron. The annihilation, either by two or three photon decay, is signaled by the detection of the characteristic radiation. These time intervals are then stored as events in a composite time spectrum. Each spectrum is taken at a fixed temperature and applied electric field.

2.1.2 Analysis of Time Spectrum

A typical time spectrum is shown in Figure 1. The characteristics of such a spectrum can be divided into four areas. The first of these is the negative time region characterized by the presence of a random coincidence background. Operation with a portion of the time spectrum in the negative time region is obtained by electronically delaying the stop signal so that random coincidence events, in which the start signal is preceded by a stop signal, are recorded. The random coincidence background which is the sole component in this region occurs at a constant level throughout the rest of the spectrum as well.

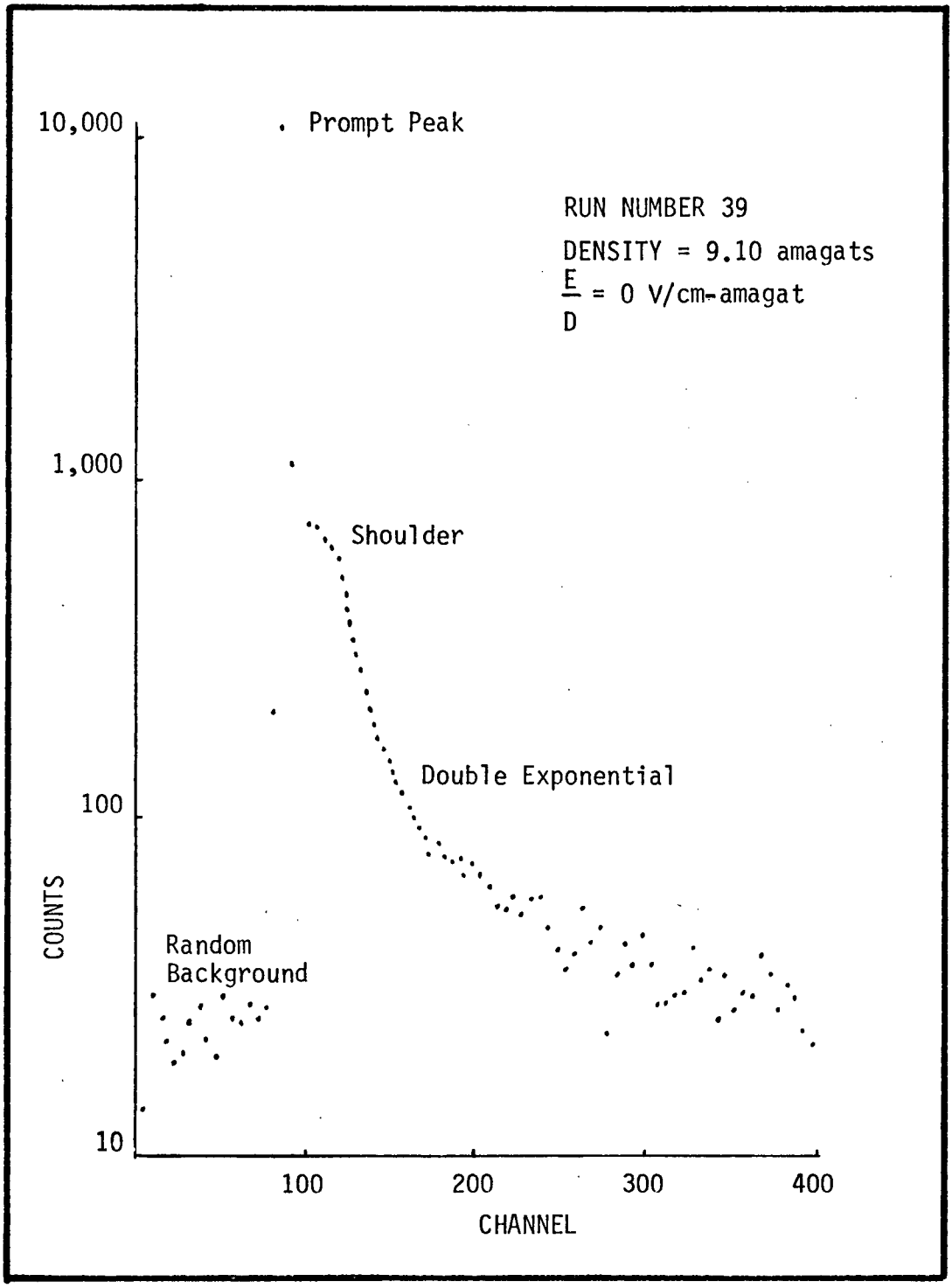

Figure 1 Typical Time Spectrum

The second region is the "prompt peak" which occurs at zero relative time. This peak corresponds to the detection of annihilations of the positrons within the source, the source holder, or chamber walls and also from parapositronium decay. The width of the prompt peak, defining the instrumental resolution for the experiment, was typically 5 nanoseconds.

The third region is the "shoulder" area which, as mentioned earlier (Section 1.3.1), is due mainly to annihilations of free positrons before they reach thermal equilibrium in the gas and partly to orthopositronium decay. The typical density-width product of the shoulder region in argon is 350 nsec amagats, where the width is defined as the time between the prompt peak and the estimated beginning of the double exponential decay. This feature of the spectrum is very sensitive to impurities (Paul (1964), Orth (1966)) and can therefore be used as an indication of gas purity.

The fourth region is that characterized by annihilation of free positrons in thermal equilibrium with the host gas and by the decay of thermalized orthopositronium. The removal of free positrons from the equilibrium distribution is described by

$$\frac{dN(t)}{dt} = -(\lambda_d + \lambda_f + \lambda_c)N(t) \qquad 2\text{-}1$$

where λ_d is the direct annihilation rate

λ_f is the positronium formation rate

λ_c is the molecular complex formation rate if such exists

and $N(t)$ is the total thermalized positron population integrated over the velocity distribution

solving $$N(t) = N(0)e^{-(\lambda_d + \lambda_f + \lambda_c)t} \qquad 2\text{–}2$$

or the observed rate for decay from the free positron distribution is

$$R_f(t) = \epsilon_2\left(\lambda_d + \frac{\lambda_f}{4} + \lambda_c\right) N(0)e^{-(\lambda_d + \lambda_f + \lambda_c)t}$$

where ϵ_2 is the detection efficiency for two-photon decay, taking into account both detector efficiency and solid angle, and it is assumed that all parapositronium and any molecular complexes formed annihilate immediately. (Parapositronium lifetime is 1.25×10^{-10} seconds and can therefore be considered as depopulating the distribution directly.) For the low electric fields such as employed in this experiment no positronium formation occurs, so for this experiment

$$R_f = \epsilon_2(\lambda_d + \lambda_c)N(0)e^{-(\lambda_d + \lambda_c)t}. \qquad 2\text{–}3$$

The orthopositronium population is given by

$$\frac{dN_o(t)}{dt} = -(\lambda_o + \lambda_q)N_o(t) + \frac{3}{4}\lambda_f N(t) \qquad 2\text{–}4$$

where λ_o is the free orthopositronium decay rate

λ_q is the orthopositronium quenching rate.

Again, for low electric fields, no positronium formation occurs from the thermalized positron distribution and therefore 2–4 can be written

$$\frac{dN_o(t)}{dt} = -(\lambda_o + \lambda_q)N_o(t)$$

solving $$N_o(t) = N_o(0)e^{-(\lambda_o + \lambda_q)t}. \qquad 2\text{–}5$$

The observed rate from orthopositronium decay is therefore

$$R_o(T) = \epsilon_2\lambda_q N_o(t) + \epsilon_3\lambda_o N_o(t) \qquad 2\text{–}6$$

where ϵ_3 is the detection efficiency for three-photon decays.

Combining 2-3 and 2-6 the observed annihilation spectrum from the thermalized components is

$$R(t) = R_f(t) + R_o(t)$$
$$= I_1 e^{-\lambda_1 t} + I_2 e^{-\lambda_2 t} \qquad 2\text{-}7$$

where
$$I_1 = \epsilon_2(\lambda_d + \lambda_c)N(0)$$
$$I_2 = (\epsilon_2\lambda_q + \epsilon_3\lambda_o)N_o(0)$$
$$\lambda_1 = \lambda_d + \lambda_c$$
$$\lambda_2 = \lambda_o + \lambda_q$$

It is assumed that for the low electric fields encountered in this experiment no positronium formation occurs from the free positron thermalized distribution, that is, $\lambda_f = 0$. It is evident from 2-7 that if molecular complexes are formed they would be experimentally indistinguishable from direct annihilations. For the purposes of this thesis the short-lived component obtained from a two-component analysis of the equilibrium part of the spectrum has been designated as the "direct rate" although it would contain any molecular complex channels if they exist.

2.2 Experimental Method

2.2.1 Chamber Configuration

2.2.1.1 Chamber Design

The chamber used for this work was basically that used by Miller (1968) and is illustrated in Figure 2. Modifications to Miller's system were

i. inclusion of a titanium gas purifier

ii. provision for eleven high voltage feedthroughs in order to be able to externally bias the electric field grid

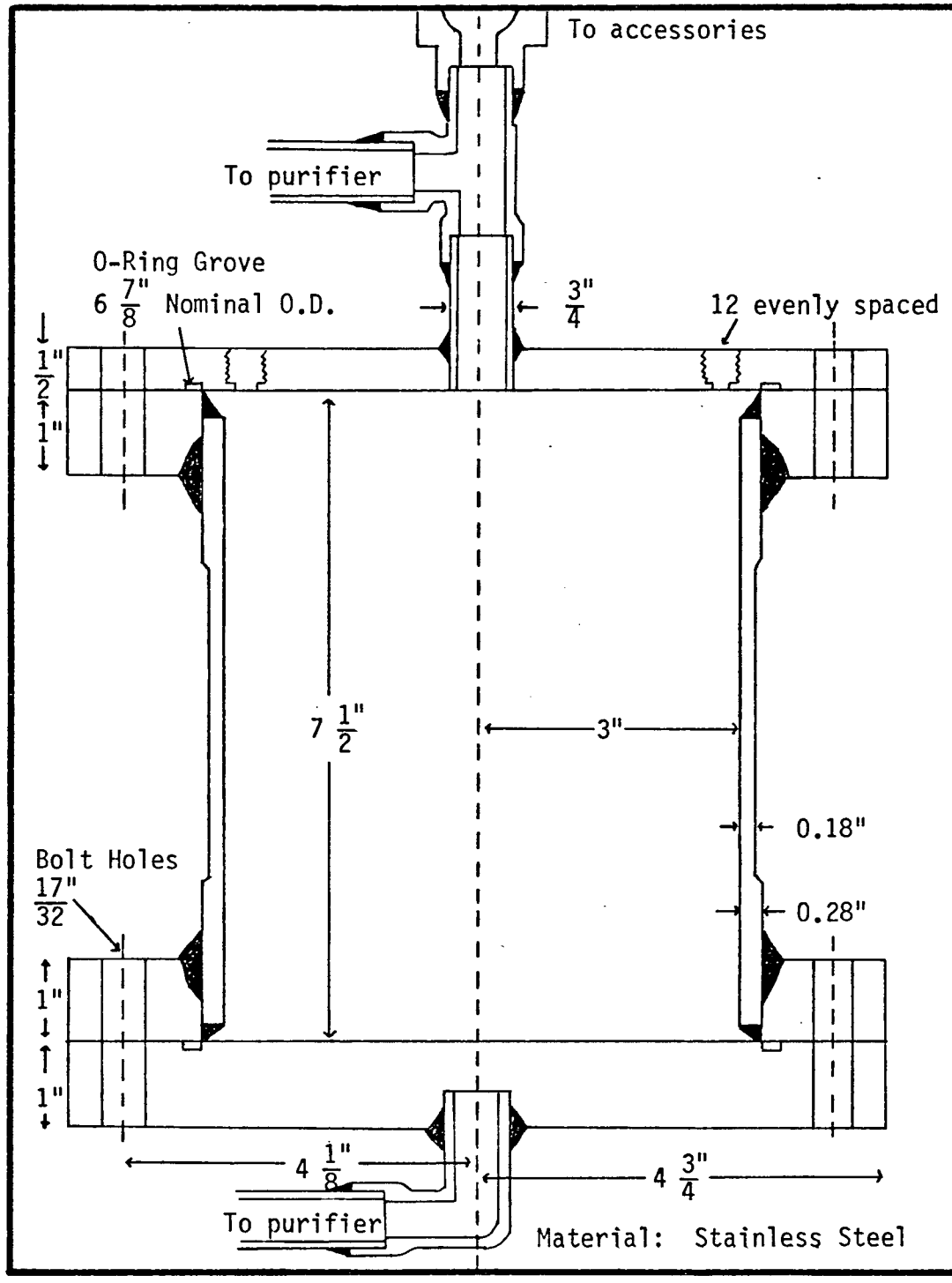

Figure 2 Experimental Chamber

(Section 2.2.1.2)

iii. an iron-constantan thermocouple.

The external fixtures such as sample bottles, pressure gauges, and so forth were attached as shown in Figure 3. The pressure gauges were connected to the chamber by stainless steel tubing a meter long to ensure that the gauge readings would be unaffected by temperature changes. The chamber and purifier were hydraulically pressure tested to 500 p.s.i.g. at room temperature, sufficient to ensure its capability of withstanding 250 p.s.i.g. at 350^{o} C.

The high voltage and thermocouple feedthroughs were Ceramaseal type 800A0211-1 purchased from Ceramaseal Incorporated, New York. In order to facilitate replacement of defective units these were held in place mechanically as shown in Figure 4 rather than being welded. Solder, of course, could not be used because of the high temperatures to which the chamber was raised. The limiting feature of these feedthroughs was their rather low breakdown voltage which although rated at 3.1 kV was in practice somewhat less. This restricted the size of the electric field that could be attained (Section 2.2.1.2)

The chamber was baked at 650 K under vacuum (estimated at less than 0.01 mm Hg) for forty-eight hours before filling with 99.999% ultra pure argon gas (Section 2.4.6). All pumping was done either by absorption pumping (roughing out of chamber) or by a conventional diffusion pump system. In the latter system a cold trap was employed in the vacuum line to reduce the backstreaming and contamination of the chamber by mechanical or diffusion pump oil.

2.2.1.2 Electric Field Grid

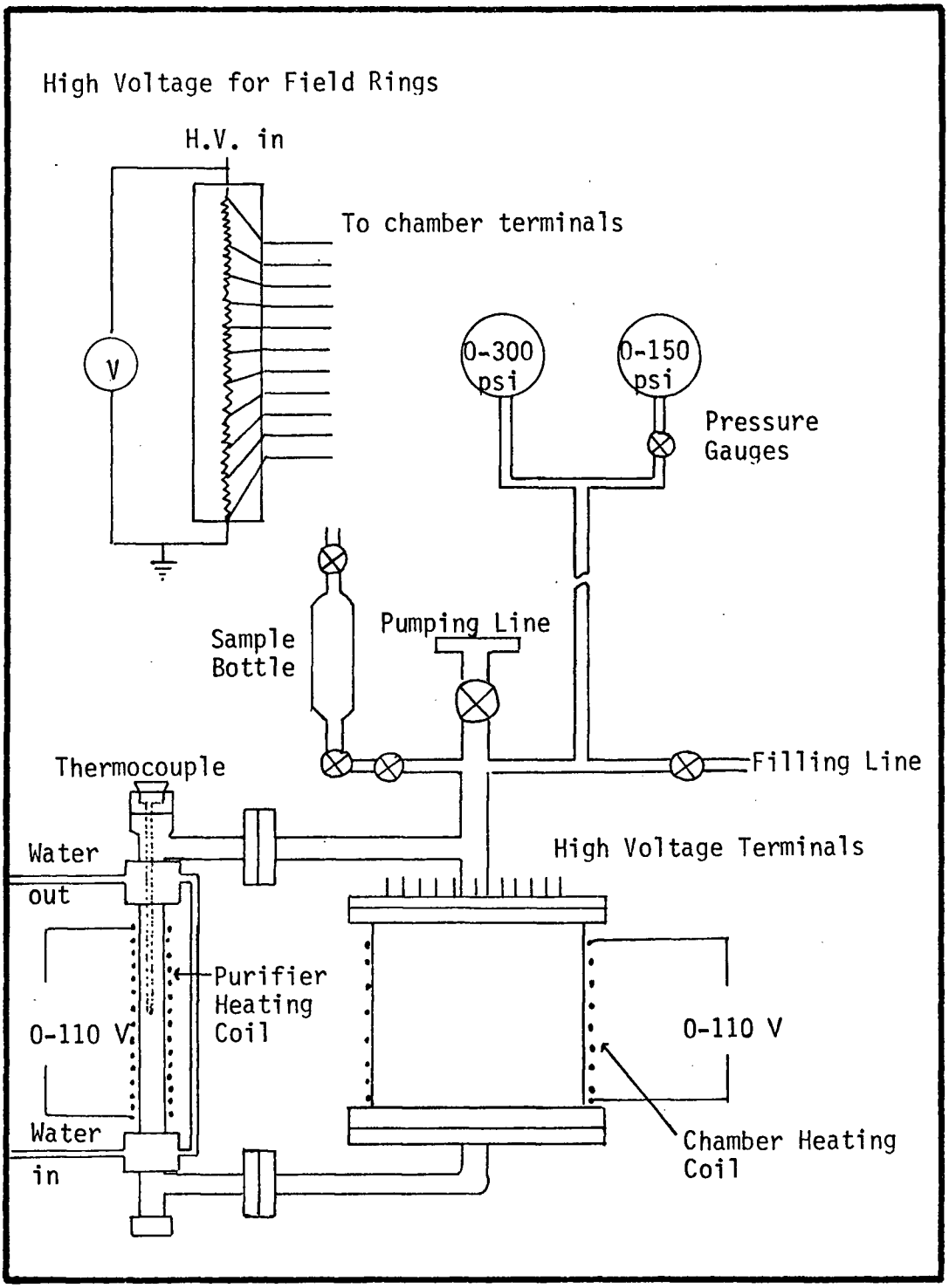

Figure 3 Chamber Configuration - External Features

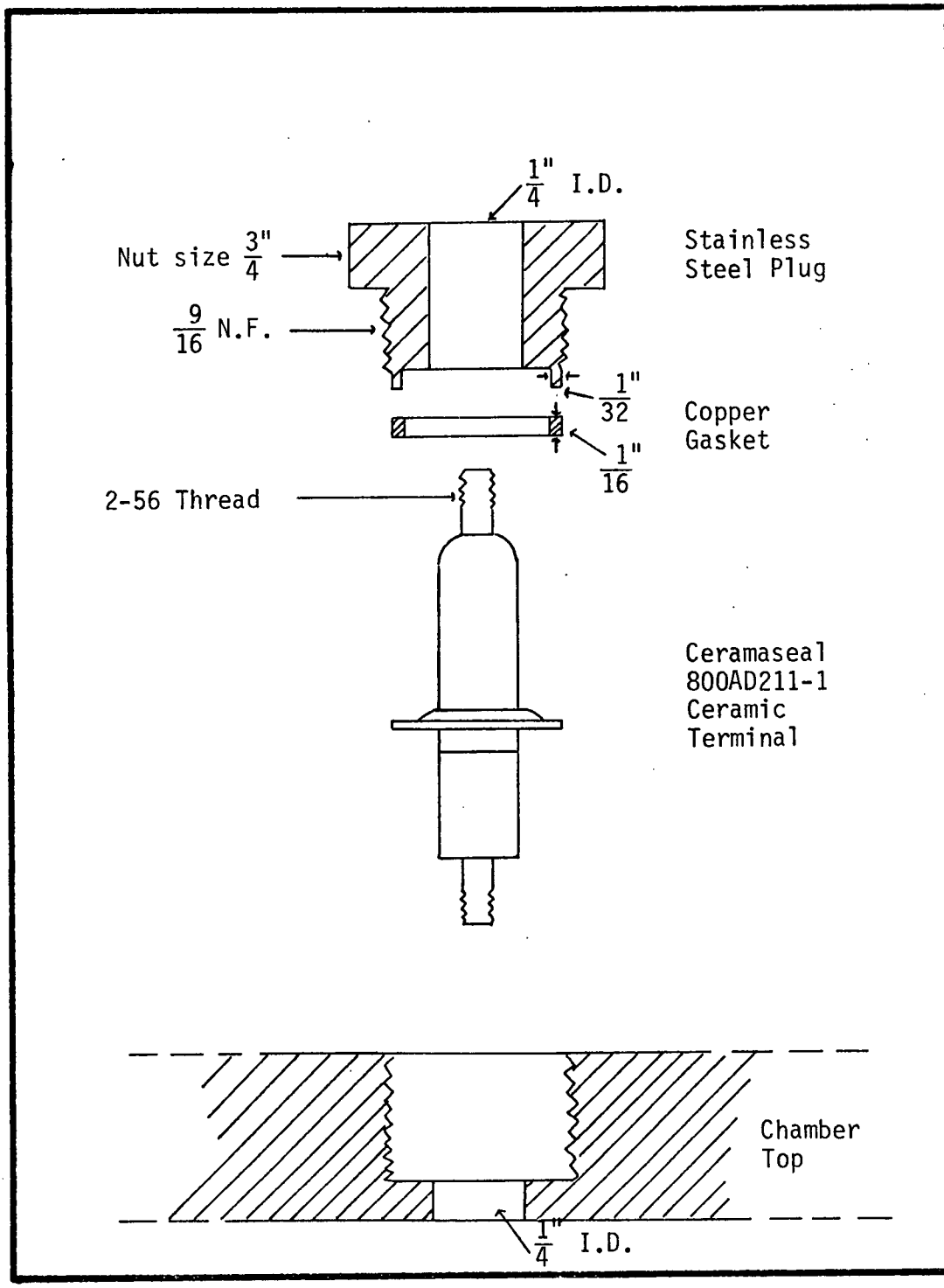

Figure 4 High Voltage Electrical Feedthroughs

The large temperature variation to which the chamber was subjected in the experiment required that the electric field grid be externally biased, unlike previous field configurations (Falk (1965), Orth (1966)) in which the resistor chain was inside the chamber. The field rings were $5\frac{1}{2}$ inches in outer diameter and were made of polished copper $\frac{1}{8}$ inch in cross-section. The spacers between rings consisted of $\frac{3}{8}$ inch ceramic terminals, giving a center-to-center spacing of $\frac{1}{2}$ inch on the rings. Ceramic spacers were chosen because of their good electrical insulating properties over a wide temperature range and their chemical stability at high temperatures (unlike Teflon which had been previously used). Figure 5 shows the electric field assembly. The end plates were $\frac{1}{8}$ inch brass and the source ring consisted of a fine wire mesh similar to that of Falk (1965). As no part of the field assembly was internally grounded, the voltage gradient could be applied from end-to-end or, as in previous experiments (Falk (1965), Orth (1966)), from the center to each end. In order to attain a wider range of voltage gradients and also to check the consistency of operation both of these configurations were used (Section 2.2.2.4).

2.2.1.3 Source Construction and Strength

The source, placed in the center of the electric field grid, was composed of radioactive $^{22}NaCl$ salt deposited on a single layer of 30 μinch nickel foil. Its strength, 15 μCi, was larger than that previously used (Falk (1965), Orth (1966), Miller (1968), Lee (1969)) but the disadvantages of increased random background were felt to be outweighed by the advantages of a shorter counting time while doing a temperature controlled experiment. Nickel foil was used rather than

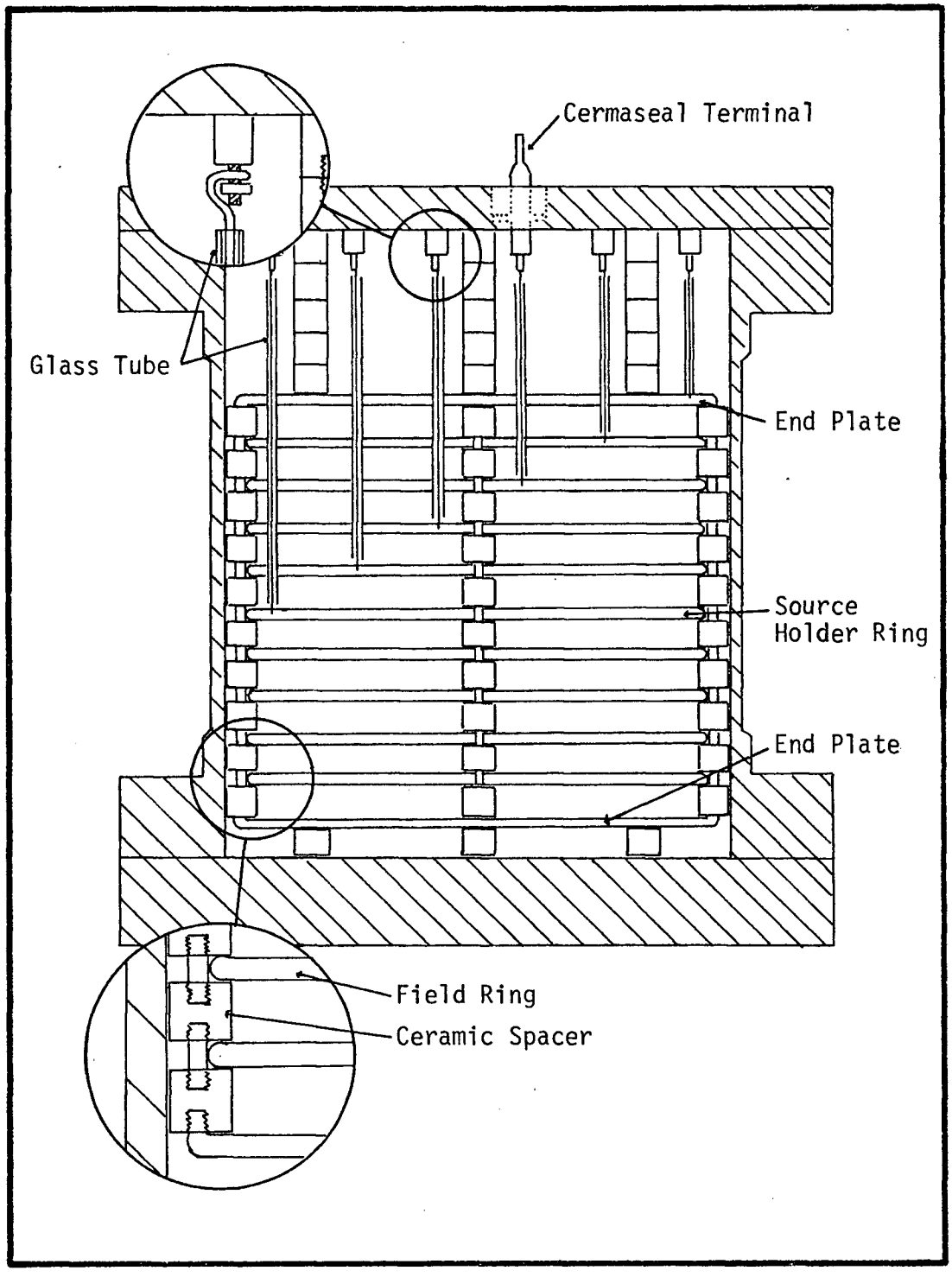

Figure 5 Electric Field Assembly

aluminum foil since it was found that $AlCl_3$ was formed when the radioactive salt was deposited, this compound subliming at 178° C. The result was a large hole where the source was originally situated. The somewhat higher atomic weight of the nickel foil increases slightly the fraction of positrons that annihilate in the source and consequently increases the random background and prompt peak. These effects were considered to be satisfactorily small.

2.2.1.4 Purifier Design and Operation

The use of the closed loop titanium purifier is illustrated in Figure 3. Previous work (Lee (1969)) on positron annihilation in helium had demonstrated the effectiveness of such a purifier for removing non-noble gases. The necessity of a thermocouple to measure the titanium temperature was also demonstrated since gas at high density is an efficient coolant. Before operating the purifier it was first heated in vacuum to 450° C. Titanium absorbs significant amounts of hydrogen gas at room temperature and this is re-emitted at temperatures above 400° C. (Stout and Gibbons (1955)). No other gases are re-emitted once absorbed. In the steady state operation of the purifier the temperature was held constant at 650° C.

Tests with nitrogen impurity added to the argon indicated that impurities were removed within twenty-four hours after turning on the purifier. Figure 6 compares a spectrum taken with 2% nitrogen added to one taken after running the purifier for forty-eight hours. It can be seen that the increase in shoulder width, to the acceptable level of 350 nsec amagats, is evidence of the effectiveness of the purifier. As standard procedure during the experiment the purifier

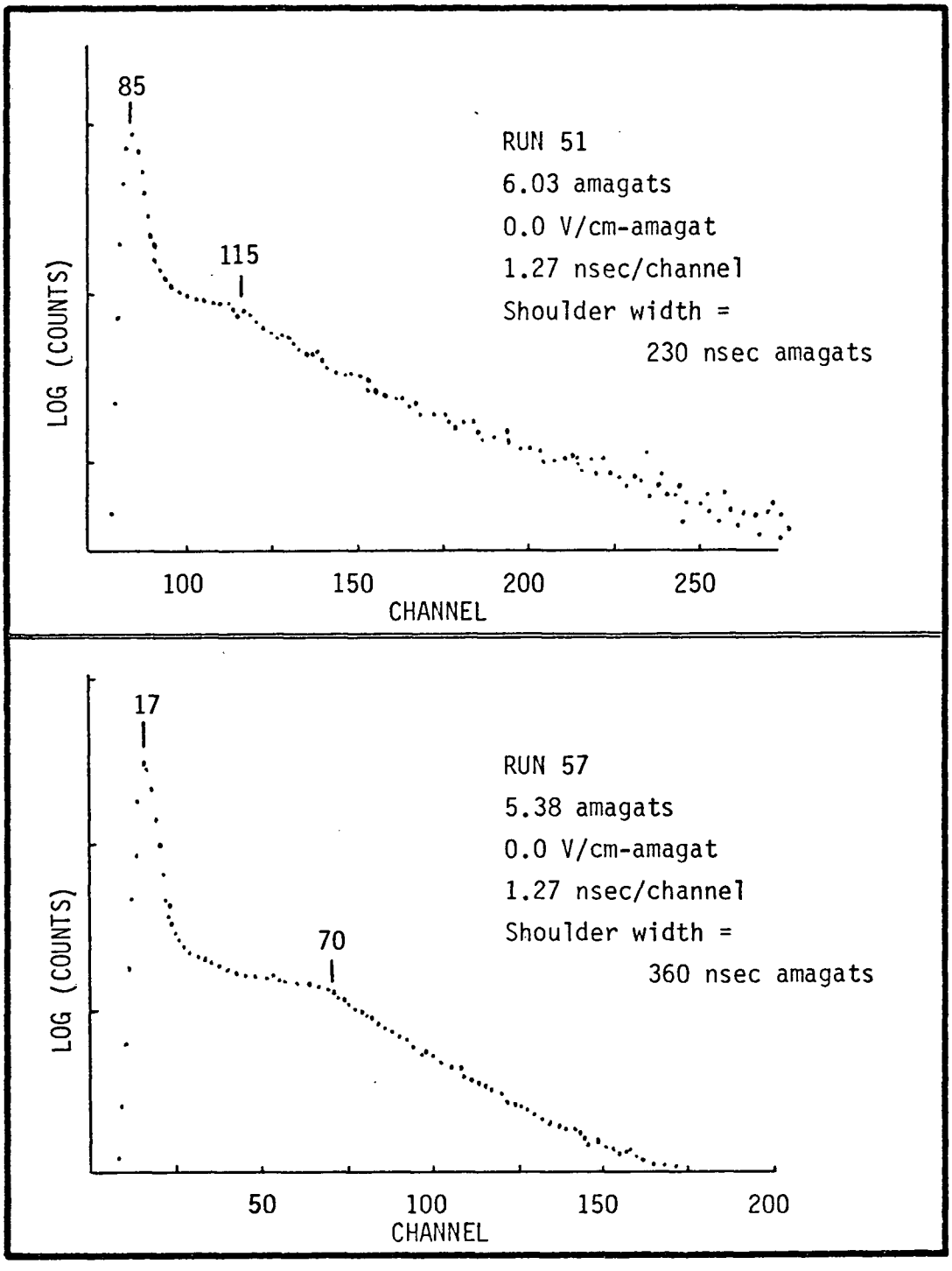

Figure 6 Effect of Purifier

Top spectrum taken with added N_2.
Bottom spectrum taken after purification.

was turned on for a minimum of forty-eight hours whenever new gas was added to the chamber or whenever the temperature of the chamber was increased.

2.2.2 Parameter Control and Measurement

2.2.2.1 High Temperatures

The chamber was heated with a coil of #22 nichrome wire wrapped around the central area and covered with asbestos. The whole chamber was then wrapped in aluminum foil. The a.c. heating current was drawn, via a variac, from the regulated voltage lines to reduce fluctuations. It was found that once a steady state was attained the subsequent temperature variation was less than 5° C. depending mainly upon the changes in room temperature. Since this degree of stability was tolerable no further control was used. The temperature was measured using an iron-constantan thermocouple and a Hewlett-Packard Model 425A microvoltmeter. The reference point for the thermocouple was an ice bath at 0° C. Tests of the temperature measurement system at liquid nitrogen temperature and at the boiling point of water indicated that the error in the system was dominated by the uncertainty in reading the voltmeter. Depending upon the temperature, and therefore the voltage range, this uncertainty varied from less than 1° C. at temperatures near 0° C. to 5° C. at temperatures above 190° C. The output of the voltmeter was connected to a chart recorder to facilitate continual monitoring of the temperature fluctuations during a run.

2.2.2.2 Low Temperatures

The method used to attain low temperatures involved a simple control

system designed to cool the chamber by adding a small amount of liquid nitrogen as required, followed by slow warming back to the temperature at which the liquid nitrogen control system was activated. The low temperature configuration is shown in Figure 7. The chamber was placed in a styrospan container lined with a layer of aluminized mylar. Stainless steel tubes were inserted into the container through which liquid nitrogen was forced. The liquid nitrogen flow was controlled by a voltage sensor circuit (Figure 7) attached to the thermocouple micro-voltmeter output. Although the sensitivity of this control system was less than 2° C. the intrinsic hysteresis of the pressurized liquid nitrogen system was such that the actual temperature variation was between 5° C. and 10° C. For safety reasons compressed nitrogen rather than compressed air was used to pressurize the liquid nitrogen system. The same thermocouple and micro-voltmeter were used for temperature measurement as for the high temperature case.

2.2.2.3 Pressure

The pressure of the gas contained within the chamber was measured using two test gauges. One, manufactured by Marsh, read from 0 to 150 p.s.i.g. (2% mirror backed) and the other, manufactured by Ashcroft, read from 0 to 300 p.s.i.g. (2% mirror backed). Calibrations obtained using a dead weight tester (Civil Engineering Department, U.B.C.) enabled pressure to be obtained to an error of less than 1%. In order to be able to neglect temperature effects on the gauges themselves connections to the chamber were made via one meter stainless steel tubing ($\frac{1}{8}$ inch inner diameter) and the gauges were kept at room temperature.

The pressure variation over a run because of lost gas was negligible

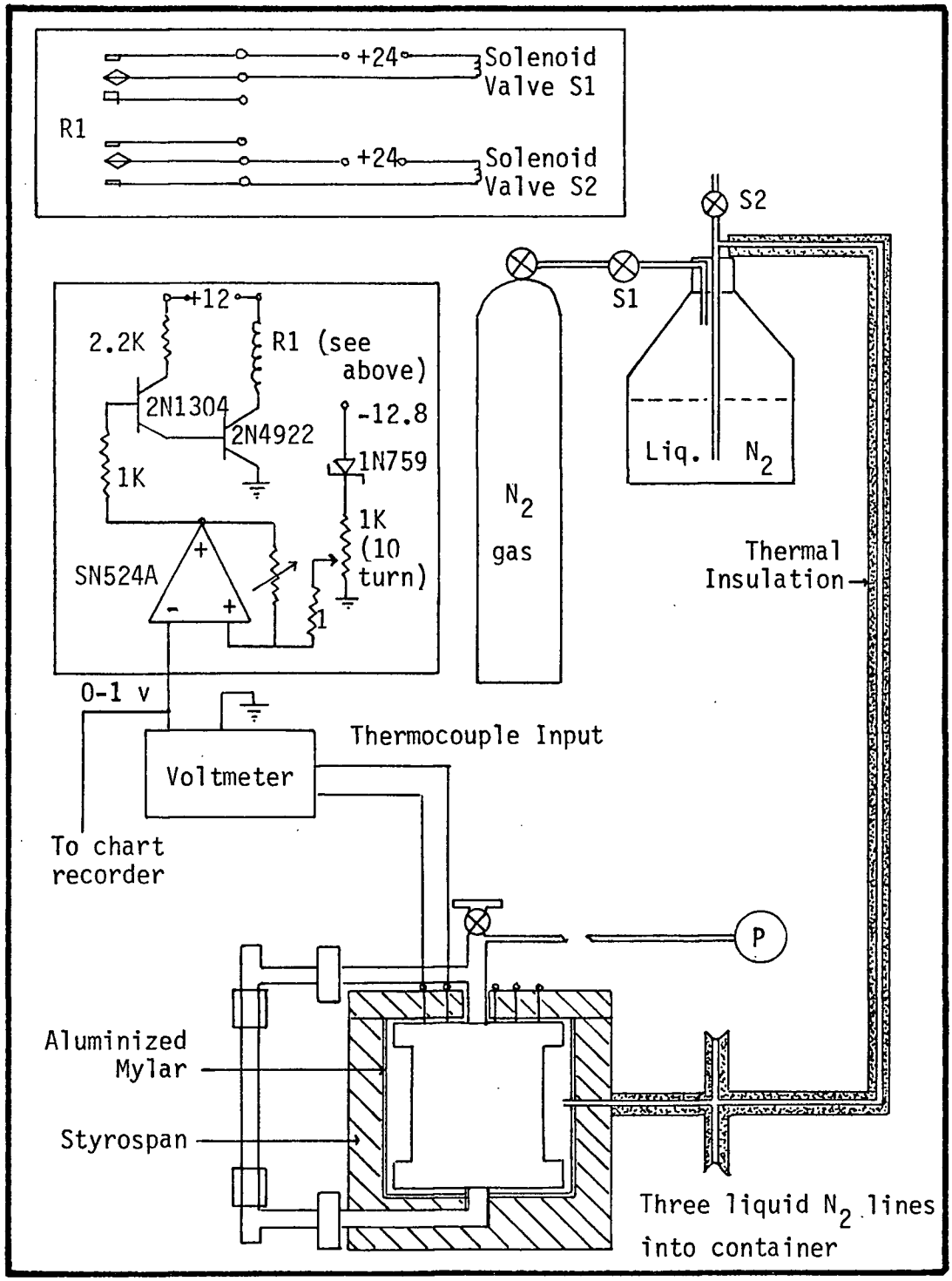

Figure 7 Low Temperature Chamber Configuration

at high temperatures but was measurable at room temperature and below. The cause of such leaks is uncertain but was probably due to the large number of electrical feedthroughs and the effect of thermal expansion. During such runs the pressure difference from start to finish, normalized for slight temperature variations, was always less than 3%. The pressure used to calculate the gas density was, of course, the average pressure over the run.

2.2.2.4 Electric Field

The electric field grid (Section 2.2.1.2) was externally biased by a resistive chain consisting of ten 130 KΩ 1% wire-wound resistors. The voltage was supplied by a Northeast Scientific Corporation regulated high voltage supply capable of 5 kV at 10 mA. Previous workers had used only a line regulated supply (Falk (1965), Orth (1966), Lee (1969)) since they required much higher voltages. The voltage was measured using an Avometer (2% full scale accuracy) in parallel with the resistor chain. The calibration of this meter with a Fluke 853A null-meter indicated the validity of this quoted accuracy. The uncertainty in the high voltage due to this measurement was therefore the 2% error associated with the meter.

Two configurations of the electric field were used in this experiment. In the first, the one used for most of the work, the highest voltage was put on the top plate of the electric field grid and the bottom plate was attached to ground. The source was then at an intermediate potential. Previous workers in this laboratory (Falk (1965), Orth (1966), Lee (1966)) had connected the source to high voltage and kept both end plates at ground. This latter configuration is capable of

yielding a higher electric field gradient since the distance is halved, high fields being of interest to the previous workers. For the low fields required in this experiment the first configuration was sufficient, simpler, and presumably yielded a field gradient of better uniformity. As a consistency check, however, the second configuration was used for some runs at room temperatures and higher fields.

2.2.3 Electronics

2.2.3.1 General Description

The data acquisition system employed a standard fast-slow coincidence circuit similar to that used by Orth (1966), Miller (1968), and Lee (1969). Modifications to the previous system (Lee (1969)) included the following.

i. The RCA 7046 photomultipliers were replaced by Philips 58AVP photomultipliers. The biasing circuit for these is illustrated in Figure 8.

ii. The home-made discriminators, pile-up-rejectors, and time-to-amplitude converters were replaced by standard fast commercial NIM units. The slow coincidence circuit remained the same as that used previously.

Figure 9 outlines the electronic configuration used.

2.2.3.2 System Linearity

2.2.3.2.1 Integral Linearity

The integral linearity was measured by the method of Taylor (1968) using a frequency generator and fixed delay. The complete system is shown in Figure 10. For a fixed delay, d, the time between two conseq-

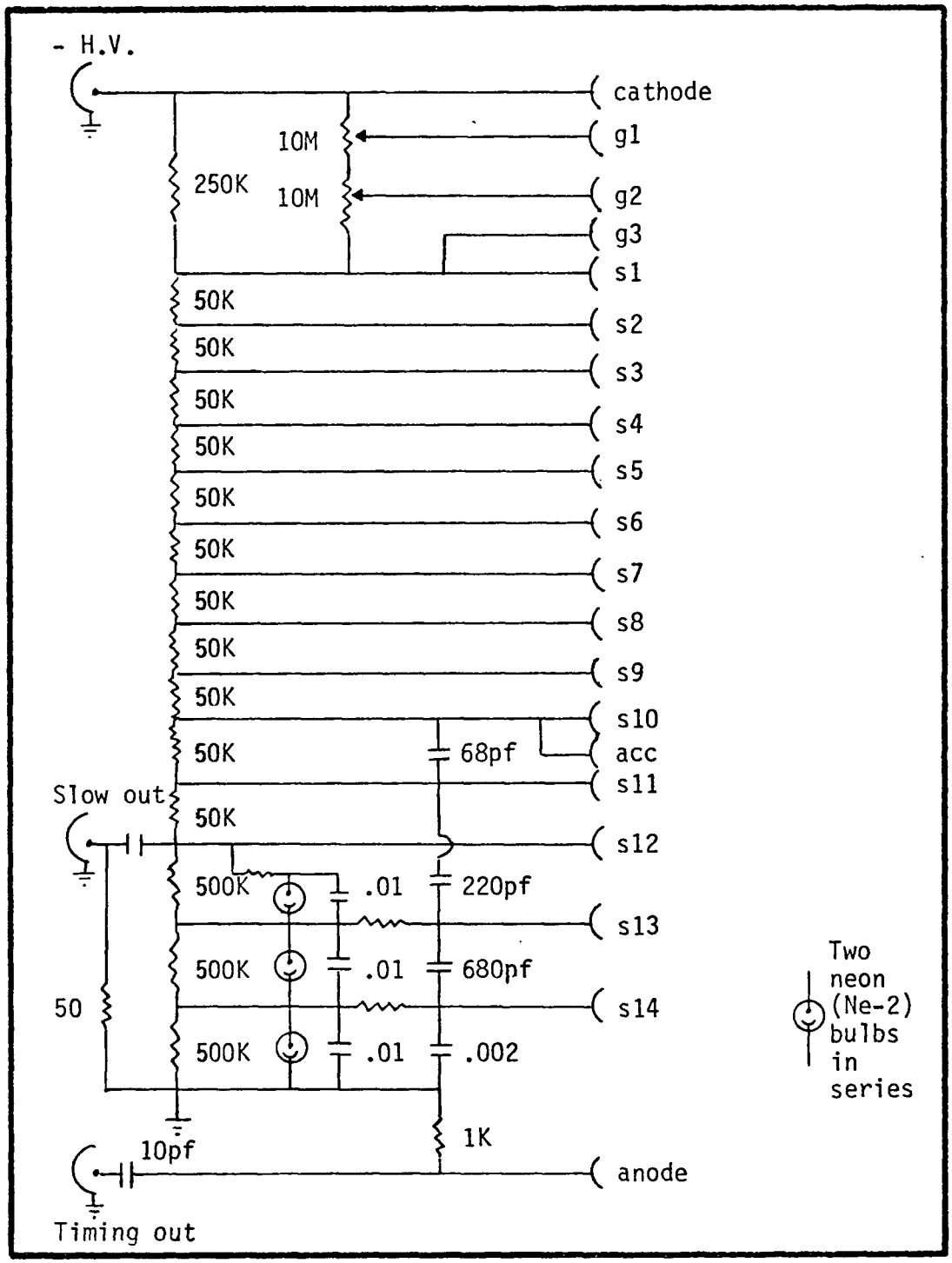

Figure 8 Photomultiplier Circuit

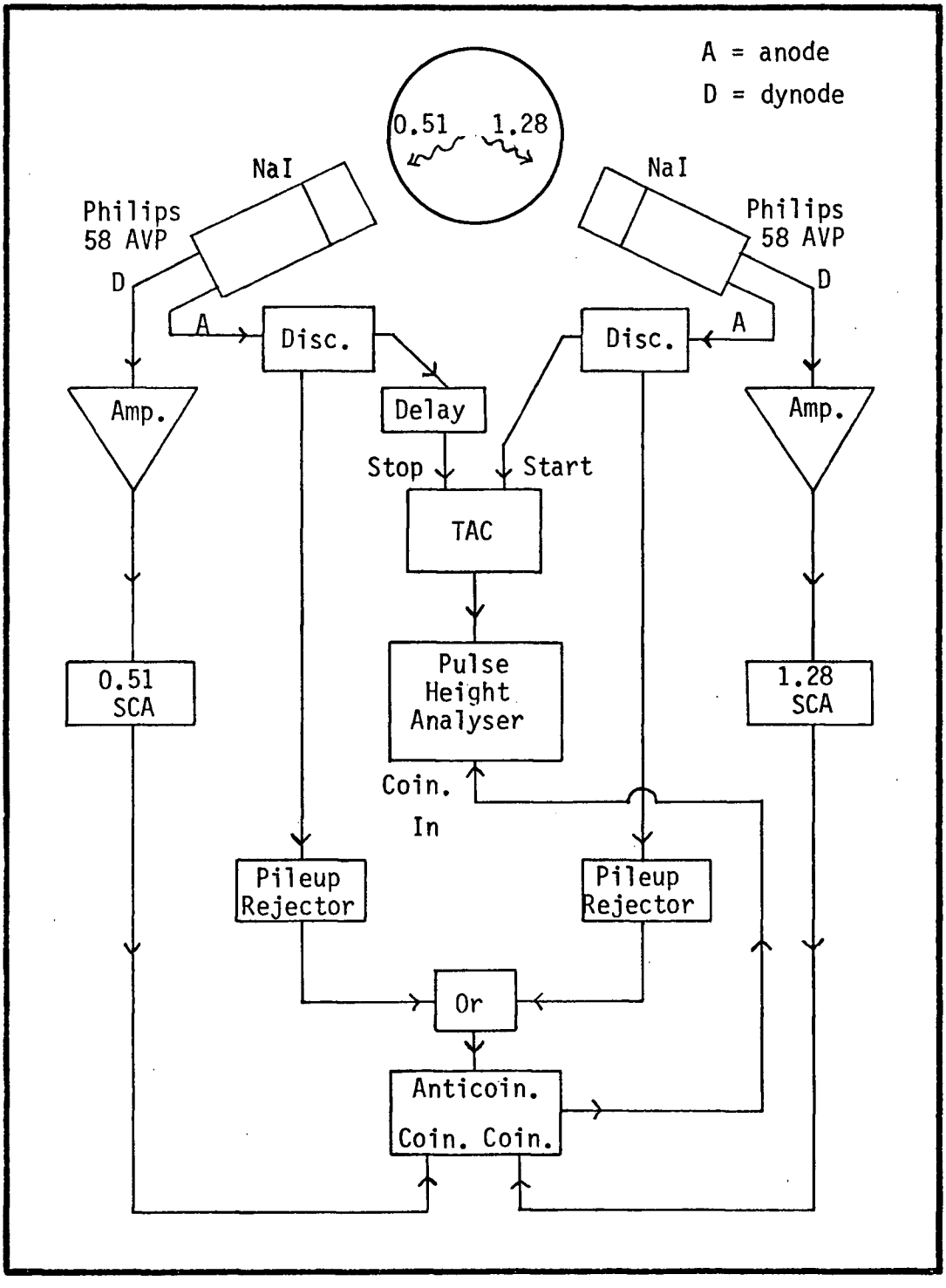

Figure 9 Electronic Configuration

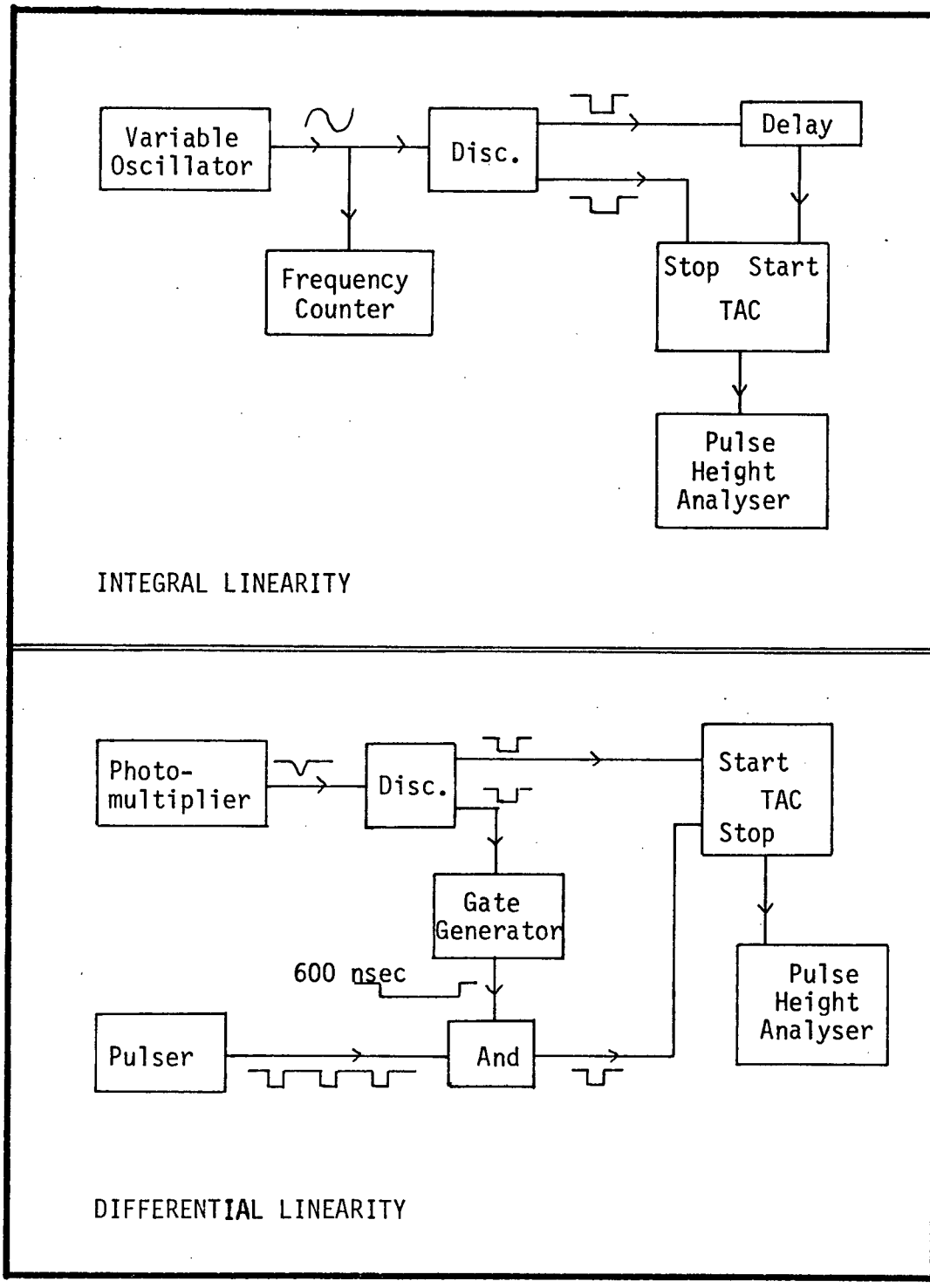

Figure 10 Electronic Configuration for Linearity Measurements

utive peaks obtained on the pulse-height-analyser is, as a function of frequency,

$$t_{f_1 f} = \left(\frac{1}{f_1} - d\right) - \left(\frac{1}{f} - d\right)$$

or

$$t_{f_1 f} = \frac{1}{f_1} - \frac{1}{f}$$

A plot of 1/f versus channel number is given in Figure 11. The straight line fitted to the data corresponds to an integral linearity of the system of 1.27 $\pm$ .01 nsec/channel.

2.2.3.2.2 Differential Linearity

The differential linearity was measured using the method of Falk et al. (1965). The electronic configuration is shown in Figure 10. The start pulses are generated from nuclear radiations detected by a scintillation counter and are thus random in nature. The stop pulses, however, are produced by the pulser. For a completely linear system, the counts per channel accumulated are equal within statistics. Non-linearities to a level of $\frac{1}{2}\%$ were determined by accumulating fifty thousand counts in each channel. The relative channel widths so determined were used in the data analysis. The differential linearity was essentially counstant (within $\frac{1}{2}\%$) over the region from channels 5 to 399 on the 400 channel pulse-height-analyser.

2.2.3.3 Time Resolution of System

The timing resolution of the electronic system, as measured by the width of the positron lifetime spectrum characterizing Na^{22} in aluminum, was found to decrease, as might be expected, both for lower discriminator settings and for higher applied voltage to the photomultipliers. The procedure used to define these settings was as follows.

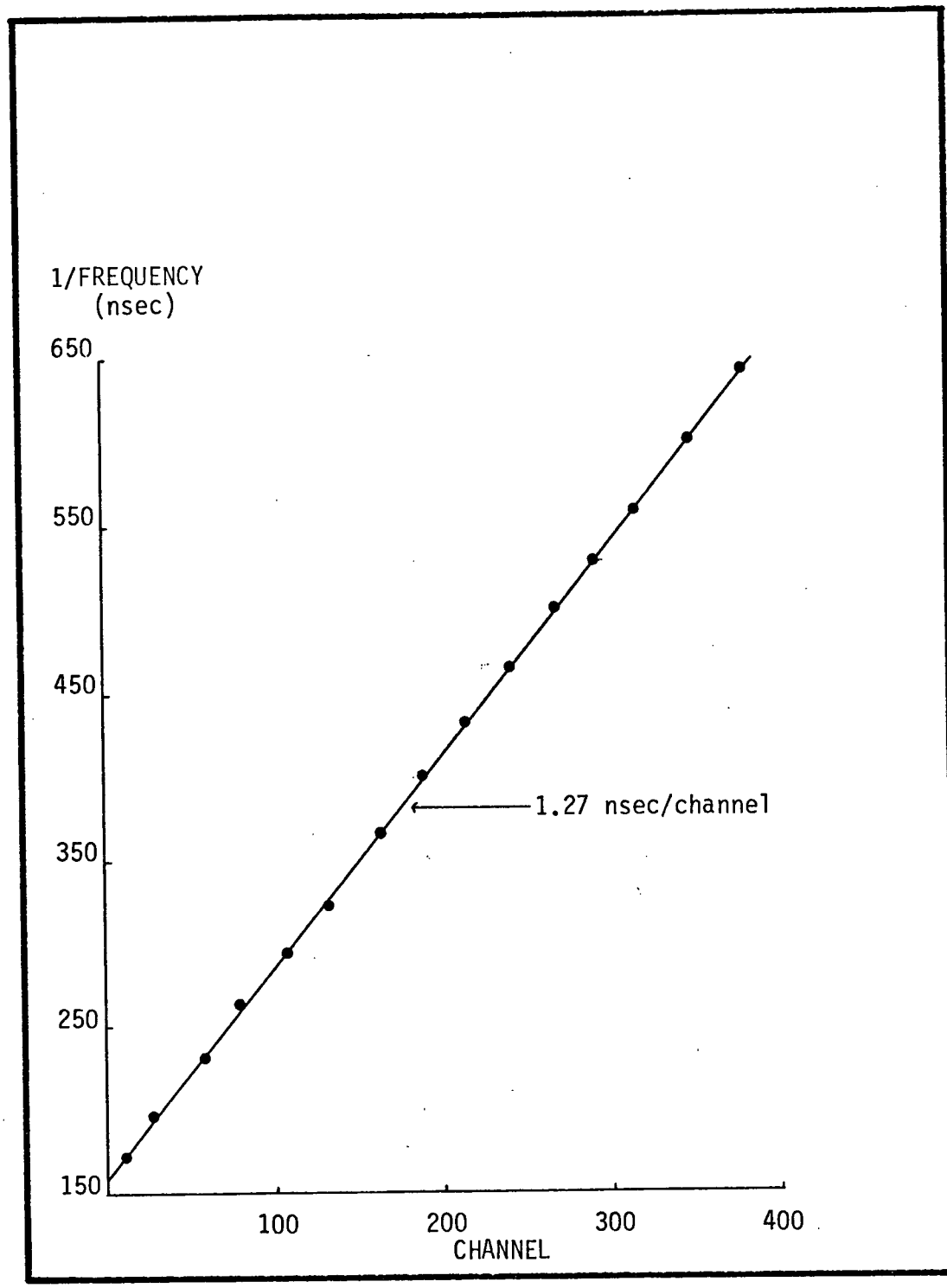

Figure 11 Integral Linearity

Plot of frequency^{-1} versus channel number.

The discriminator setting was required to be above that corresponding to triggering by thermal noise in order to maintain a low random background. Since the discriminators had only a small range of threshold settings (100 mV to 500 mV) this limited the photomultiplier H.T. to about 2400 volts. The best resolution obtained in this manner was less than 4 nsec full-width-half-maximum for Na^{22} in aluminum. During the experimental runs, resolution was about 5 nsec since a background problem required that the discriminator level be set significantly higher than the noise (Section 2.2.3.4).

2.2.3.4 Pulse Pile-up and Effects on the Random Background

The effect of a high count rate manifested itself in several ways. The first effect was that of time-slewing due to pile-up causing a baseline shift in the a.c. coupling between the photomultiplier and discriminator. This effect was also observed by Falk (1965) and it was demonstrated that the use of a pile-up gate would eliminate the problem.

The other major effect of high count rates is an increase in the random coincidence background. This effect arises for one of the following reasons. The first is the straightforward one of detection of uncorrelated events which happen to satisfy the energy window criteria and occur within the time interval spanned by the system. The probability of such random events can be shown to be constant in time for low count rates (less than 10^4/sec) from the slow coincidence stop single channel analysers (Appendix A). For this experiment the count rates were low enough to satisfy this condition.

The second random background effect is more troublesome since

it leads to a non-uniform random coincidence time spectrum in which the random background on the negative time region of the spectrum is affected to a greater extent than on the positive time side. This effect is discussed in detail in Appendix A. Even if such an effect causes a difference of only a few percent between the negative and positive time backgrounds, it manifests itself as an apparent increase in the orthopositronium quenching rate when the time spectrum is analysed assuming a constant background equal in both time regions.

Use of a pile-up-rejector reduces this second effect only if the pile-up-rejector has a deadtime that is short compared to the mean period between counts from the single-channel analyser. Miller (1968) observed anomalously low orthopositronium lifetimes which he interpreted as large quenching rates. Since he used a strong source and pile-up-rejectors whose deadtime was 1 μsec (Falk (1965)) the explanation for these results could easily be that just discussed. Miller's results ($\lambda_q = .39\ \mu sec^{-1}\ amagat^{-1}$) were similar to those obtained in this work before this problem was detected. For the much weaker sources used by Orth (1966) and Lee (1969) this effect was not observed.

The inherent limitations of the operation of the pile-up-rejector illustrated in Figure 9 is the output pulse width of the discriminator. Pile-ups occuring within this time cannot be detected by the pile-up-rejector. For the updating discriminators used, the width is determined by the length of the input pulse from the photomultipliers. This pulse, originally in excess of 300 nsec, was shortened by differentiating the photomultiplier anode pulse through a 10 pf capacitor in series with the 50 Ω load. In this way the length of the pulse at threshold

was shortened to 150 nsec and consequently the limitations on the pile-up-rejector were reduced to 150 nsec. In addition, the count rate was reduced by raising the discriminator level slightly. This reduced the number of longer output pulses (and thus longer deadtimes) which are caused by the updating of the discriminator when a second pulse exceeds the triggering threshold within 150 nsec.

The use of an a.c. coupled system could lead to time-slewing problems due to baseline shifts, as earlier mentioned. Falk (1965) demonstrated that the use of pile-up-rejectors removes this problem although he observed a prompt peak broadening at very high count rates even with the pile-up-rejectors in operation. At similar count rates no significant broadening in the prompt peak of Na^{22} in aluminum was observed in this experiment with the pile-up-rejectors in use. The effect noticed by Falk could easily be due to the rather long deadtime (1μsec) of his pile-up-rejectors.

2.2.4 Analysis of Results

2.2.4.1 Density Corrections

The density of argon differs from that calculated using the perfect gas law by an amount that depends on the temperature and the pressure. A complete tabulation (N.B.S. Circular 564 (1955)) of such corrections was used to determine the appropriate densities in this work. For the results presented here the perfect gas density was corrected by as much as 5% and the resulting density was estimated to be accurate to within 1%.

2.2.4.2 Curve Fitting Techniques

Throughout this thesis all curves were fitted using maximum likelihood techniques (Orear (1959)). Since the applicability of this method to Poisson and Gaussian statistics has been described by Orth et al. (1968) only a brief summary will be given here.

For Poisson statistics the probability of an experimental value N is

$$P_P = \frac{Y^N e^{-Y}}{N!}$$

where Y is the mean value.

For Gaussian statistics

$$P_G = \frac{1}{\sigma_N \sqrt{2\pi}} e^{-\frac{1}{2}\left(\frac{N - Y}{\sigma_N}\right)^2}$$

where σ_N^2 is the variance associated with the experimental value N.

The joint probability, or likelihood, of m specific values N_i being attained is

$$L = \prod_{i=1}^{m} P_i .$$

If Y depends upon some undetermined parameters, a_i, then those values of a_i which maximize L are the best values a_i^*.

Generally one maximizes the logarithm of L,

$$W = \ln L,$$

by solving the system of equations

$$\frac{\partial W}{\partial a_i} = 0 \qquad i = 1,p \qquad 2\text{-}8$$

where p is the number of parameters, a_i, to be fitted.

The solution of 2-8 is easily obtained if Y is a linear function of the a_i. Otherwise iterative methods may be required.

For the case where L is approximated by a multi-dimensional gaussian

in the neighbourhood of the maximum, the variances associated with the a_i^* are

$$\overline{(a_i - a_i^*)(a_j - a_j^*)} = (H^{-1})_{ij} \qquad 2\text{-}9$$

where

$$H_{ij} = -\left.\frac{\partial^2 W}{\partial a_i \partial a_j}\right|_{a_i^*, a_j^*}$$

If a physical quantity X is a function of the a_i, that is,

$$X = X(a_1, a_2, \ldots a_m)$$

then the best value for X, X^*, and the uncertainty in X, ΔX, are given by

$$X^* = X(a_i^*)$$

$$\Delta X_{RMS} = \left(\sum_i \sum_j \frac{\partial X}{\partial a_i} \frac{\partial X}{\partial a_j} (H^{-1})_{ij} \right)^{\frac{1}{2}} \qquad 2\text{-}10$$

The iterative method used to solve 2-8 was that of Orth et al. (1968) in which the partial derivatives in 2-8 are Taylor expanded about the initial (or best) fit and the resulting simultaneous equations are solved for the first order corrections.

The application of this program to the fitting of a function consisting of the sum of two exponentials plus a constant random background has been described by Orth et al. (1968). Essentially the same procedure was used in this work. The one difference was that for each exponential, instead of fitting to the intensity at zero time and the lifetime, the fit was made to the area under the curve ($I\tau$ product) and the lifetime. This resulted in somewhat faster convergence due to the reduced degree of correlation between these variables (Appendix B).

The fitting of electric field and temperature results also used the same basic maximum likelihood technique. All physical quantities determined from these results were calculated according to 2-10.

2.3 Presentation of Results

2.3.1 Acceptability of Data

Appendix C contains a summary of the accepted data. There were a total of 160 runs taken of which 34 were discarded for various reasons. Acceptance was based on the following criteria.

2.3.1.1 Random Background and Electronic Stability

The initial forty spectra indicated an anomalously short orthopositronium lifetime. This was attributed to the background problem outlined in Section 2.2.3.4. Once the corrective measures described in Section 2.2.3.4 were taken, however, the orthopositronium quenching rate deduced from the data was found to be consistent with expectations. As the discriminator level was set near noise, this condition was very susceptible to small changes in the gain of the photomultiplier and thus was dependent upon the stability of the H.T. supply. Occasionally such gain shifts did occur resulting in the generation of non-uniform random backgrounds. The positions of the 0.51 MeV and 1.28 MeV energy peaks were periodically monitored. When a shift in these indicated that the photomultiplier gain had varied, the data from the immediately preceding runs was neglected if the orthopositronium quenching rate was statistically high compared to the rest of the experimental values for that temperature. Such shifts occured five times. As a result four single runs and one group of twelve runs were compromised. The electronics was readjusted before continuing.

2.3.1.2 Convergence of Fitting Procedure

No runs were accepted unless the spectrum-fitting procedure con-

verged while varying all five parameters. Convergence could normally be attained in difficult cases by first holding one or more parameters constant and so obtain better estimates for the remaining parameters before allowing simultaneous fitting to all five parameters. The starting channel for the fit was normally chosen to be that point, no less than 5 channels away from the end of the shoulder, at which both convergence and an acceptable chi-squared (Section 2.3.1.3) were obtained. If the starting position was too close to the shoulder the chi-squared goodness-of-fit was reduced even though convergence was attained. For starting positions further away from the shoulder the chi-squared values were comparable but the errors in the parameters increased. Comparison of the values of the parameters obtained from fits starting further away indicated that, within statistics, the choice of starting channel had no effect. For difficult cases the choice of starting position had little effect on the rate of convergence.

A total of thirteen runs were rejected on this basis and all of these were at low densities where convergence is known to be difficult to attain (Orth (1966)). For these low densities even fixing the long lifetime did not result in good enough statistics to make this approach worthwhile.

2.3.1.3 Goodness-of-Fit

The chi-squared probability was calculated for all spectrum fits both for the complete data as well as after combining channels to get better statistics (Orth (1966)). Individual channel counts were normally sufficiently large that these two values were consistent. The criteria for acceptability of a run was that either of the chi-squared probabilities

described be greater than 0.1. Only two runs were rejected on this basis. The chi-squared was found to be essentially independent of the starting position provided this position was out of the region of the shoulder.

2.3.1.4 Equipment Failure

Two runs were rejected due to electrical and mechanical failure and one was rejected because of a temperature variation that was unacceptable.

2.3.2 Orthopositronium Quenching Rate

2.3.2.1 Temperature Dependence

The statistical errors on the orthopositronium lifetimes were poor since the primary interest was the direct annihilation rate and hence the lifetime spectra were taken in a direct enhanced mode (Orth (1966)). That is, the stop signal single channel analyser was centered about the 0.51 MeV peak. In order to obtain any significant information about the orthopositronium quenching rate, λ_q, the theoretical value for the free orthopositronium rate of 7.2×10^6 sec^{-1} was assumed and the orthopositronium lifetime, λ_2, was fitted to the functional relationship

$$\lambda_2 = 7.2 + \lambda_q D \ \mu sec^{-1} \qquad 2\text{-}11$$

for all values of λ_2 at a particular temperature. No attempt was made to find a dependence upon electric field since no effect was expected and previous work (Orth (1966)) had failed to observe such an effect. The results of these fits are shown in Table I and Figure 12. From these it can be seen that there is no statistical evidence for a temperature dependence in the orthopositronium quenching rate. The averaged

TABLE I

Temperature Dependence of Orthopositronium Quenching Rate

Temperature (K)	Average Quenching Rate (μsec^{-1} $amagat^{-1}$)	Number of Points Averaged
573	$.27 \pm .06$	17
465	$.18 \pm .14$	9
367	$.22 \pm .04$	13
298	$.255 \pm .009$	48
209	$.23 \pm .02$	14
135	$.24 \pm .08$	8
298	$.23 \pm .03$	39
298	$.23 \pm .02$	22

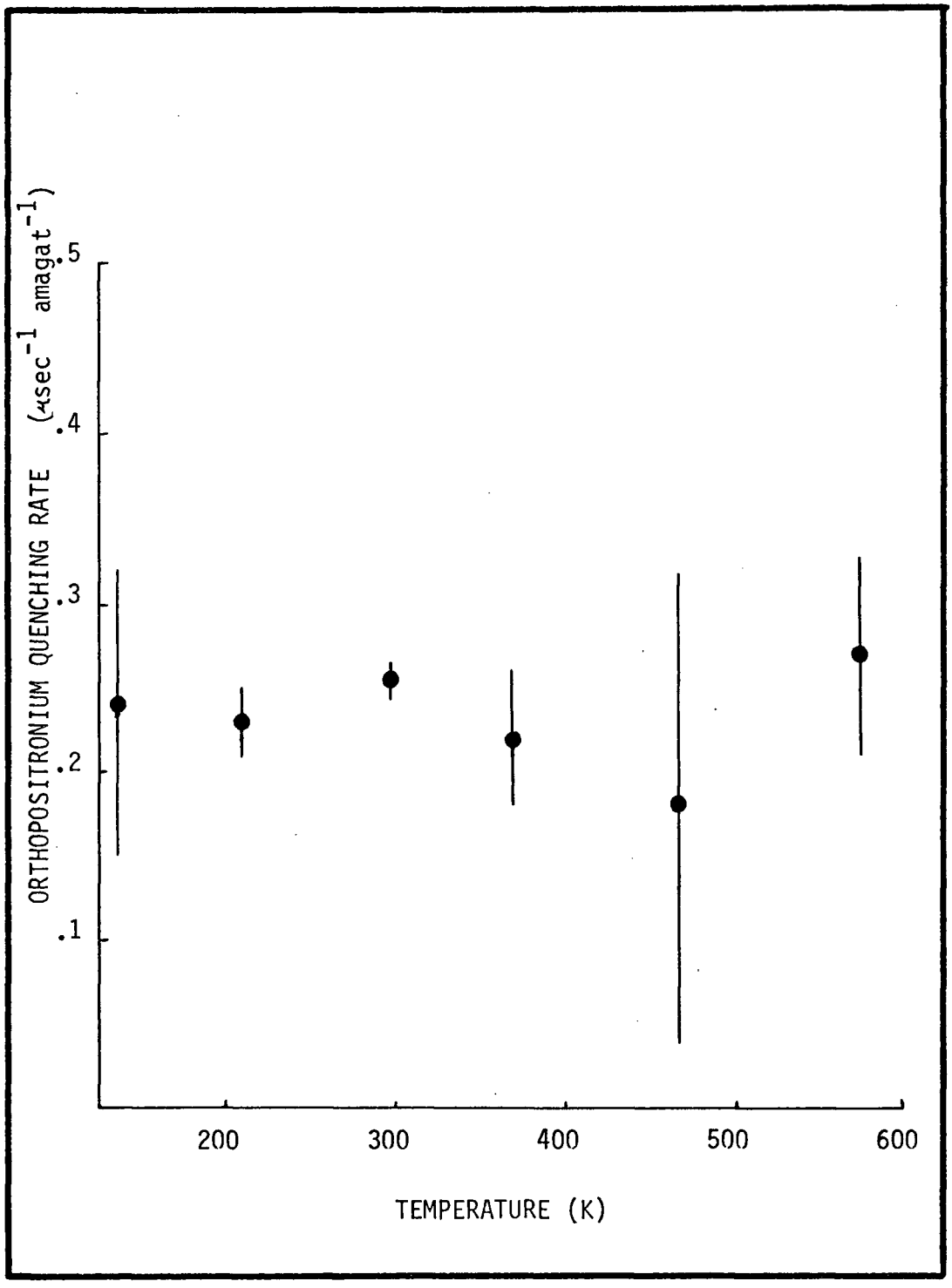

Figure 12 Temperature Dependence of Orthopositronium Quenching Rate

results for the quenching rates obtained below room temperature were

$$\lambda_q = .23 \pm .02 \text{ ⁄sec}^{-1} \text{ amagat}^{-1}$$

and for temperatures above room temperature

$$\lambda_q = .23 \pm .03 \text{ ⁄sec}^{-1} \text{ amagat}^{-1}.$$

The results for room temperature,

$$\lambda_q = 0.255 \pm .009 \text{ ⁄sec}^{-1} \text{ amagat}^{-1}$$

are in excellent agreement with the recently reported results of Tao (1970) of $\lambda_q = 0.255 \pm .015$ ⁄sec^{-1} amagat^{-1}.

For the room temperature results there were enough data points to get a good fit without constraining the free orthopositronium lifetime.

Thus $$\lambda_2 = \lambda_o + \lambda_q D \text{ ⁄sec}^{-1} \qquad 2\text{-}12$$

and the resulting fit was

$$\lambda_2 = (7.35 \pm .4) + (.235 \pm .05)D \text{ ⁄sec}^{-1}$$

which is again in good agreement with previous results (Tao (1970), Beers and Hughes (1968)).

2.3.3 Direct Annihilation Rate

2.3.3.1 Temperature Results

The temperature dependence of the zero field direct annihilation rate is shown in Figure 13. The function fitted to these results was of the form

$$\frac{\Delta}{D} = aT^b \text{ ⁄sec}^{-1} \text{ amagat}^{-1} \qquad 2\text{-}13$$

and the resulting best values obtained were

$$a = 21.43 \pm 2.33$$

$$b = -0.24 \pm .02.$$

The error matrix obtained from this fitting procedure is shown in Table II. This matrix is necessary in order to calculate results

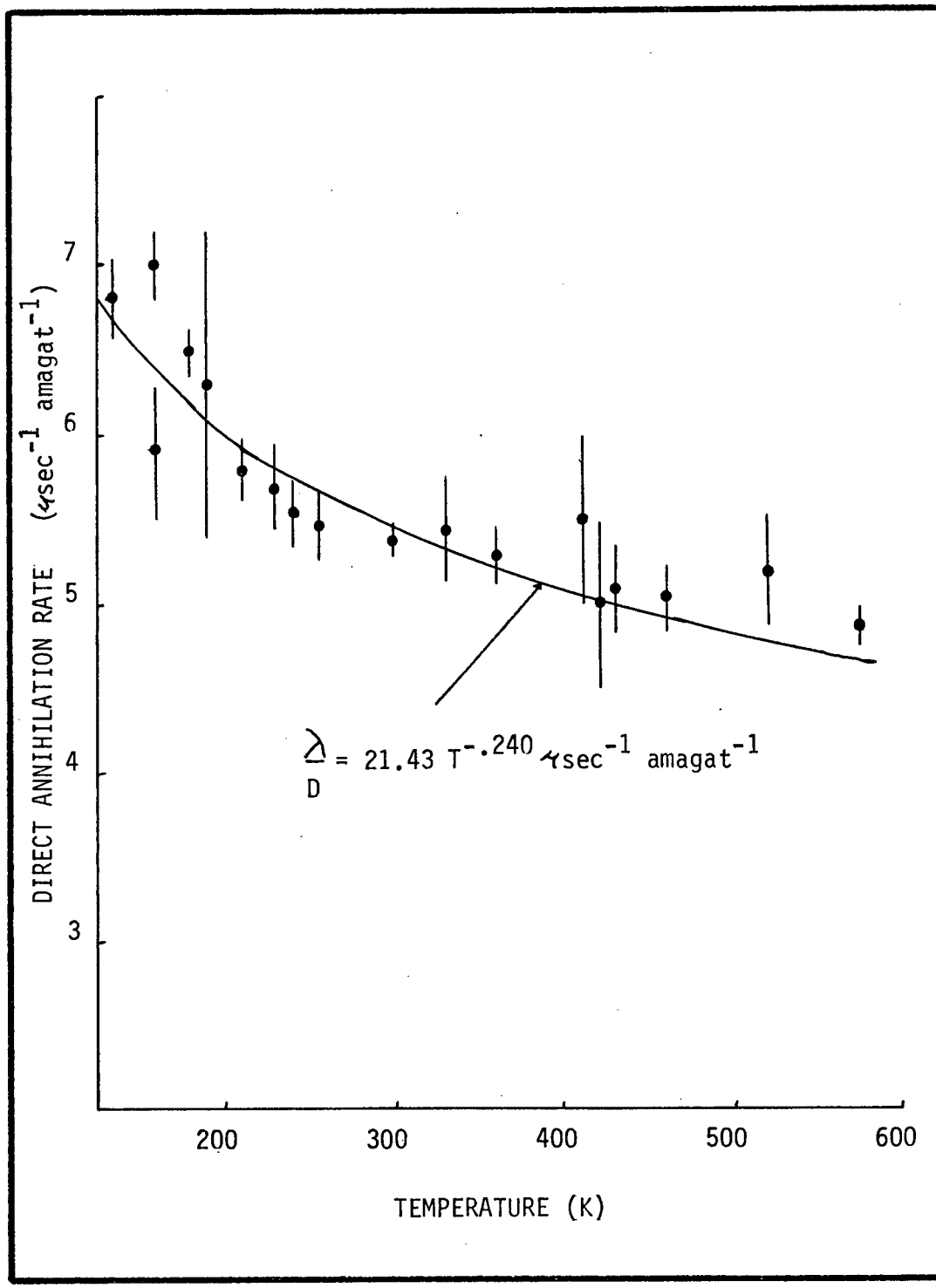

Figure 13 Temperature Dependence of Direct Annihilation Rate at Zero Electric Field

TABLE II

Error Matrix Resulting from Fit to Zero Field Temperature Results

	a	b
a	5.44	-.0455
b	-.0455	.000381

TABLE III

Results of Fitting Electric Field Data

Temp. (K)	a_o	$a_1 \times 10^2$	b_o	$b_1 \times 10^2$	$b_2 \times 10^6$
135	$6.8 \pm .2$	$-.45 \pm .17$	$6.7 \pm .2$	$-.46 \pm .16$	1.8 ± 1.2
209	$5.80 \pm .08$	$-.40 \pm .05$	$5.80 \pm .08$	$-.52 \pm .10$	4.5 ± 2.0
298	$5.35 \pm .03$	$-.28 \pm .05$	$5.35 \pm .03$	$-.27 \pm .03$	1.0 ± 0.2
367	$5.32 \pm .16$	$-.23 \pm .05$	$5.33 \pm .16$	$-.27 \pm .08$	1.0 ± 0.8
465	$5.10 \pm .18$	$-.21 \pm .06$	$5.10 \pm .20$	$-.24 \pm .13$	0.8 ± 1.7
573	$4.89 \pm .11$	$-.20 \pm .09$	$4.90 \pm .11$	$-.23 \pm .11$	1.0 ± 1.2

using 2-10. The errors quoted, and the error matrix presented, are based upon the assumption that the likelihood function resulting from the fit to 2-13 is a two dimensional gaussian in the region of the best values (Orear (1958)). That this is the case is demonstrated in Figure 14 where the relative likelihood is plotted for points near the best values obtained.

The current results are slightly different from those of Miller (1968) in that the dependence upon temperature is somewhat less. This is attributable to the fact that this earlier work (Miller et al. (1968)) did not take into account the density correction necessary at low temperatures (Section 2.2.4.1). If in fact the current results are fitted using values of λ/D uncorrected for this density change the agreement with Miller is good.

2.3.3.2 Electric Field Results

The electric field results at various temperatures are shown in Figures 15 through 20. At each temperature the data was fitted to the power series expansions

$$\frac{\lambda}{D} = a_0 + a_1 \left(\frac{E}{D}\right)^2 \text{ sec}^{-1} \text{ amagat}^{-1} \qquad 2\text{-}14(a)$$

and

$$\frac{\lambda}{D} = b_0 + b_1 \left(\frac{E}{D}\right)^2 + b_2 \left(\frac{E}{D}\right)^4 \text{ sec}^{-1} \text{ amagat}^{-1} \qquad 2\text{-}14(b)$$

depending upon the magnitude of the electric fields included in the data. A power series expansion was chosen because knowledge of the derivative $\partial(\lambda/D)/\partial(E/D)^2$ at zero field is required in order to obtain values for the scattering cross-sections (Section 3.3).

The results of this fitting procedure are summarized in Table III. It is seen that for low electric fields ($E/D < 25$ V cm^{-1} amagat^{-1} for T

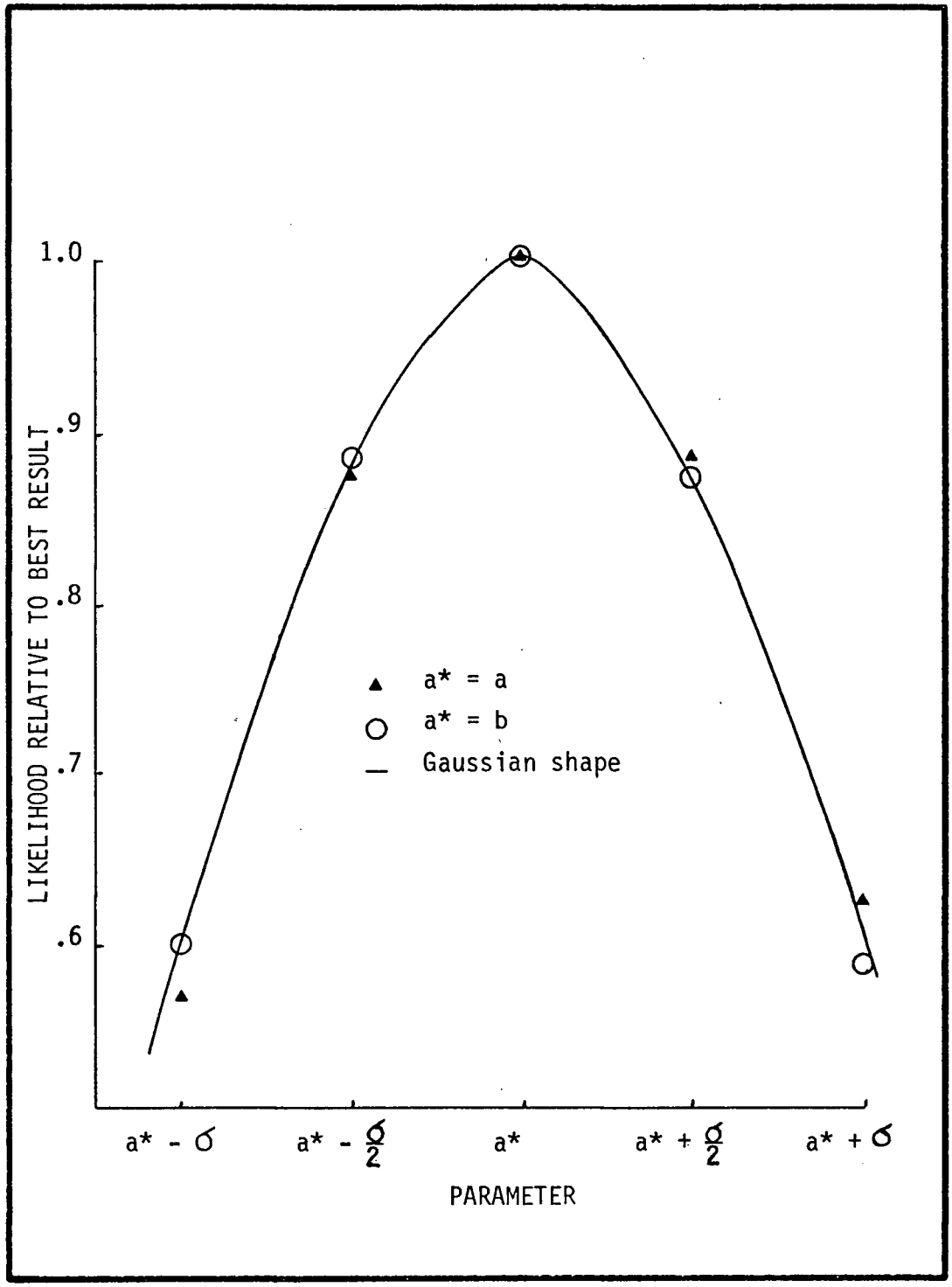

Figure 14 Dependence of Likelihood Function on Parameters Involved in Fit of λ/D versus Temperature

One parameter was varied while the other was held at its best value.

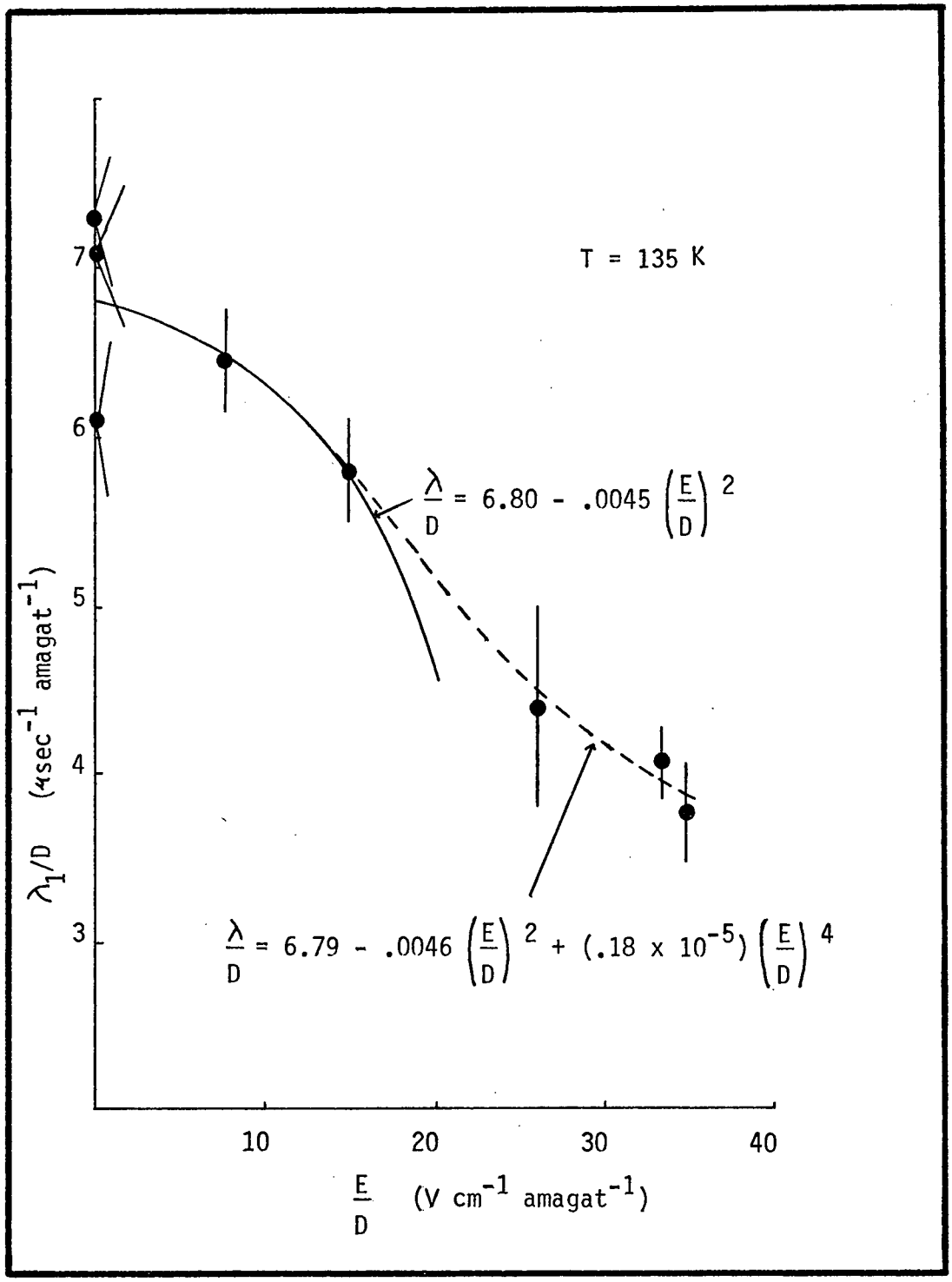

Figure 15 Electric Field Dependence of Direct Annihilation Rate at T = 135 K

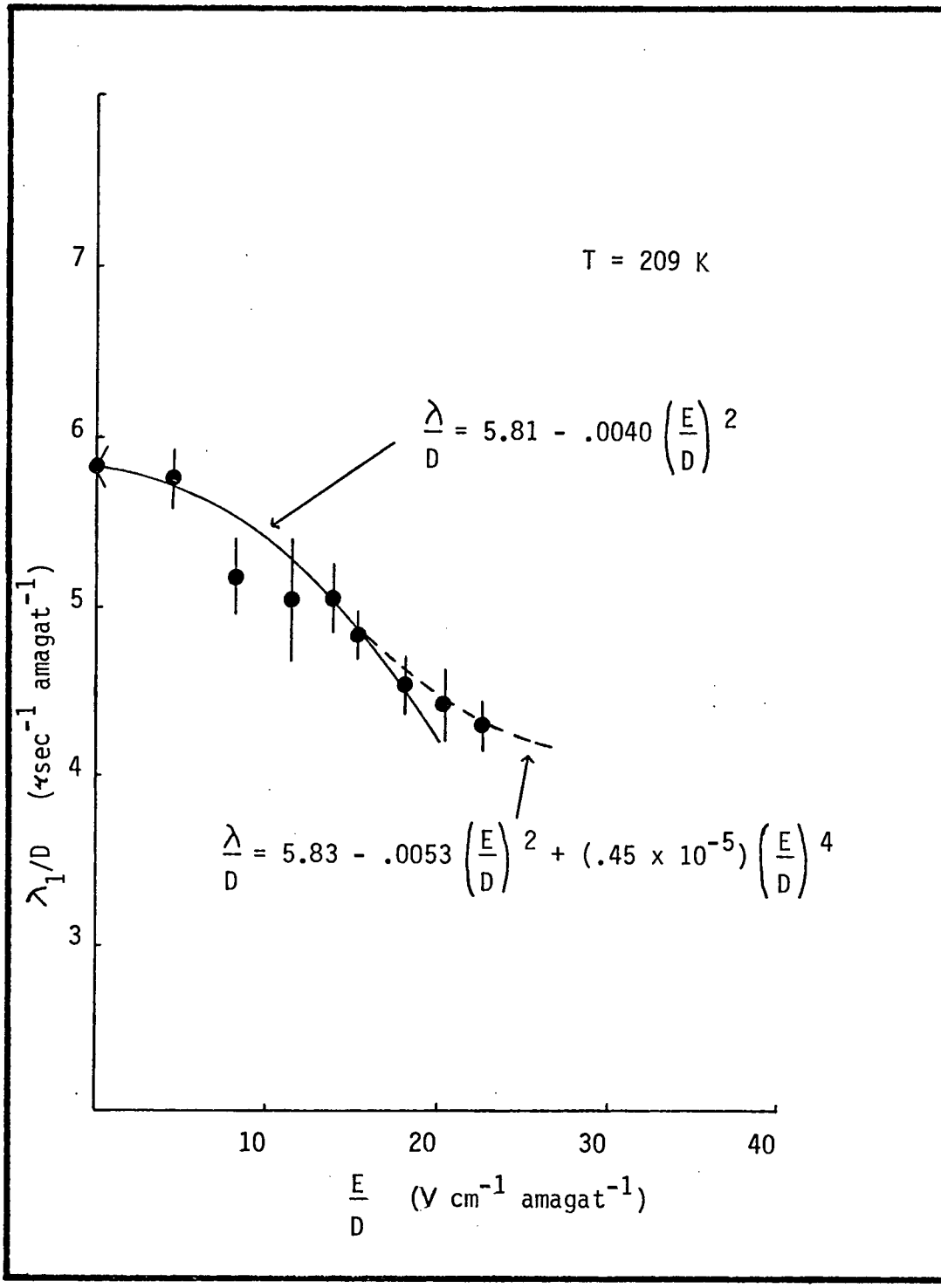

Figure 16 Electric Field Dependence of Direct Annihilation Rate at T = 209 K

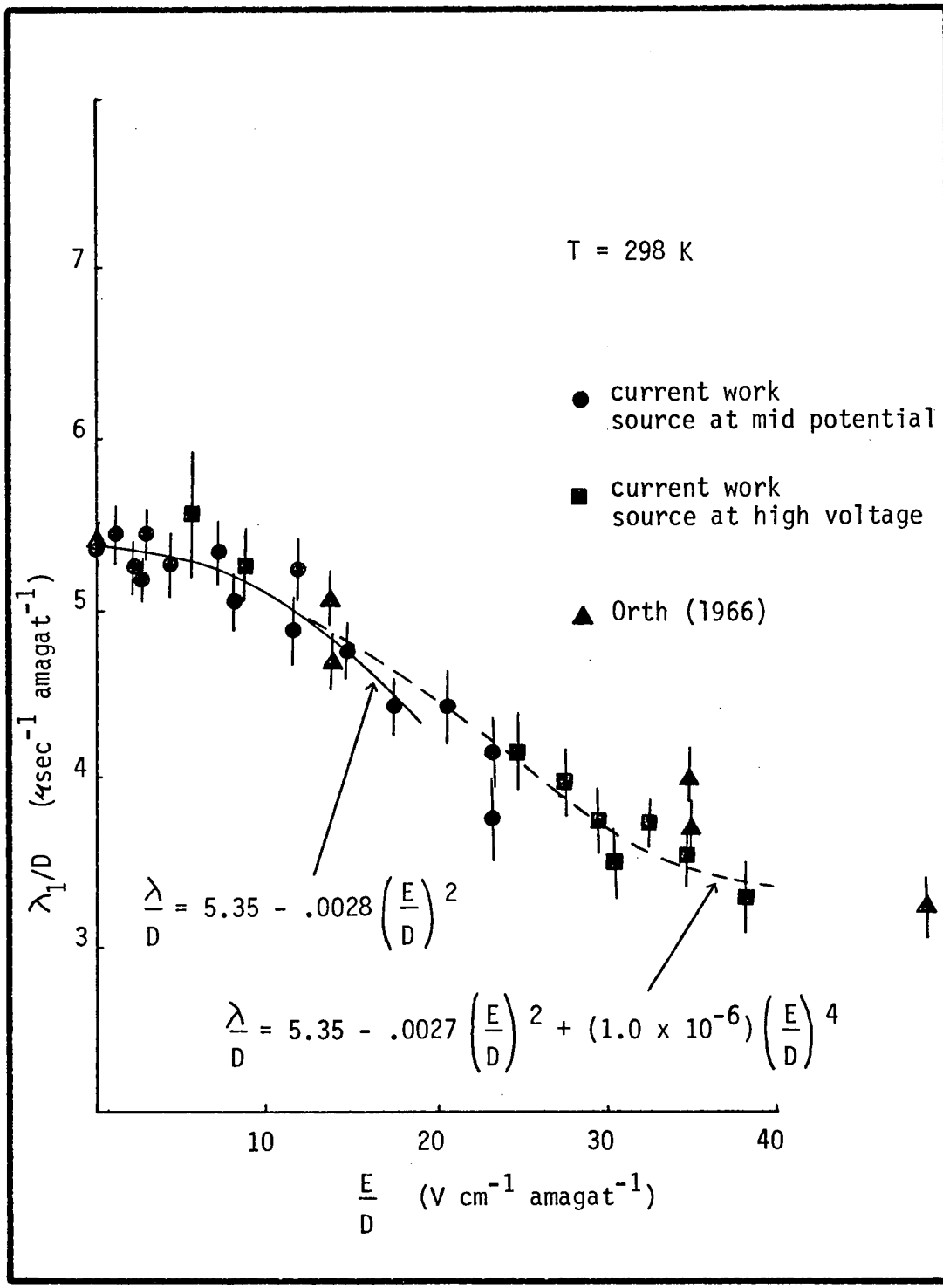

Figure 17 Electric Field Dependence of Direct Annihilation Rate at T = 298 K

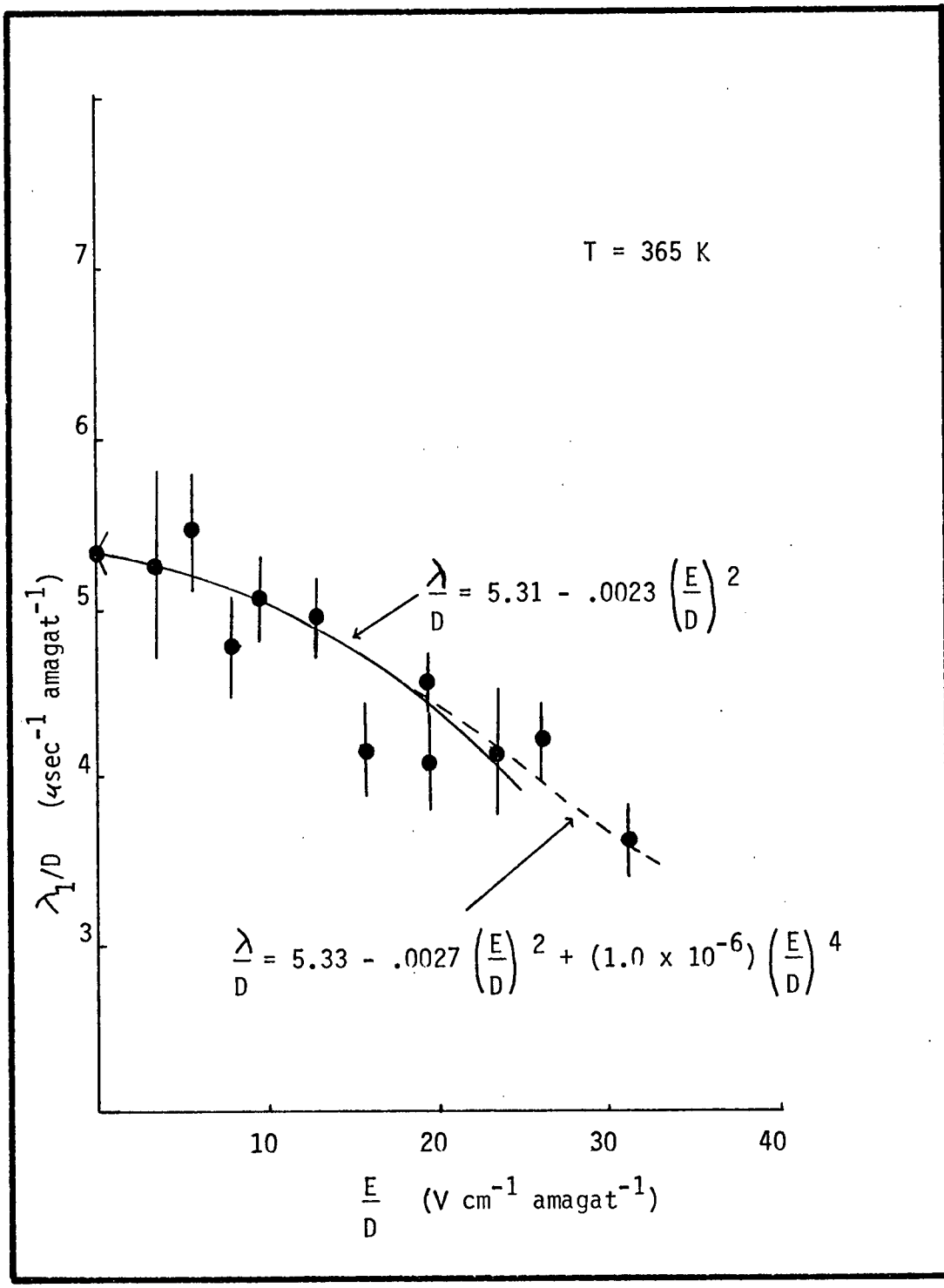

Figure 18 Electric Field Dependence of Direct Annihilation Rate at T = 365 K

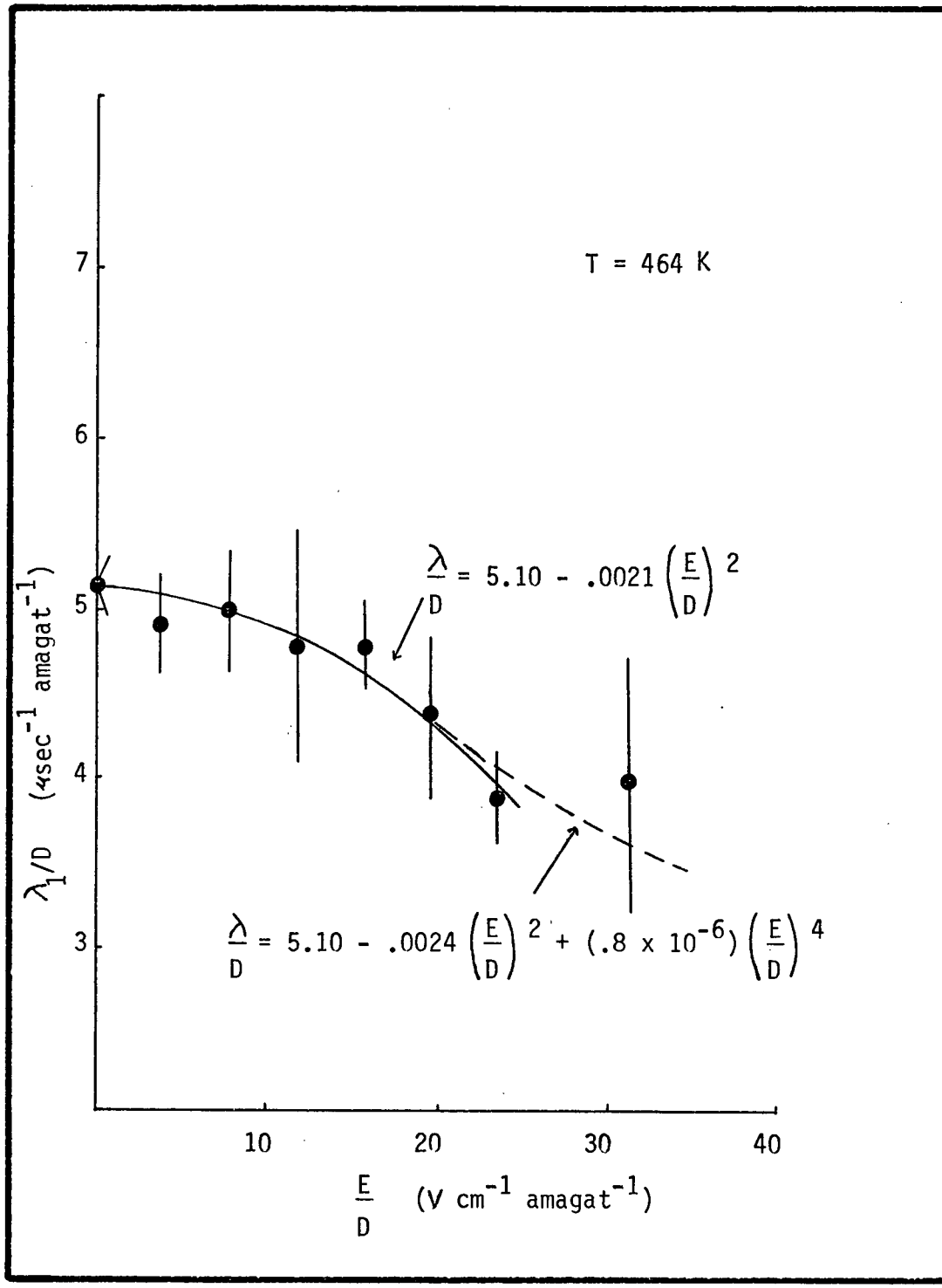

Figure 19 Electric Field Dependence of Direct Annihilation Rate at T = 464 K

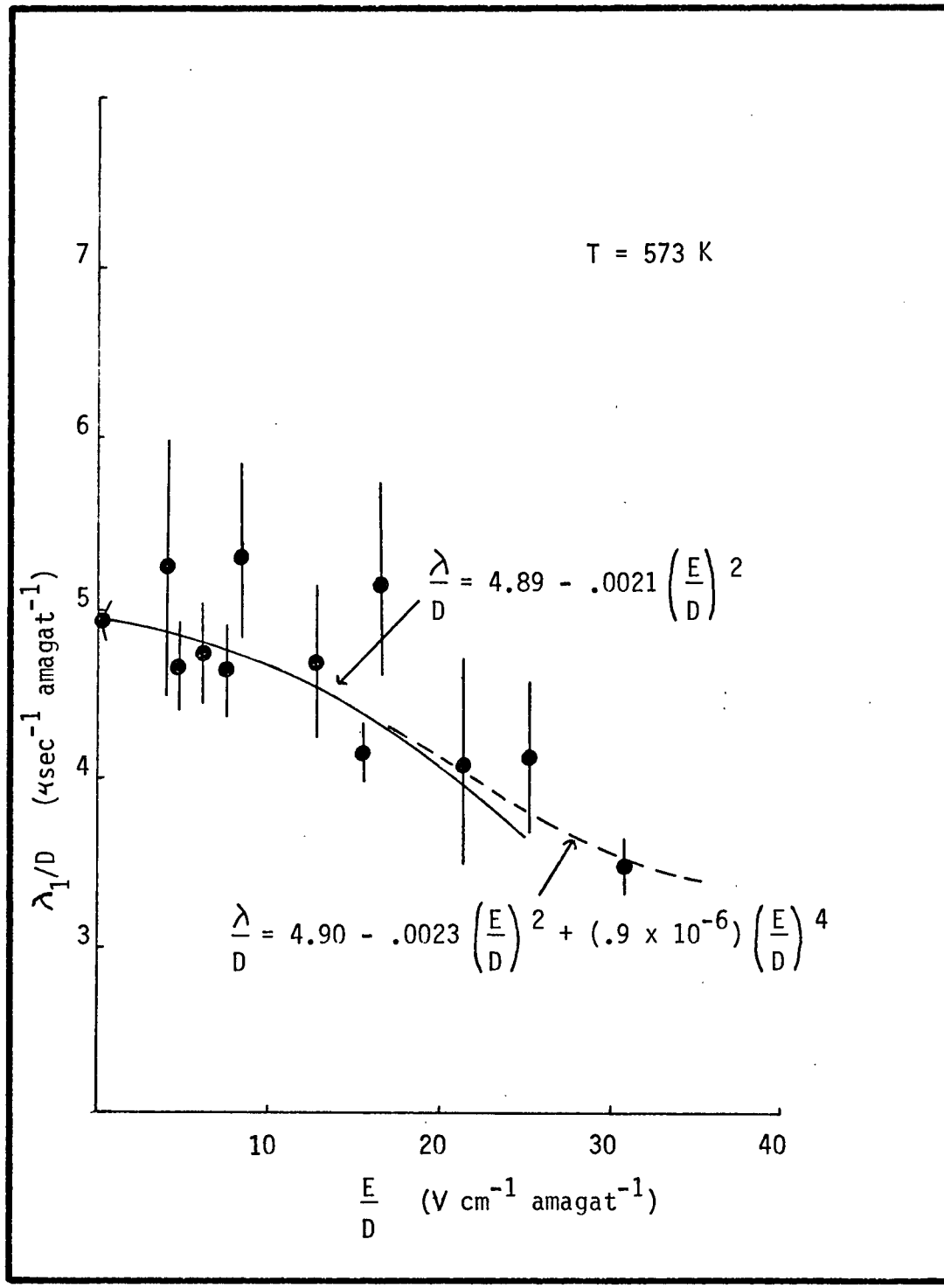

Figure 20 Electric Field Dependence of Direct Annihilation Rate at T = 573 K

>300 K and $E/D < 20$ V cm^{-1} amagat^{-1} for $T < 300$ K) the values of a_1 so determined agree within statistics with the value of b_1 obtained by fitting over a larger range of electric fields ($E/D < 40$ V cm^{-1} amagat^{-1}). The difference in the electric field limits as a function of temperature arises since one expects, on theoretical grounds, that the higher order terms in the power series expansion have a greater effect at lower temperatures (Appendix D). It would thus appear that for low fields the expansion containing only the first term in $(E/D)^2$ (Equation 2-14(a)) adequately represents the data.

Comparison with previous results is shown in Figure 17 where the results of Orth (1966) are also plotted. In this figure the higher electric field results were, as indicated in the figure, taken with the central or source plane at high voltage and the end plates at ground (Section 2.2.2.4). The results do not appear to depend upon the electric field configuration used and agreement with the results of Orth is excellent.

2.4 Error Analysis

2.4.1 Counting Statistics and Uncertainty in λ/D

Standard deviations of the fitted parameters due to counting statistics were determined from the maximum likelihood fitting procedure (Equation 2-9) with the assumption that the likelihood function is gaussian in shape near the best values. This assumption was substantiated by Orth (1966) fitting similar data using an intensity-lifetime function. The validity of this assumption for the case of fitting an area-lifetime function (Section 2.2.4.2) is demonstrated in Figure 21. The likelihood space is in fact more gaussian-like for the latter case, possibly

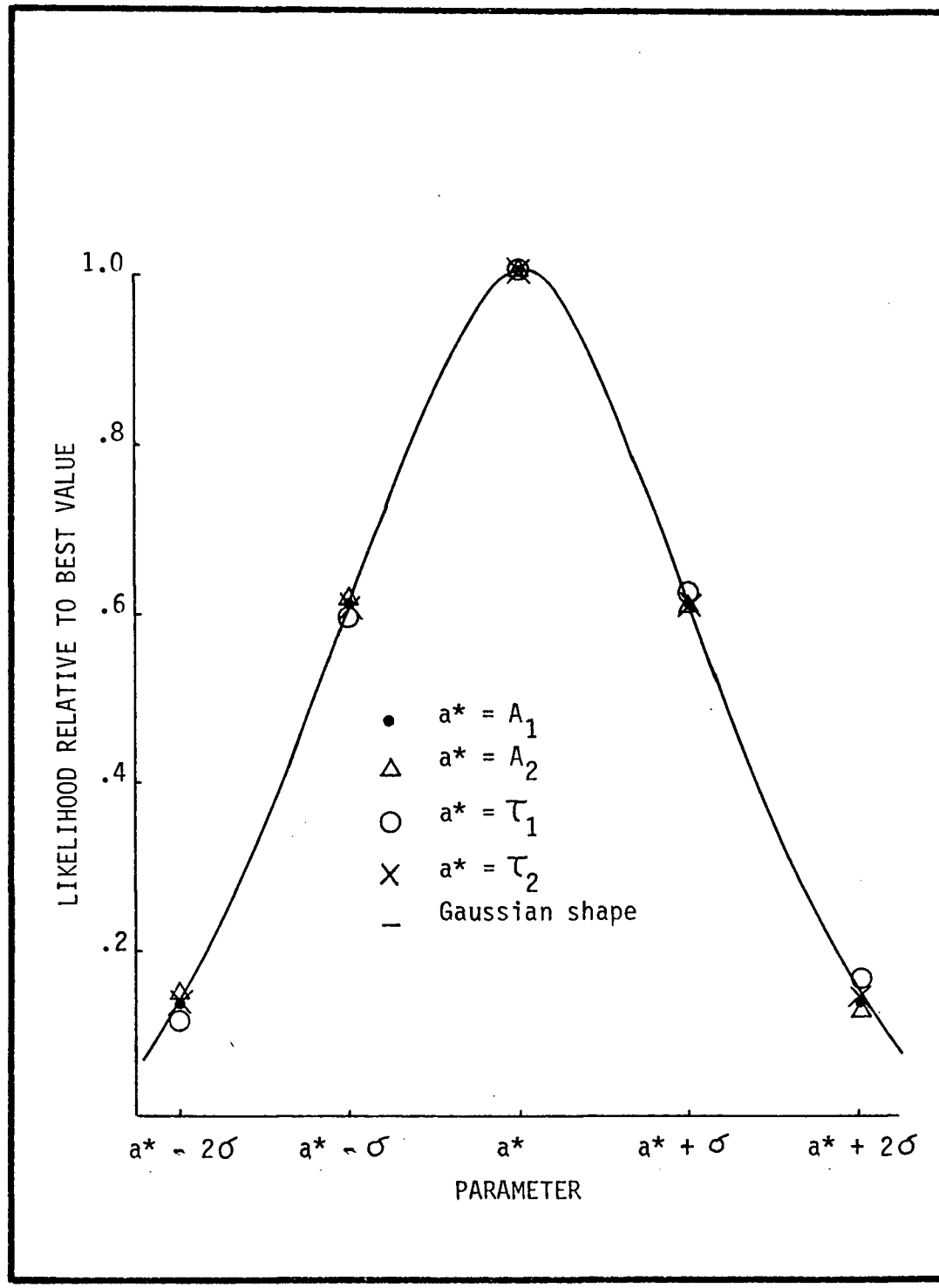

Figure 21 Dependence of the Likelihood Function on Parameters Involved in Area Fitting of Double Exponential

Each parameter was varied with the other three held fixed at their best values.

reflecting the reduced degree of correlation between the parameters. All errors displayed in Figures 15 to 20 characterize such statistical fits to the data.

Additional uncertainties in λ/D, arising from electronic instability (Section 2.4.1.1) and uncertainties in gas density (Section 2.4.1.3) are approximately 3.2%, obtained by combining the RMS uncertainties in these parameters. As this uncertainty is less than that contributed by counting statistics (about 5%), the overall uncertainty obtained by combining these is comparable, that is, less than 6%. For this reason the uncertainties due to density and electronic stability were not considered when fitting the electric field and temperature results of Section 2.3.3.

In addition, the values of E/D and T were assumed to be well defined while the fits to 2-13 and 2-14 were carried out. The errors in E/D (Section 2.4.1.4) and T (Section 2.4.1.2) are small and are equivalent, for the dependencies obtained in 2-13 and 2-14, to a change in λ/D of less than 1%.

2.4.1.1 Electronic Stability

As mentioned in Section 2.3.1.1 electronic instability was responsible for the rejection of certain runs. During an acceptable run the effects of electronic instability on the timing were almost certainly less than the inherent resolution of the apparatus (5 nsec). No shift in the prompt peak by even as much as 1 channel (1.27 nsec) was noted during a run.

Uncertainties in timing due to the integral and differential linearity are of the order of 1%. The absolute error in the integral linearity

(Section 2.2.3.2.1) is less than 0.8% and the uncertainty in the differential linearity is about 0.4% (Section 2.2.3.2.2). Since the differential linearity is already a correction term, the total uncertainty in timing due to linearity measurements is less than 1%.

2.4.1.2 Temperature

The temperature of the chamber was measured with an iron-constantan thermocouple and H.P. 425A micro-voltmeter (Section 2.2.2.1). The uncertainty in temperature thus varied between 1^{o} and 5^{o} C. depending upon the temperature range. The major temperature uncertainty over a run was the inaccuracy due to temperature fluctuations, rather than measuring inaccuracy, and these fluctuations were within a maximum of 10^{o} C. Thus the maximum error in temperature due to measurement was about 1.5%, whereas the total error in temperature over a run was about 5%.

2.4.1.3 Gas Density

The gas density was determined from measurements of pressure and temperature by using the perfect gas law together with published corrections for the non-ideal nature of argon (Section 2.2.4.1). The uncertainty in the gas density, obtained by combining the errors in pressure (Section 2.2.2.3), temperature (Section 2.4.1.2), and the correction, is therefore of the order of 2%. The major uncertainty, however, was due to gas leakage during a run and amounted to a maximum of 3% for any one run. As an upper limit on the error in gas density this value of 3% is used.

2.4.1.4 Electric Field

The spatial uniformity of the electric field within the chamber for a grid structure similar to the one used in this experiment was investigated by Falk (1965). He found that the non-uniformities were confined to a region immediately surrounding the field rings encompassing about 8% of the volume. The uniformity of the field for the current geometry is assumed to be similar. The reproducibility of the E/D lifetime results over a range of densities is evidence of the unimportance of this small non-uniformity since the number of positrons reaching the neighbourhood of the rings is pressure dependent.

The accuracy of the electric field gradient depends in turn on the measurement accuracy of both the applied voltage and the spatial distances. For the grid assembly used, the distance between end-plates (5 inches) was known to $\frac{1}{16}$ inch, or 1.3%. As the applied voltage was measured to 2% accuracy (Section 2.2.2.4), the combined uncertainty is of the order of 2.3%. There is also some possible non-uniformity in the field arising from variations in the values of the bias resistors. The resistors, which are external to the chamber and at room temperature, are accurate to 1%. This effect and the non-uniformity introduced by variations in ring spacing are a perturbation on the average field as calculated above. For the relatively slight dependence of the positron lifetime with electric field, an upper estimate for the effect on the measured lifetime of the non-uniformity due to bias resistors and ring spacing is 1%. The combined error in the electric field is therefore less than 3%.

The error in E/D obtained by combining the error in E and D is then 4.2%.

2.4.2 Gas Purity

The gas purity was monitored by constant checking of the "shoulder width"-density product which has been found to depend strongly on the presence of impurities (Falk (1965), Paul (1964)). This product was found to be about 350 nsec amagats. The gas used to fill the chamber was Matheson Gold Label Ultra Pure, 99.999% pure. The Matheson Company analysis of the gas was

$CO_2 < 1$ ppm

$O_2 < 5$ ppm

$H_2 < 1$ ppm

$CO < 1$ ppm

$N_2 < 5$ ppm

$CH_4 < 2$ ppm

$H_2O < 4$ ppm.

The chamber was outgassed under vacuum (0.01 mm Hg) for forty-eight hours at 650° K before filling and the purifier (Section 2.2.1.4) was used after every filling and after every addition of gas since it was felt that significant contamination could arise from the valves and filling lines which were exposed to atmosphere between usage. Tests of the purifier (Section 2.2.1.4) showed its effectiveness in this respect. In order to obtain a more quantitative estimate of the purity of the gas contained in the chamber during a series of runs, a sample bottle was attached to the chamber and used to obtain a gas sample for analysis. An analysis performed by Gollob Analytical Service Corporation of New Jersey (recommended by Matheson Company) indicated the impurity levels as

N_2	30 ppm	
O_2	< 4 ppm	detectable limits
CO_2	< 4 ppm	
H_2	< 4 ppm	
He	< 4 ppm	
Hydrocarbons	< 0.5 ppm	
H_2O	< 20 ppm.	

The impurity level of all gases, with the exception of nitrogen, was below the detection limit. The small, but detectable amount of nitrogen gas, is difficult to explain but could be due to outgassing of the sample bottle or chamber walls since nitrogen was added to the chamber for a test of the purifier at an earlier time. In support of this hypothesis, an earlier sample analysis indicated greater than 1000 ppm nitrogen yet the shoulder width was as good. This earlier sample had been obtained without first baking out the sample bottle and the large impurity level indicated is attributed to outgassing from its walls.

That the results agree well with previous room temperature results (Orth (1966), Tao (1969)), particularly the agreement in the ortho-positronium quenching rate, corroborates the results of the quantitative analysis.

CHAPTER THREE

ANALYSIS OF RESULTS AND EXTRACTION OF CROSS-SECTIONS

3.1 Outline of Procedure

From the discussion of Section 1.3 it is evident that the positron lifetime in argon depends upon the temperature of the gas, the electric field applied, and the velocity dependence of the momentum-transfer and annihilation cross-sections. The equation relating the measured annihilation rate, $\lambda(T)$, and the velocity dependent annihilation rate, $\nu_a(v)$, (Equation 1-5) is

$$\lambda(T) = \frac{\int_0^\infty \nu_a(v) v^2 f(v) dv}{\int_0^\infty v^2 f(v) dv}. \qquad 3\text{-}1$$

Given $\nu_a(v)$, the relationship (Equation 1-4)

$$f(v) = C\exp\left(- \int_0^v \frac{v'}{\left(\frac{e^2E^2}{3m\nu_d^2} + \frac{kT}{m} \right)} dv' \right) \qquad 3\text{-}2$$

in principle outlines a method for obtaining the momentum-transfer rate, $\nu_d(v)$. The momentum-transfer cross-section can be parameterized and the $f(v)$ of 3-2 written in terms of these parameters. This $f(v)$, used in 3-1, in principle allows the experimental results, $\lambda(T)$, to be expressed in terms of these same parameters. In practice, however, an analytic solution to 3-1 and 3-2 is not possible for non-zero electric fields.

A more practical technique involves consideration of the quantity $\partial(\lambda/D)/\partial(E/D)^2$ at $E = 0$. An analytic solution of the resulting equations

is possible for certain parameterizations of $\nu_d(v)$ and an equation relating $\partial(\lambda/D)/\partial(E/D)^2$ at E = 0 with these parameters can be obtained.

By fitting the set of experimental values at different temperatures, T, with this expression, the best values of these parameters and thus $\nu_d(v)$ can be obtained. This technique was the one adapted for analysis of results in this thesis.

3.2 Calculation of Velocity Dependent Annihilation Rate

3.2.1 Zero Field Thermal Positron Velocity Distribution

The zero field thermal positron velocity distribution, with the approximation that the velocity dependence of the annihilation rate does not appreciably affect the shape of the distribution, is given by $v^2 f(v)$ where $f(v)$ is given in 3-2 with E = 0. Thus

$$f(v) = C\exp\left(-\frac{mv^2}{2kT}\right) \qquad 3\text{-}3$$

and $v^2 f(v)$ is recognized as the Maxwell-Boltzmann distribution at temperature T.

3.2.2 Determination of Velocity Dependent Annihilation Rate

For a positron velocity distribution of the form 3-3 the experimentally determined annihilation rate at temperature T is related to $\nu_a(v)$ by

$$\lambda(T) = \frac{\int_0^\infty \nu_a(v) v^2 e^{-\frac{mv^2}{2kT}} dv}{\left(\frac{k}{m}\right)^{\frac{3}{2}} \sqrt{\frac{\pi}{2}}\, T^{\frac{3}{2}}}. \qquad 3\text{-}4$$

If in 3-4 the experimental values of the annihilation rate are fitted by the functional form of 2-13, that is by

$$\frac{\lambda}{D} = aT^b \text{ sec}^{-1} \text{ amagat}^{-1}, \qquad 3\text{-}5$$

then the solution of 3-4 for $\lambda_a(v)$ is readily obtained analytically (Appendix E) and is given by

$$\lambda_a(v) = \frac{a\sqrt{\pi}}{2\Gamma\left(\frac{3}{2}+b\right)}\left(\frac{m}{2k}\right)^b v^{2b} \text{ sec}^{-1} \text{ amagat}^{-1} \qquad 3\text{-}6$$

where a, b are the best fit values to 3-5

m = mass of positron

k = Boltzmann's constant.

Hence from the experimental data $\lambda_a(v)$ can be determined over the velocity range encountered in the experiment. The result is model-independent but does depend on the assumptions that the annihilation rate does not affect the positron velocity distribution (Section 4.5.2.1) and that the data can be adequately represented by the form of 2-13 over the velocity range involved. Using the results of Section 2.3.3.1 for a and b,

$$\lambda_a(v) = 1.195v^{-.480} \text{ sec}^{-1} \text{ amagat}^{-1}. \qquad 3\text{-}7$$

The error in $\lambda_a(v)$ is determined using 2-10 and is therefore velocity dependent. The result (Equation 3-7) with its associated errors (Section 2.3.3.1) is displayed in Figure 22 where for comparison various theoretical results are also displayed. It is seen that the curves of Falk et al. (1965) and Montgomery and LaBahn (3p-d) (1970) most closely reproduce the experimentally derived velocity dependence. The curve of Falk et al. (1965) was not, however, the result of a theoretical calculation but was derived from a semi-empirical fit of lifetime spectra.

3.3 Calculation of Velocity Dependent Momentum-Transfer Cross-Section

3.3.1 Thermalized Positron Velocity Distribution with Electric Field

Again, the approximation is made that the annihilations do not affect

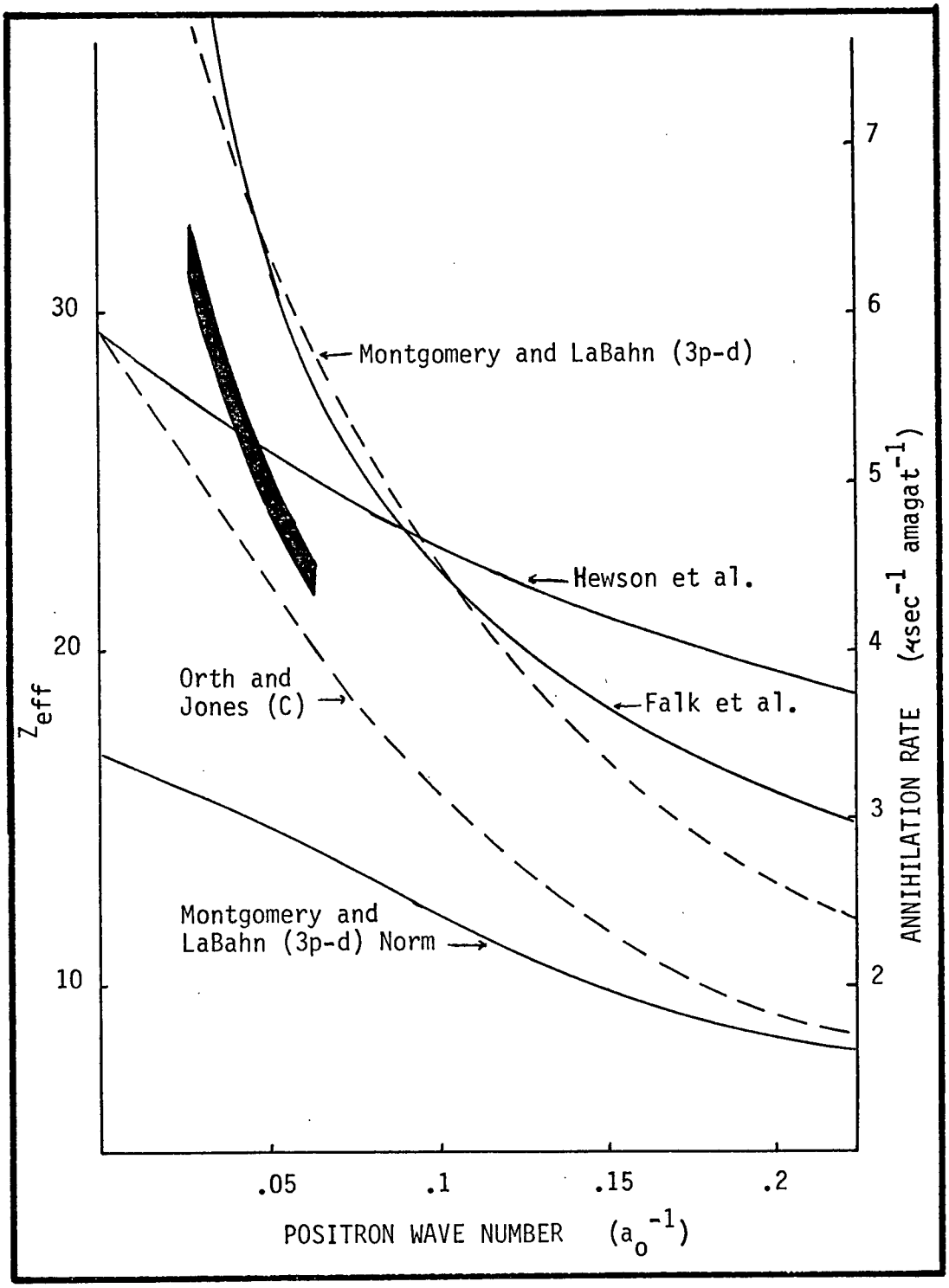

Figure 22 Velocity Dependence of Annihilation Rate

the shape of the positron velocity distribution. Hence the steady state distribution is of the form $v^2 f$ with f given by 3-2. The validity of this approximation is checked in Section 4.5.2.2.

3.3.2 Determination of Momentum-Transfer Cross-Section

3.3.2.1 Comparison of Electric Field and Temperature Results

Previous workers (Orth and Jones (1969b)) derived a value for the momentum-transfer cross-section ($\sigma_d = 39\pi a_o^2$) at v = 0.045 atomic units ($e^2/\hbar$) by comparing the relative effects of temperature and electric field at room temperature. An obvious extension of this procedure involves comparison of electric field effects at various temperatures.

3.3.2.2 Method of Determination

The momentum-transfer cross-section calculation of Orth and Jones (1969b) was based upon the assumption that the momentum-transfer rate was essentially constant over the positron velocity distribution. This restriction is unnecessarily stringent. It is only necessary for the method described here to require that the momentum-transfer rate, $\nu_d(v)$, be adequately represented, over the velocity range of interest, by the parameterization $\nu_d(v) = Av^B \text{ sec}^{-1} \text{ amagat}^{-1}$ 3-8

The analysis technique used involves consideration of the effect of electric fields in the limit of zero field and thus the rate of change of the theoretical annihilation rate (Equation 3-1) with respect to the square of the electric field at E = 0 is calculated. That is,

$$\left.\frac{\partial\left(\frac{\lambda}{N}\right)}{\partial\left(\frac{E}{N}\right)^2}\right|_{E=0} = \frac{\partial}{\partial\left(\frac{E}{N}\right)^2}\left(\frac{\int_0^\infty \nu_a(v) v^2 f(v)\,dv}{\int_0^\infty v^2 f(v)\,dv}\right)\Bigg|_{E=0}$$

where $f(v)$ is given by 3-2.

This expression can be analytically evaluated using 3-7 and 3-8, yielding the result (Appendix D)

$$\left.\frac{\partial\left(\frac{\lambda}{D}\right)}{\partial\left(\frac{E}{D}\right)^2}\right|_{E=0} = \frac{2e^2}{3\mu k^2 T^2}\frac{S}{\pi A^2(1-B)}\left(\frac{2kT}{m}\right)^{1-B-\frac{R}{2}} \times\left(\frac{\sqrt{\pi}}{2}\Gamma\left(\frac{5}{2}-B-\frac{R}{2}\right)-\Gamma\left(\frac{3}{2}-\frac{R}{2}\right)\Gamma\left(\frac{5}{2}-B\right)\right) \quad 3\text{-}9$$

where A, B are the parameters defined by 3-8

S, R are the parameters from $\nu_a(v) = Sv^{-R}$ of 3-7

e = charge of positron

T = temperature (K)

k = Boltzmann's constant

μ = reduced mass = $\frac{m}{M}$

m = mass of positron

M = mass of host gas atom.

This function (Equation 3-9) when fitted to the experimental results of Section 2.3.3.2 yields the best values and errors of the parameters A and B and thus the magnitude and velocity dependence of $\nu_d(v)$. The momentum-transfer cross-section, $\sigma_d(v)$, is thus given by

$$\sigma_d(v) = \frac{\nu_d(v)}{Nv} \quad 3\text{-}10$$

where N is the number density of atoms.

3.3.2.3 Evaluation of Velocity Dependence

The experimental values of $\partial(\lambda/D)/\partial(E/D)^2$ at E = 0 used in the fit of 3-9 are the a_1 listed in Table III. A plot of these values

as a function of temperature together with the corresponding maximum likelihood best fit is given in Figure 23. The best fit parameters to 3-9 are

$$A = (2.11 \pm 1.43) \times 10^{11}$$
$$B = -.49 \pm .24 \qquad 3\text{-}11$$

for v of 3-9 in atomic units ($e^2/\hbar$).

The rather large errors on these parameters are a direct result of the very strong correlation between them. The likelihood contour plot shown in Figure 24 gives visual evidence of the degree of this correlation. It is evident that although the range of uncertainty in either A or B is large the combined error applicable to σ_d is much less. The error matrix characterizing this fitting procedure is given in Table IV.

TABLE IV

Error Matrix Resulting from Fit to Equation 3-9

	A	B
A	2.032	.3344
B	.3344	.0553

The momentum-transfer cross-section given by 3-10 can now be written

$$\sigma_d(v) = \frac{Av^B}{(5.171 \times 10^{11})v} \pi a_o^2 \qquad 3\text{-}12$$

where v is in atomic units

and A, B are given in 3-11.

The uncertainty in $\sigma_d(v)$ is velocity dependent since the errors

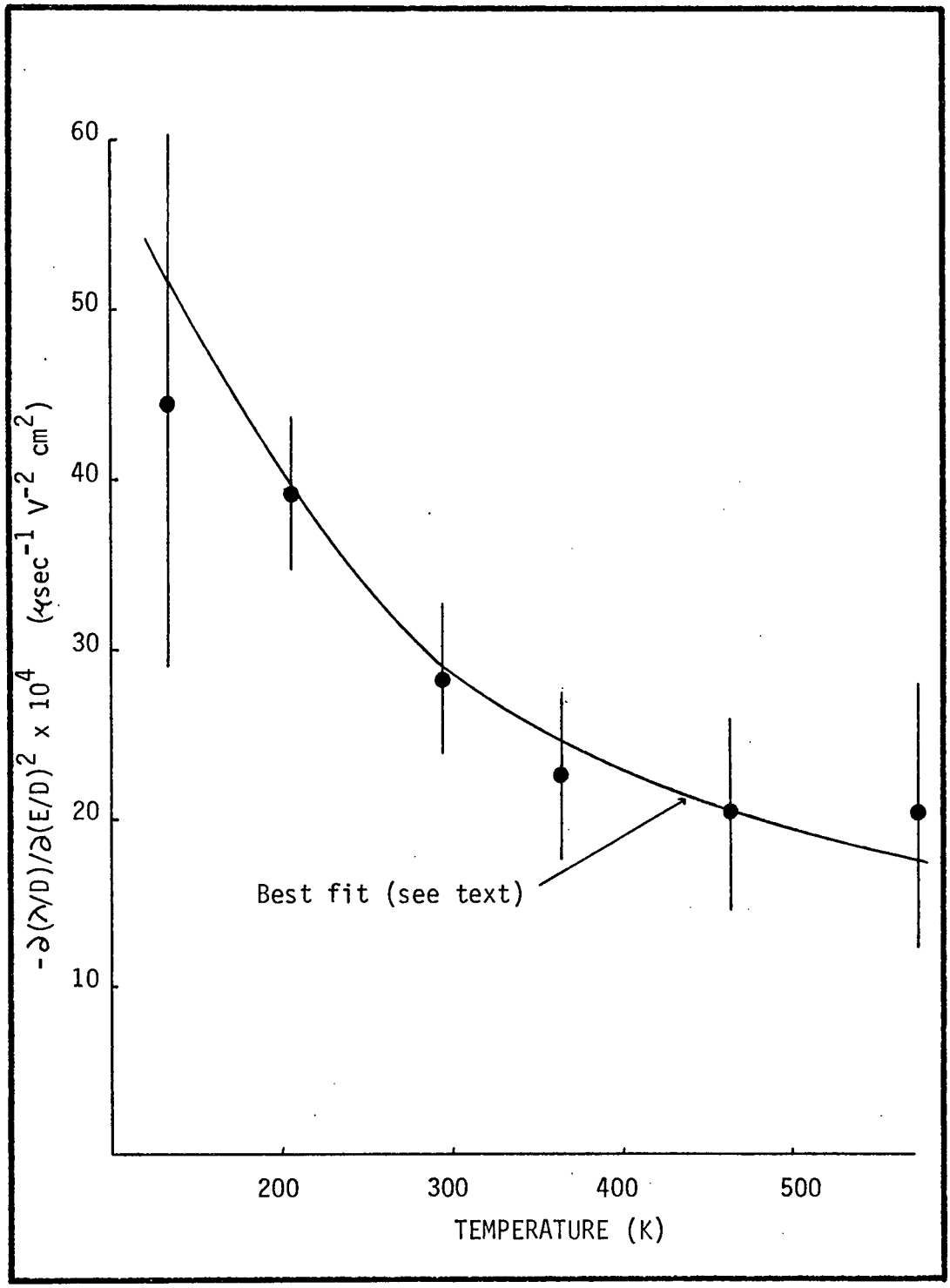

Figure 23 Temperature Dependence of $\partial(\lambda/D)/\partial(E/D)^2$

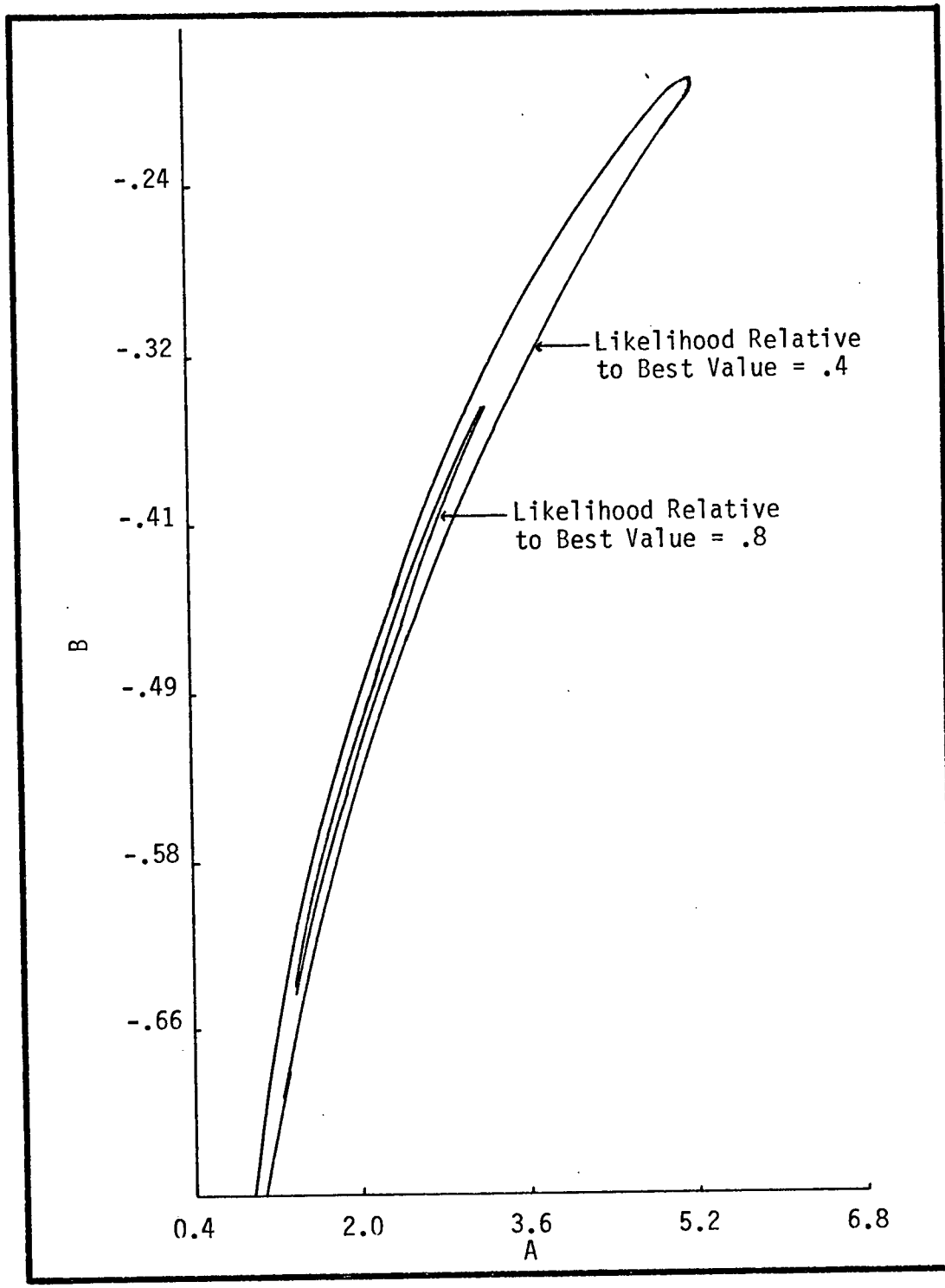

Figure 24 Likelihood Contour of Parameters from Fitting $\partial(\lambda/D)/\partial(E/D)^2$ as a Function of Temperature

are calculated using 2-10. In addition to these statistical errors resulting from the fit to 3-9 there is additional uncertainty from the errors in S and R used in 3-9. These errors reflect the uncertainty in the fitting procedure to the temperature results of Section 2.3.3.1. Again the errors in a and b of 2-13 are strongly correlated and the degree of correlation is demonstrated in Figure 25. Since the extremities in the allowable range for the parameters a and b are at points X and Y, the function 3-9 was fitted for A and B using the values of S and R corresponding to these points. The uncertainty in $\sigma_d(v)$ was then taken as the largest of the deviations between the best value, $\sigma_d^*(v)$, and the values obtained from the calculation of $\sigma_d^X(v)$ and $\sigma_d^Y(v)$ and the corresponding range of uncertainty in each of these results. The best value, $\sigma_d^*(v)$, and the resulting uncertainty is shown in Figure 26.

The errors as calculated from 2-10 depend upon the assumption that the likelihood space is gaussian in the region of its maximum. The validity of this assumption was checked for the fit to 3-5 and is demonstrated in Figure 27. It can be seen that the likelihood function closely approximates a gaussian for the parameter B but is somewhat skew for the parameter A. In order to check the effect this might have on the uncertainty in $\sigma_d(v)$ the values of $\sigma_d(v)$ at points A_1 and A_2 were calculated. These points enclose an area of roughly 68% of the skew curve and therefore are analogous to the definition of error for the gaussian case. The values B_1 and B_2 used to find $\sigma_d(v)$ were those which maximized the likelihood at A_1 and A_2. It is evident that the results, shown in Figure 26 and labelled 1 and 2, are within the

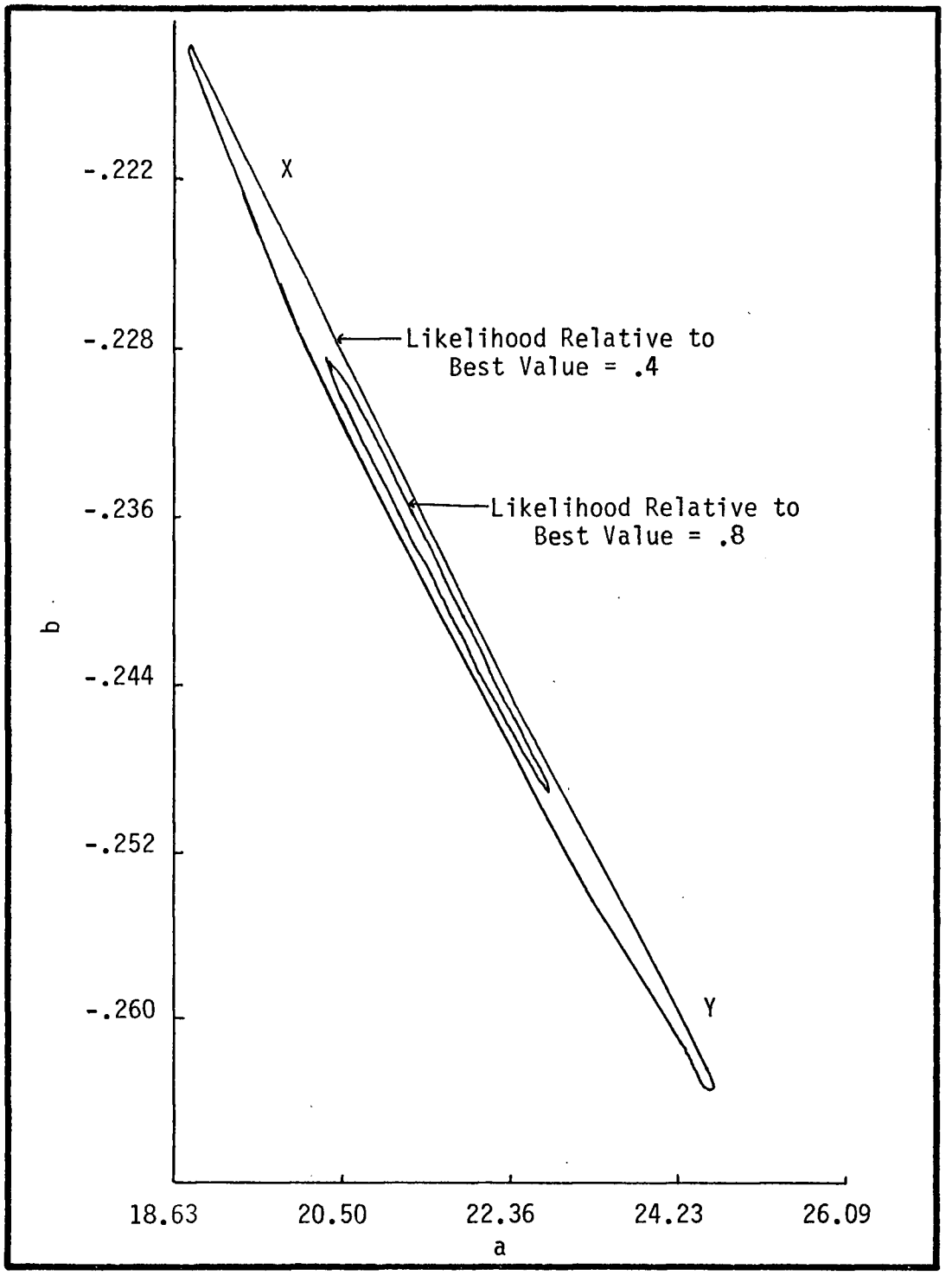

Figure 25 Likelihood Contour of Parameters from Fitting λ/D as a Function of Temperature

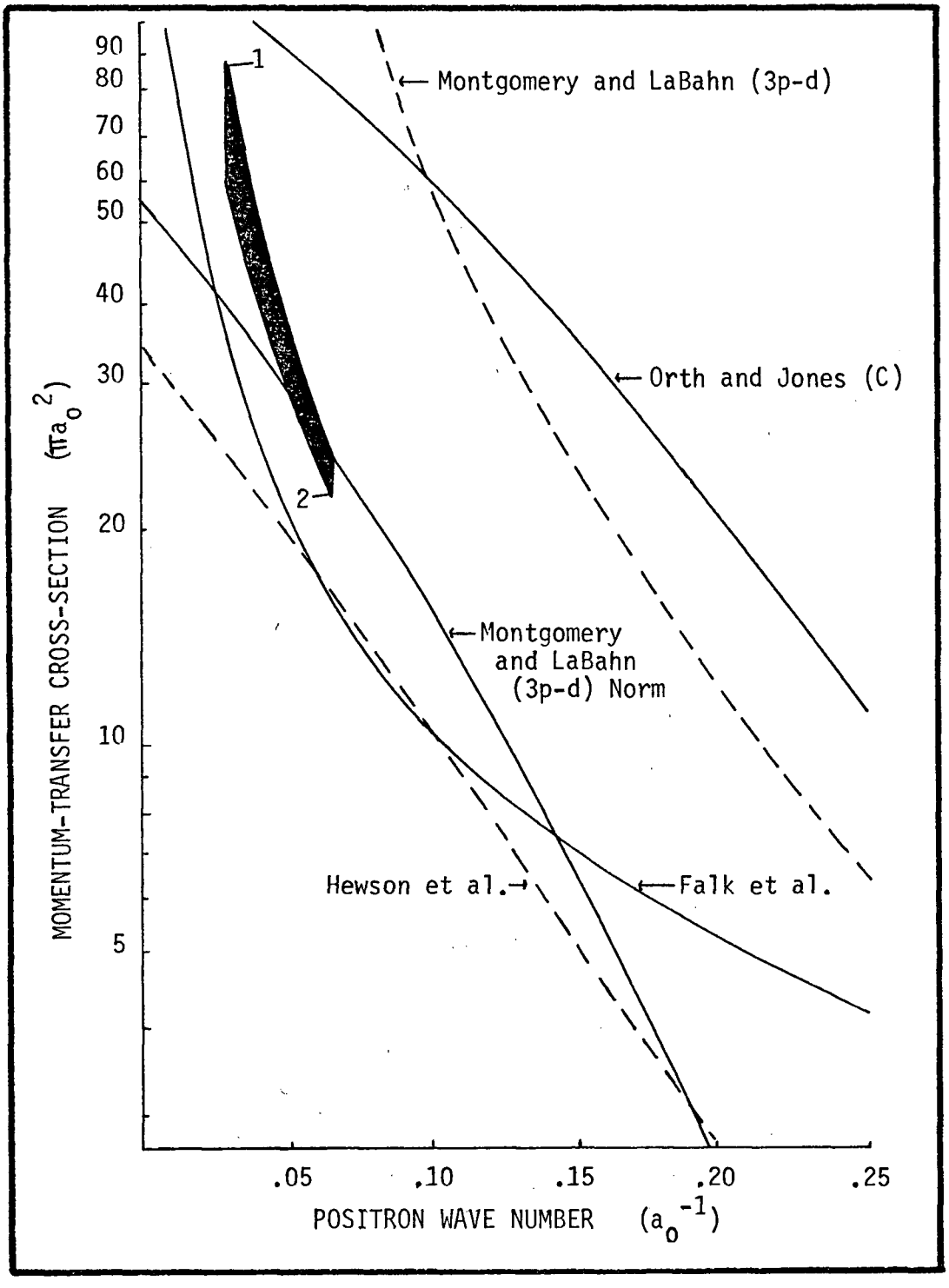

Figure 26 Velocity Dependence of Momentum-Transfer Cross-Section

Experimental result is darkened area.

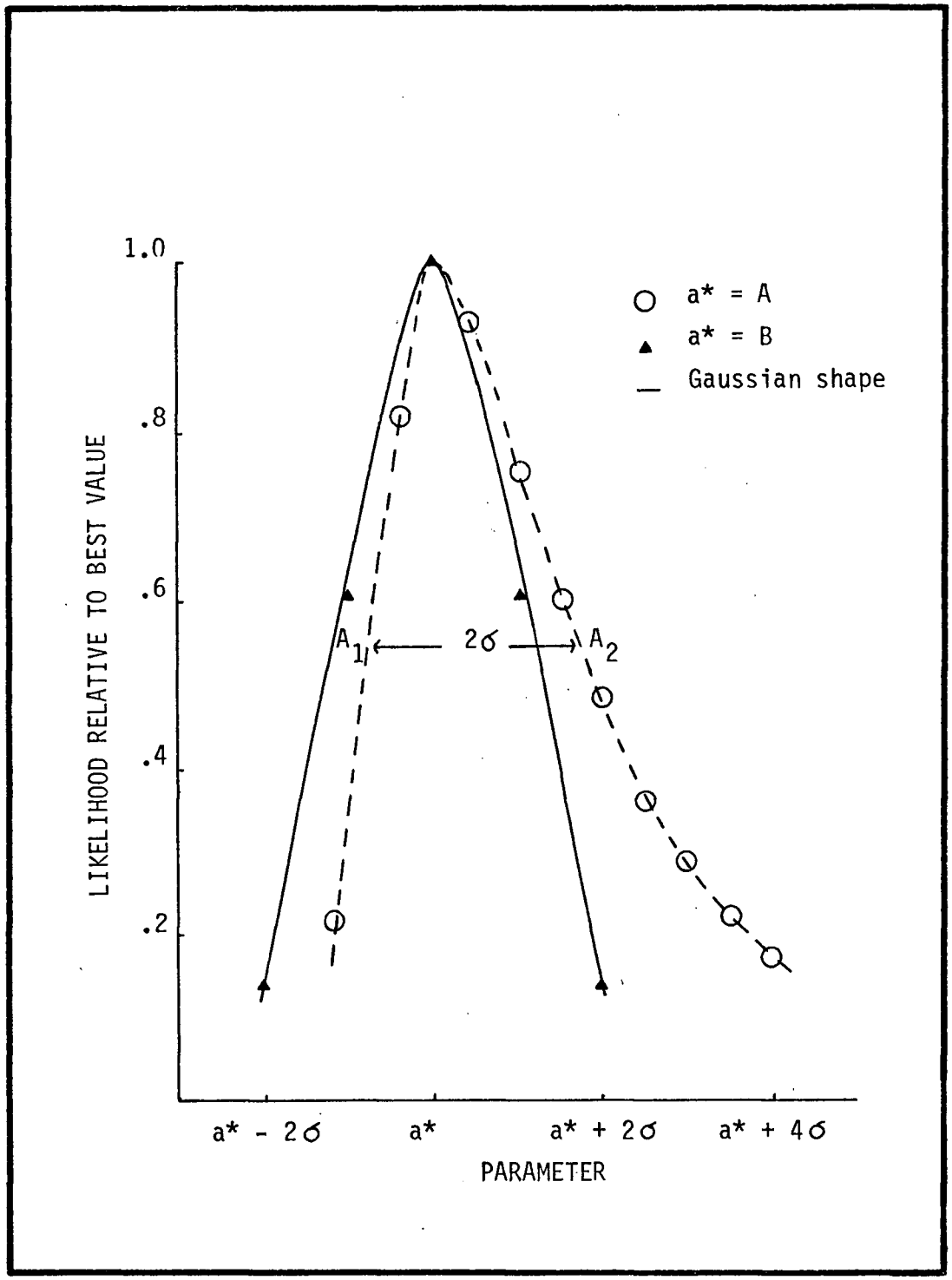

Figure 27 Dependence of the Likelihood Function on Parameters Involved in Fit of $\partial(\lambda/D)/\partial(E/D)^2$ versus Temperature

One parameter was varied while the other was held at its best value.

errors as quoted. From this it can be assumed that the effects of deviation from the gaussian shapes of the likelihood function for parameter A can be neglected.

For comparison, the results of published theoretical estimates are also displayed in Figure 26.

3.4 Velocity Dependence of Orthopositronium Quenching Rate

The orthopositronium velocity distribution is presumed to be that of a Maxwell-Boltzmann distribution at temperature T. No change in the distribution occurs when electric fields are applied since orthopositronium is electrically neutral.

Since no change in the quenching rate is observed as the temperature is varied, the quenching rate over the velocity region corresponding to the temperature extremes is constant, at least within the errors shown in Figure 12.

CHAPTER FOUR

DISCUSSION OF RESULTS

4.1 Annihilation Rate Dependence on Density

4.1.1 Theoretical Discussion

The assumption that has been made throughout this thesis is that the positron interacts with only one atom at a time and that the annihilation and scattering rates are therefore linearly dependent upon density. Thus the experimental annihilation rate, $\lambda(T)$, is

$$\lambda = A_1 D.$$

If such was not the case, for example at very high densities or low temperatures, then clearly λ/D is no longer density independent and the analysis of Chapters Two and Three is invalid.

4.1.2 Experimental Evidence

Near room temperature there is good experimental evidence for an annihilation rate linearly dependent upon density up to 50 amagats (Tao (1970)). Orth (1966) showed some evidence of non-linearity at densities greater than 20 amagats but these probably arose from systematic errors in the analysis techniques.

A non-linearity in the positron annihilation rate in argon at high density (greater than 20 amagats) and low temperature (less than 180 K) has been reported (Canter and Roellig (1971)). The extent of this non-linearity is shown in Figure 28 where λ_1/D versus D for various temperatures is plotted. The values for densities greater than 20 amagats are those quoted by Canter and Roellig and the lower density values are results from Miller (1968) and the present work. The extent

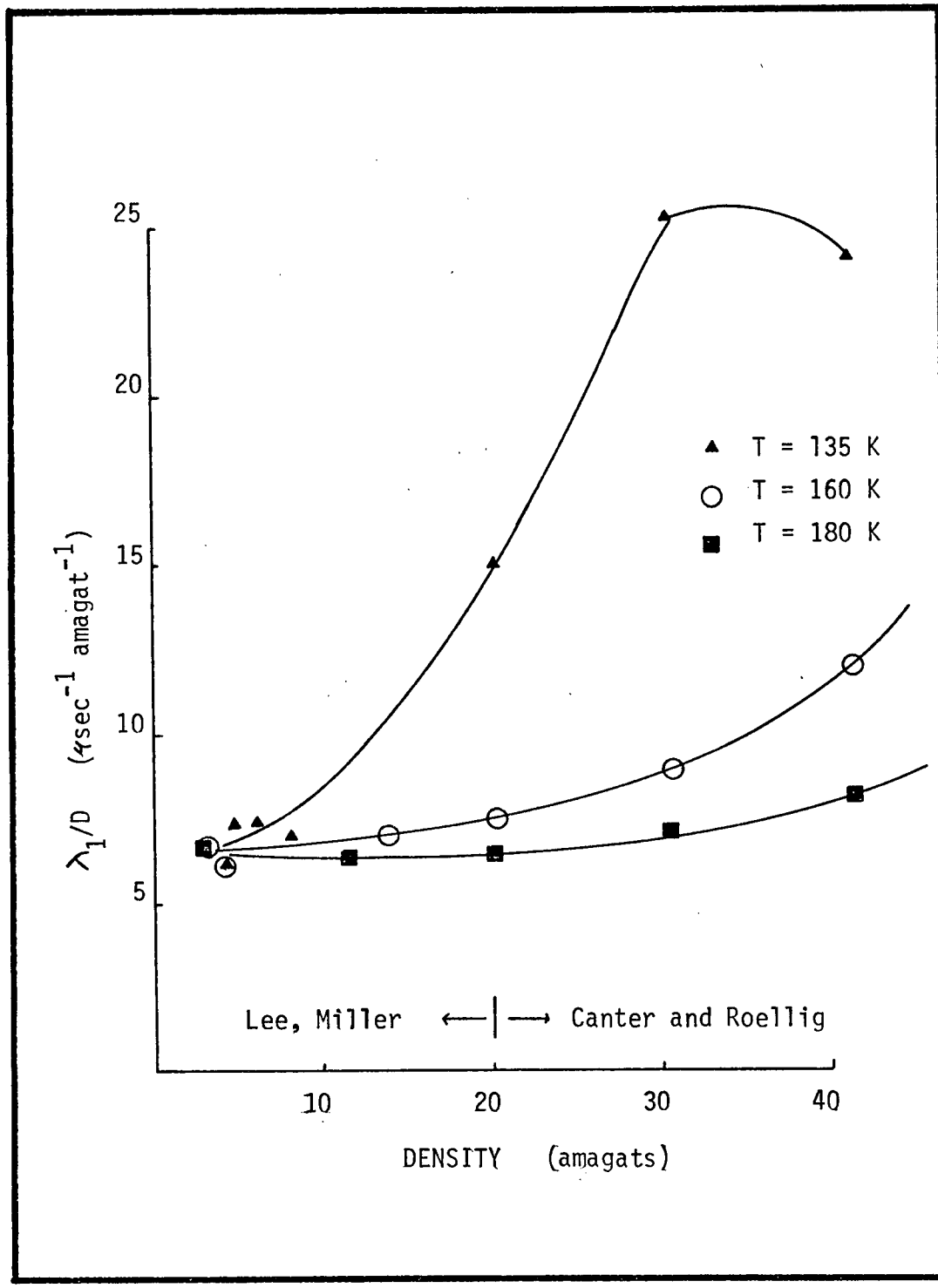

Figure 28 λ_1/D versus D for Several Temperatures

of the non-linearities for densities less than 6 amagats at 135 K and less than 15 amagats at 160 K is negligible. As these were the upper limits for the densities employed for this work the assumption of linearity is assumed to be valid.

4.2 Comparison to Published Theoretical Results

Generally the theoretical results do not reproduce the large velocity dependences observed (Figures 22 and 26). The semi-empirical fit to lifetime spectra of Falk (1965) and the (3p–d) curve of Montgomery and LaBahn are the two that most closely reproduce the velocity dependences, although not the magnitudes, of $\nu_a(v)$ and $\nu_d(v)$.

The Montgomery and LaBahn (3p–d) result is derived from a polarized orbital calculation (Temkin (1957), Temkin and Lamkin (1961)) which approximates the distortion interaction by a dipole polarization potential. The unperturbed wavefunctions were taken to be the Hartree-Fock wavefunctions of argon. The correction which accounts for the distortion was calculated using perturbation theory to first order. The label (3p–d) is a designation of the perturbed orbital components considered. For argon the (3p–d) component calculated in this fashion was found to give too high a value for the theoretical polarizability so was normalized to give the experimental polarizability and labeled (3p–d) Norm. Although these two results, (3p–d) and (3p–d) Norm, were found to give better agreement with experiment than other components, (3p–s) and (3s–p), this agreement is still poor (Figure 31).

A semi-phenomenological model of Hewson et al. (1971) gives reasonable agreement with electric field results at room temperature (Figure 31) but does not reproduce the temperature dependence (Figure 30). In

this work the effect of the positron on a Thomas-Fermi model of the atom is calculated. Increased electron density or enhancement, effective charge, and effective mass are calculated and used to predict the experimental dependencies. The ability of a theoretical model to give good agreement with electric field effects at room temperature but to fail completely to reproduce the correct velocity dependences of the individual cross-sections is well demonstrated by this example.

Other results (Orth and Jones (1969a)) used a Hartree-Fock potential and an empirical polarization potential, a combination which had been used in fitting the electron-argon case (Holtzmark (1929), Kivel (1959)). The velocity dependence arising from this method is too small. This is probably due to neglect of positron-electron correlations near or inside the atom.

4.3 Modified Effective Range Theory

4.3.1 Description

Effective range theory describes the scattering and momentum-transfer cross-sections in terms of two parameters, the scattering length, A, and the effective range, r_o. This approximation is valid for low energies. It is derived by expanding the phase-shifts, d_L, about a selected value of the wavenumber, k, corresponding to a low energy and then using these approximations in the standard expressions for the cross-sections. The derivation of effective range theory is discussed by Mott and Massey (1965).

Standard effective range theory requires the asymptotic value of the potential to decrease faster than $1/r^5$ (Mott and Massey (1965)). This is not the case for a $1/r^4$ polarization potential. O'Malley,

Spruch, and Rosenburg (1961) have developed a modified effective range theory that takes into account the $1/r^4$ dependence explicitly. For the case of scattering of a charged particle by a neutral polarizable system (O'Malley (1963)) the result is

$$\sigma_d = 4\left(A^2 + \frac{8}{3a_o}A^2\alpha k^2 \ln(ka_o) + \frac{4}{5a_o}A\alpha k + Ck^2 + \ldots\right) \qquad 4\text{–}1$$

where σ_d is in units of πa_o^2

A is in units of a_o where A is the zeroth order scattering length

k is in units of a_o^{-1}

α is in units of a_o^3 where α is the polarizability

C depends upon both the first order scattering length and the zeroth order effective range (r_o)

A and C are parameters to be determined from experiment.

This expression differs from that of standard effective range theory in that terms in k and $k^2 \ln k$ are present.

This formula, 4–1, is based upon the assumption that there is no permanent dipole distortion of the target atom, low incident energy (small k), and only single channel elastic scattering. It does not hold for bound state formation (Section 4.1.2). This formula is valid for values of k such that the appropriate terms in the phase shift expansions are small. In particular (O'Malley (1963))

$$\frac{\pi\alpha k^2}{3} \ll 1 \quad \text{or} \quad k \ll .29\, a_o^{-1} \text{ for argon.} \qquad 4\text{–}2$$

4.3.2 Effect of Bound State

The existence of a weakly bound state requires significant modification

to 4-1. In fact, the usual effective range formula is applicable for a bound state system (O'Malley et al. (1961)). Taking the expansion about the energy of the bound state rather than zero energy, the approximate solution for low energies is

$$\sigma_d = 4(A'^2 + C'k^2 + \ldots) \qquad 4\text{-}3$$

where σ_d is in πa_o^2

A' and C' are again determined by experiment.

For a bound state of energy, E_γ, such that $\gamma^2 = -2mE_\gamma/\hbar^2$, the coefficients A' and C' for the momentum-transfer cross-section are both dependent upon γ and the zeroth and first order (L = 0, L = 1) scattering lengths and effective ranges in such a manner that a value for γ, the scattering length, or the effective range cannot be deduced from knowledge only of the A' and C' values (O'Malley et al. (1962)). It is interesting that a similar situation characterizes the modified theory of 4-1. The coefficient A is the zeroth order scattering length, but C depends on the zeroth order effective range and the first order scattering length, A_1. Therefore the effective range cannot be obtained from knowledge of A and C. Only for the total scattering cross-section expansions (rather than momentum-transfer cross-sections) is the k^2 coefficient unambiguously related to the zeroth order effective range (O'Malley et al. (1961)).

4.3.3 Calculation of Parameters from Results

Values for the coefficients in 4-1 and 4-3 were obtained by a maximum likelihood fit to the momentum-transfer cross-section of Figure 26. The results of these fits and the chi-squared goodness-of-fit are shown in Table V. The best chi-squared was attained from the fitting

of 4-1, the modified effective range theory. However, as Figure 29 indicates, there is little difference in the two curves for $\sigma_d(v)$ in the region of the experimental values.

TABLE V

Values of Effective Range Parameters

	A (a_o)	C (a_o^4)	Chi-Squared Probability
Modified Effective Range	$-4.38 \pm .16$	181 ± 217	.59
Standard Effective Range	$-3.89 \pm .15$	-2292 ± 348	.35

The standard deviations in Table V are statistical. The actual uncertainty is larger since the assumed shape ($\nu_d = Av^B$) is different from the shape predicted by the modified E.R.T. From consideration of the cross-section at v = 0 an estimated value for the zeroth order scattering length is $A = -4.4 \pm .5\ a_o$. This is significantly larger in magnitude than the corresponding result for electrons, $A_e = -1.70\ a_o$ (O'Malley (1963)).

4.4 Positron-Argon Complexes

If a bound state, as previously mentioned in the discussion of effective range theory, exists it would significantly enhance the positron annihilation rate at low velocities. Canter and Roellig (1971) postulate the existence of a positron-argon complex, which is stable at low temperatures and high densities, in order to explain the very high annihilation

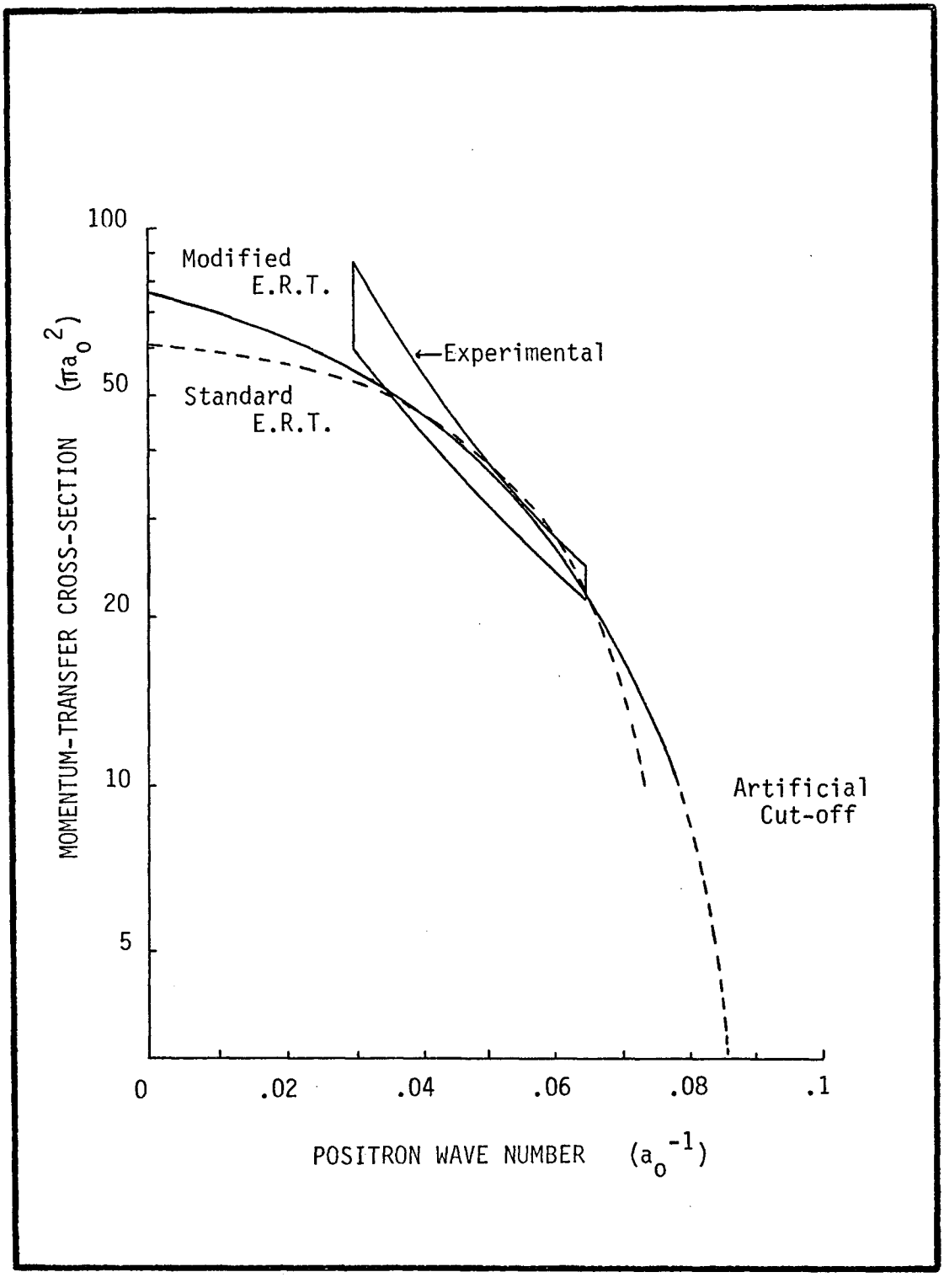

Figure 29 Effective Range Fits to Experimentally Obtained Momentum-Transfer Cross-Section

rates obtained. It is not clear, however, if such effects could not also be due to interactions of the positron with more than one atom.

Resonance scattering (Paul and Smith (1970)) could also account for an increased annihilation rate. However, such a resonance would be expected to be above thermal energies and therefore should have the effect of increasing the annihilation rate at higher temperatures and electric fields. These effects are not observed.

4.5 Numerical Solution of Diffusion Equation

4.5.1 Technique of Solution

The numerical methods employed to solve the diffusion equation (Equation 1-1) were those developed by Orth (1966). This iterative method assumes the zeroth order solution to be that of Equation 1-4, that is

$$f_0(v) = C\exp\left(-\int_0^v \frac{v'}{\left(\frac{a^2}{3\nu_d(v')^2} + \frac{kT}{m}\right)}dv'\right). \qquad 4\text{-}4$$

The zeroth order solution for λ is then given as in 1-2

$$\lambda_0 = \int_0^\infty \nu_a(v)v^2 f_0 dv. \qquad 4\text{-}5$$

This expression, using the appropriate $\nu_d(v)$ and $\nu_a(v)$, was evaluated using eight-point gaussian integration. The initial values obtained, $f_0(v)$ and λ_0, were then used in the right hand side of Equation 1-3 which was solved for the next approximation, $f_1(v)$. Hence

$$f_1(v) = f_0(v)\left(\gamma + \int_0^v \frac{g(v')}{f_0(v')}dv'\right) \qquad 4\text{-}6$$

where

$$g(v) = \frac{4\nu_d(v)}{\left(\frac{a^2}{3\nu_d(v)^2} + \frac{kT}{m}\right)} \int_0^v (\nu_a(v) - \lambda_0(v'))v'^2 f_0(v')dv'.$$

The constant γ is required since, in general, the limit $v \to 0$ of $f_1(v)/f_0(v)$ is not unity. This constant was evaluated by requiring the integral of $f_1(v)$ and $f_0(v)$ to be normalized. In a similar manner any approximation $f_{j+1}(v)$ can be evaluated in terms of $f_j(v)$ and λ_j. λ_j is calculated, as indicated for zero order, by 4-5. Numerical solution of 4-6 was carried out using Simpson's rule integral techniques. In most cases the iterative method described converged within four iterations.

4.5.2 Use in Consistency Tests

The numerical solution of the diffusion equation does not involve any approximations about the shape of the distribution nor does it neglect the effect of annihilations on this shape. Throughout the analysis of Chapters Two and Three the explicit assumption was made that the effect of the annihilations was negligible. If such is indeed the case, numerical solution of the diffusion equation using the derived values of $\nu_a(v)$ and $\nu_d(v)$ should reproduce the experimental lifetime dependences. On the other hand, an inconsistency at this point would indicate that the region of applicability of the assumptions implicit in the analytic treatment was exceeded.

4.5.2.1 Application to Annihilation Rate

The temperature dependence of the annihilation rate as determined from the numerical solution of the diffusion equation using $\nu_a(v)$ from 3-7 is shown in Figure 30. The agreement between this result and the best fit to the temperature results as given by 2-13 is excellent. This agreement confirms the validity of the assumption that the effect

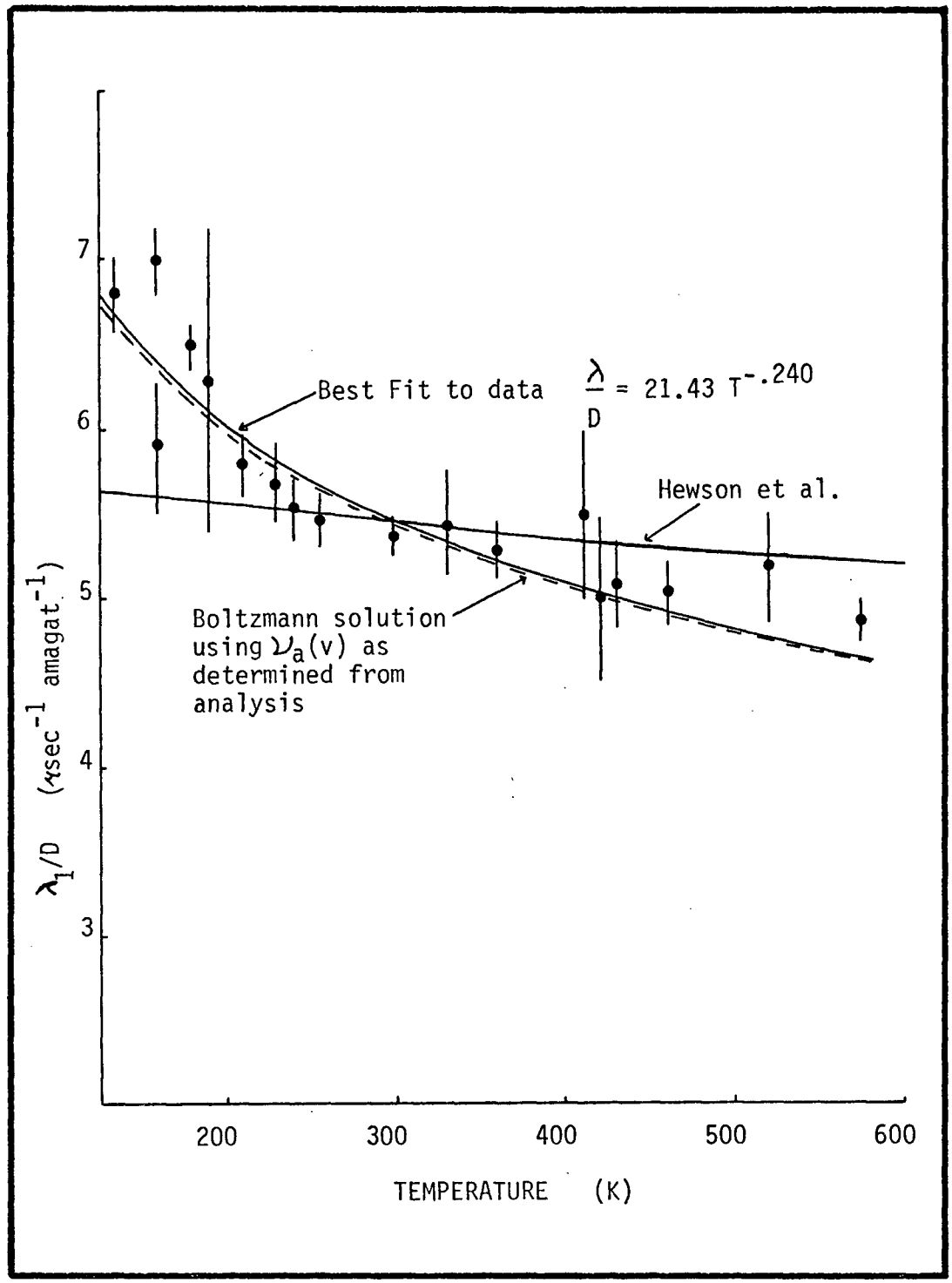

Figure 30 Temperature Dependence of Direct Annihilation Rate as Determined from Boltzmann Solution

Experimental values are shown.

of annihilations on the shape of the velocity distribution is negligible for the case of zero electric field.

4.5.2.2 Application to Momentum-Transfer Cross-Section

The room temperature electric field dependence of the positron annihilation rate as calculated by the diffusion equation is given in Figure 31. The dependence was calculated for both the $\nu_d(v)$ of 3-8 and 3-11 and the modified effective range expansion for $\sigma_d(v)$ given by 4-2 and Table V. For the modified effective range theory a cut-off was imposed to prevent $\sigma_d(v)$ from going negative for $k > .10\ a_o^{-1}$. This value (illustrated in Figure 29) was chosen to be $\sigma_d = 10\pi a_o^2$ since this gave best agreement with the experimental results.

The excellent agreement with experiment for values of E/D less than 30 volts/cm-amagat is confirmation that the approximation used to obtain the $\nu_d(v)$ of 3-11 is valid. At these low fields the fit to experiment using the modified effective range results is not as good, probably because of the artificial cut-off employed.

Further confirmation of the adequacy of the analysis carried out in Chapter Three is obtained by comparing the values of $\partial(\lambda/D)/\partial(E/D)^2$ calculated from experiment with those deduced from solution of the diffusion equations. The value so obtained was

$$\frac{\partial\left(\frac{\lambda}{D}\right)}{\partial\left(\frac{E}{D}\right)^2} = -\ .0029\ \text{sec}^{-1}\ V^{-2}\ \text{cm}^2$$

in excellent agreement with the experimental value of $-\ .0028\ \text{sec}^{-1}\ V^{-2}\ \text{cm}^2$ (Table III).

It is therefore apparent that the values for $\nu_a(v)$ and $\nu_d(v)$

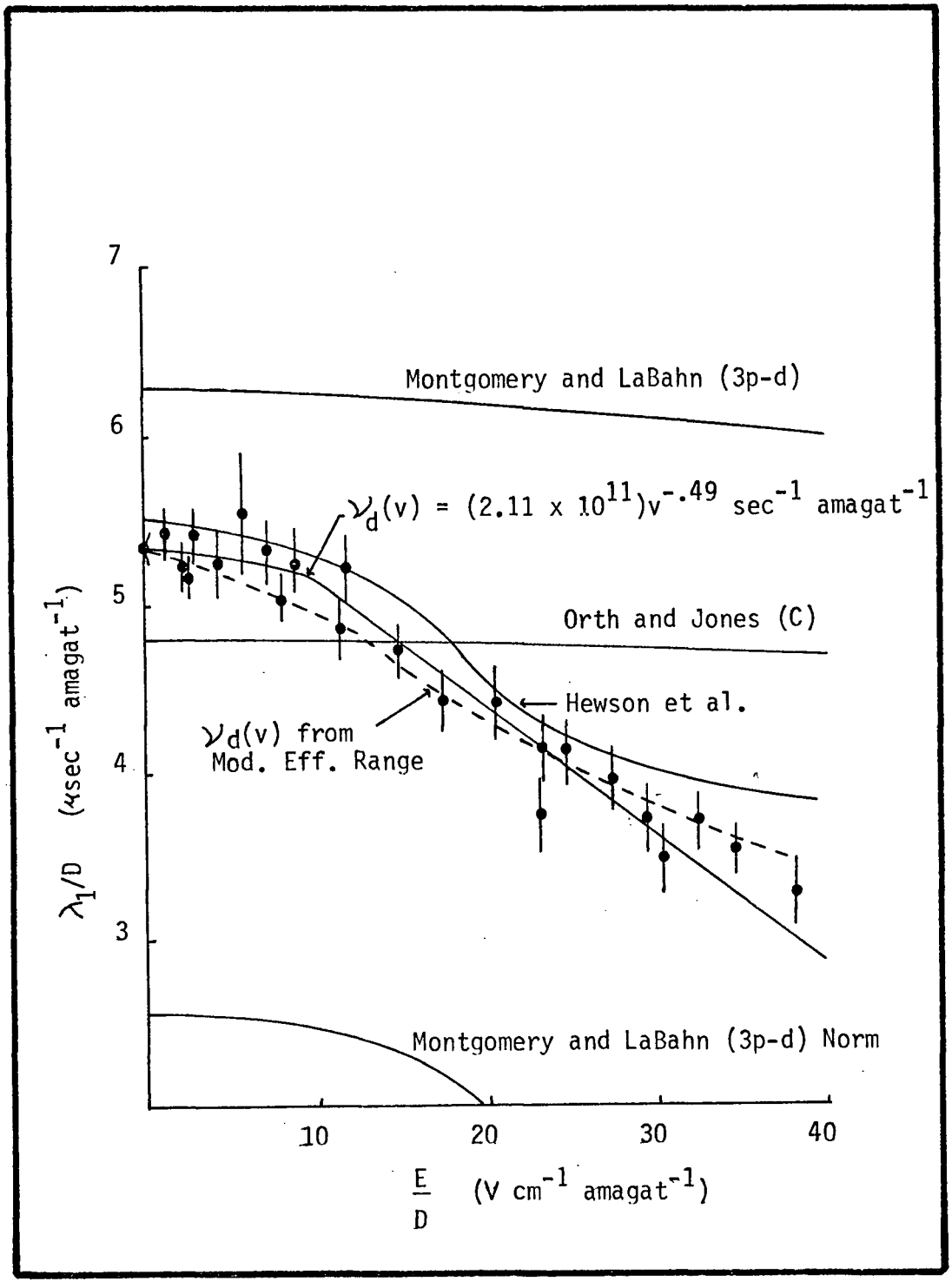

Figure 31 Electric Field Dependence of Direct Annihilation Rate at T = 298 K as Determined from Boltzmann Solution

Experimental values are shown.

obtained by the approximate analytic analysis of the experimental data do indeed yield agreement with the experimental results when an "exact" numerical solution of the relevant diffusion equation is carried out.

CHAPTER FIVE

CONCLUSIONS

5.1 Summary of Results

The velocity dependences of the annihilation rate and the momentum-transfer cross-section for free positrons in argon have been measured over the velocity range of 0.03 to 0.065 atomic units ($e^2/\hbar$) by comparing the effect on annihilation rates of electric fields and temperature changes. In terms of the mean velocity of a distribution at thermal equilibrium, this range corresponds to a temperature variation between 135 K and 573 K.

The velocity dependences of both the annihilation rate and momentum-transfer cross-section were found to be larger than that predicted by most theoretical models. This strong dependence at low velocities probably reflects strong positron-electron correlation effects during collisions between the positron and the argon atom. Further theoretical study of the effects of such correlations is now required.

No velocity dependence in the orthopositronium quenching rate was observed (within 8%) over the same temperature range.

5.2 Outline of Possible Future Studies

The experimental determination of the electric field dependence of the free positron lifetime at higher electric fields at different temperatures will contribute little in the way of additional knowledge of these cross-sections because of the difficulty of analysing such results (Section 3.1). Furthermore the available results at higher fields (Orth and Jones (1969)) are sufficient to assess the validity

at higher velocities of velocity dependences obtained from any theoretical model which reproduces the experimental velocity dependences derived in this work.

Repeating the current experiment with greater accuracy would not significantly reduce the errors in the momentum-transfer cross-section since much of this error is attributed to the assumed parameterization (which cannot completely reproduce the shape predicted by effective range theory). A less restrictive from of the cross-sections could in principle be employed but analytic solution of the pertinent equation (Section 3.1) is not possible by the techniques described. The use of numerical methods to determine the maximum likelihood fit to the data is also possible in principle but the amount of computer time required is excessive (approximately three months CPU time for the amount of data in this thesis).

Extension of the outlined technique to other noble gases would be of use only for those heavier noble gases which exhibit a significant velocity dependence in the annihilation rate as evidenced by the existence of a shoulder region (Falk and Jones (1964)). For neon and helium the shoulder is not as pronounced (Lee et al. (1969), Paul and Leung (1969), Roellig and Canter (private communication - 1971)). Therefore the velocity dependence of the annihilation rate, and consequently the electric field and temperature dependences of the positron lifetime, is small. Experimentally this makes both the measurement and analysis, in terms of velocity dependent cross-sections, extremely difficult if not impossible.

More promising is the concept of "doping" a host gas with minor

amounts of known impurities. Variation in the amount of positronium formation in a pure noble gas, an effect which can easily be measured as a function of electric field (Orth (1966), Marder et al. (1956)), depends primarily upon the momentum-transfer cross-sections of the gas atoms for positron energies near that of the positronium formation threshold (Teutsch and Hughes (1956)). For the case of impurity doping, the positron velocity distribution is determined primarily by the characteristics of the host gas. If the impurity has a low positronium formation threshold an increase in positronium formation should be observed at this threshold. Current work is being carried out using this technique (Albrecht and Jones (private communication 1971)).

There is also the possibility of analysing the non-thermalized portions of the positron annihilation lifetime spectra in order to obtain some estimate of the scattering and annihilation rates at higher velocities. Paul and Leung (1968) have made a start at this type of analysis for helium but again the difficulty of two unknowns $\nu_a(v)$ and $\nu_d(v)$ makes analysis difficult.

Development of mono-energetic positron beams would allow the determination of higher velocity cross-sections by direct measurement. Such beams are currently under development (Jaduszliwer et al. (1971)).

The non-linear density dependence of positron annihilation in argon at low temperatures is also of some interest. The cause of this effect is not understood (Canter and Roellig (1971)). Measurements are needed over a wider range of densities in order to determine the exact pressure and temperature dependence of the non-linear behavior. Experimental problems will arise, however, if densities less than four

amagats are required. The analysis of the decay spectrum into its two lifetime components becomes difficult at such a low density because the two lifetimes become comparable in magnitude.

In summary, the swarm type of experiment for positrons in argon has probably reached its limit as a source of useful information and effort should now be directed to other gases and to the determination of the momentum-transfer and annihilation cross-sections at higher velocities.

BIBLIOGRAPHY

Albrecht, R.S. and Jones, G. (1971). private communication.

Anderson, C.D. (1932). Phys. Rev. 41, 405.

Beers, R.H. and Hughes, V.W. (1968). Bull. Am. Phys. Soc. 13, 633.

Bennett, W.R., Thomas, W., Hughes, V.W. and Wu, C.S. (1961). Bull. Am. Phys. Soc. 6, 49.

Brock, R.L. and Streib, J.F. (1958). Phys. Rev. 109, 399.

Canter, K.F. and Roellig, L.O. (1971). to be published.

Deutsch, M. (1951). Phys. Rev. 83, 866.

Deutsch, M. (1953). in "Progress in Nuclear Physics" (O.R. Frisch, ed.), Vol. 3, pp. 131-158. Pergamon Press, Oxford.

Dirac, P.A.M. (1931). Proc. Roy. Soc. A126, 360.

Drachman, R.J. (1966a). Phys. Rev. 144, 25.

Drachman, R.J. (1966b). Phys. Rev. 150, 10.

Drachman, R.J. (1968). Phys. Rev. 173, 190.

Duff, B.G. and Heymann, F.F. (1963). Proc. Roy. Soc. (London) A272, 363.

Falk, W.R. (1965). Ph.D. Thesis, University of British Columbia.

Falk, W.R. and Jones, G. (1964). Can. J. Phys. 42, 1751.

Falk, W.R., Jones, G. and Orth, P.H.R. (1965). N. I. M. 33, 345.

Falk, W.R., Orth, P.H.R. and Jones, G. (1965). Phys. Rev. Letters 14, 447.

Fraser, P.A. (1968). in "Advances in Atomic and Molecular Physics" (D.R. Bates and I. Estermann, ed.), Vol. 4, pp. 63-107. Academic Press, New York.

Golden, D.E. (1966). Phys. Rev. 151, 48.

Green, J.H. and Lee, J. (1964). "Positronium Chemistry". Academic Press, New York.

Green, J.H. and Tao, S.J. (1963). J. Chem. Phys. 39, 3160.

Hewson, P.W., Jones, G. and Vogt, E.W. (1971). to be published.

Holtzmark, J. (1929). Z. Physik 55, 437.

Jaduszliver, B., Keever, W.C. and Paul, D.A.L. (1971). in "Positron Annihilation, 2nd International Conference". Queen's University, Kingston, Canada. unpublished.

Kivel, B. (1959). Phys. Rev. 116, 4.

LaBahn, R.W. and Callaway, J. (1964). Phys. Rev. 135A, 1539.

Lee, G.F. (1969). M.Sc. Thesis, University of British Columbia.

Lee, G.F., Orth, P.H.R. and Jones, G. (1969). Phys. Letters 28A, 674.

Leung, C.Y. and Paul, D.A.L. (1969). J. Phys. B 2, 1278.

Marder, S., Hughes, V.W., Wu, C.S. and Bennett, W. (1956). Phys. Rev. 103, 1258.

Massey, H.S.W. (1967). in "Positron Annihilation" (A.T. Stewart and L.O. Roellig, ed.), pp. 113-125. Academic Press, New York.

Miller, D.B. (1968). M.A.Sc. Thesis, University of British Columbia.

Miller, D.B., Orth, P.H.R. and Jones, G. (1968). Phys. Letters 27A, 649.

Mohorovicic, S. (1934). Astron. Nachr. 253, 94.

Montgomery, R.H. and LaBahn, R.W. (1970). Can. J. Phys. 48, 1288.

Mott, N.F. and Massey, H.S.W. (1965). "The Theory of Atomic Collisions" (3rd edition). Oxford Univ. Press, London and New York.

National Bureau of Standards Circular 564 (1955).

O'Malley, T.M., Spruch, L. and Rosenberg, L. (1961). J. Math. Phys. 2, 491.

O'Malley, T.M., Rosenberg, L. and Spruch, L. (1962). Phys. Rev. 125, 1300.

O'Malley, T.M. (1963). Phys. Rev. 130, 1020.

Ore, A. and Powell, J.L. (1949). Phys. Rev. 75, 1696.

Orear, J. (1958). "Notes on Statistics for Physicists", UCRL-8417 Report. Berkeley, California.

Orth, P.H.R. (1966). Ph.D. Thesis, University of British Columbia.

Orth, P.H.R., Falk, W.R. and Jones, G. (1968). N. I. M. 65, 301.

Orth, P.H.R. and Jones, G. (1966). in "Positron Annihilation" (A.T. Stewart and L.O. Roellig, ed.), pp. 401-407. Academic Press, New York.

Orth, P.H.R. and Jones, G. (1969a). Phys. Rev. 183, 7.

Orth, P.H.R. and Jones, G. (1969b). Phys. Rev. 183, 16. (There is a numerical error in this paper. The momentum-transfer cross-section obtained should be $39\pi a_o^2$.)

Osmon, P.E. (1965). Phys. Rev. 138 B, 216.

Paul, D.A.L. (1964). Proc. Phys. Soc. (London) 84, 563.

Paul, D.A.L. and Leung, C.Y. (1968). Can. J. Phys. 46, 2779.

Paul, D.A.L. and Smith, P.M. (1970). Can. J. Phys. 48, 2984.

Paul, D.A.L. and Saint-Pierre, L. (1963). Phys. Rev. Letters 11, 493.

Roellig, L.O. and Canter, K.F. (1971). private communication.

Ruark, E. (1945). Phys. Rev. 68, 278.

Stout, V.L. and Gibbon, M.D. (1955). J. A. Phys. 26, 1488.

Tao, S.J. (1970). Phys. Rev. A 1, 1257.

Tao, S.J., Bell, J. and Green, J.H. (1964). Proc. Phys. Soc. 83, 453.

Tao, S.J., Green, J.H. and Celitans, G.T. (1963). Proc. Phys. Soc. 81, 1091.

Taylor, H.E. (1968). N. I. M. 68, 160.

Temkin, A. (1957). Phys. Rev. 107, 1004.

Temkin, A. and Lamkin, J.C. (1961). Phys. Rev. 121, 788.

Thompson, D.G. (1966). Proc. Roy. Soc. A294, 160.

Teutsch, W.B. and Hughes, V.W. (1956). Phys. Rev. 103, 1266.

APPENDIX A

ELECTRONIC PILE-UP EFFECTS

High count rates have three possible effects which can influence the measured lifetime spectra (Section 2.2.3.4).

i. There may be time-slewing due to baseline shifts in a.c. coupled parts of the system.

ii. There will be an increase in the relative size of the random coincidence background.

iii. There may be a non-linearity introduced in the random background because of negative time events which are correlated.

A.1 Time-Slewing

In the electronic system used (Section 2.2.3) there was a.c. coupling between the photomultiplier and the discriminator. Time-slewing occurs if an accepted pulse triggers the discriminator while sitting on the overshoot arising from the differentiation of a previous pulse. Falk (1965) demonstrated the effectiveness of pile-up gates in removing this effect. The lack of any observable broadening of the prompt peak (the first evidence of such effects) in this experiment is attributed to the fact that pile-up gates were employed.

A.2 Random Background - Uncorrelated Coincidences

The random background due to uncorrelated coincidences is, strictly speaking, non-constant with an exponential time structure. However, for low count rates and short time scales the deviation from a constant

is negligible.

The probability of n counts per second is defined as P(n) and the probability of n counts in time t as P(n,t). If there are R counts per second on average, the probability P(n) is given by the Poisson distribution $P(n) = \frac{R^n e^{-R}}{n!}$.

Similarly, if there are Rt counts in t on average

$$P(n,t) = \frac{(Rt)^n e^{-Rt}}{n!}.$$

Hence $P(1,dt) = Rdte^{-Rdt}$.

The probability of a single count in dt when there has been no count in previous t is

$$P = P(0,t) \times P(1,dt)$$

$$P = e^{-Rt} Rdt e^{-Rdt}.$$

For small dt (dt corresponds to channel width $\approx 10^{-9}$ sec)

$$e^{-Rdt} \approx (1 - Rdt).$$

Therefore $P \approx Re^{-Rt}dt$

where terms in dt only are kept.

Hence given a start pulse the probability of the stop pulse occurring in time t to t + dt is

$$P = R_{stop} e^{-R_{stop} t} dt$$

where R_{stop} is count rate from stop side of discriminator.

For $R_{stop}t$ small this becomes

$$P = R_{stop} dt(1 - R_{stop} t + \ldots).$$

The random coincidence rate is then

$$R_{start} R_{stop} dt(1 - R_{stop} t).$$

The magnitude of this effect for the current experiment can be calculated from the observed 0.51 MeV count rate of 7500 counts/sec. The fractional effect on a 500 nsec time scale was therefore $R_{stop}t/1$

or $$\frac{7500 \times 500 \times 10^{-9}}{1} = .375 \times 10^{-5} = .38\%$$

This degree of non-constant background is small and can be neglected.

A.3 Random Background - Correlated Coincidences

The effect of correlated coincidences can be most easily seen by considering the idealized diagram of Figure 32. Since the discriminator outputs are indistinguishable regarding their origin (0.51 MeV or 1.28 MeV pulses) and since the zero time is delayed, the time-to-amplitude converter output is symmetric with respect to time as indicated. The events selected for analysis corresponding to $t > 0$ are chosen by use of the slow coincidence channel, a system which is energy sensitive.

A problem arises, however, if the deadtime of the pile-up gates is long. Consider a negative time event consisting of detection of the correlated pulses in the fast channel. For this case the slow channel is not driven since the two channels are inverted as far as energy is concerned. For long deadtimes in the pile-up gate it is possible for this event to be followed by a pair of pulses which satisfy the energy conditions in the slow channel and thereby actuate the slow coincidence circuit. This second pair may or may not be correlated. However, only the time interval between the first correlated events will be recorded for this situation. If the pile-up gate has had time to recover then a pile-up pulse is generated and such negative time events are vetoed. The length of time during which a pile-up pulse

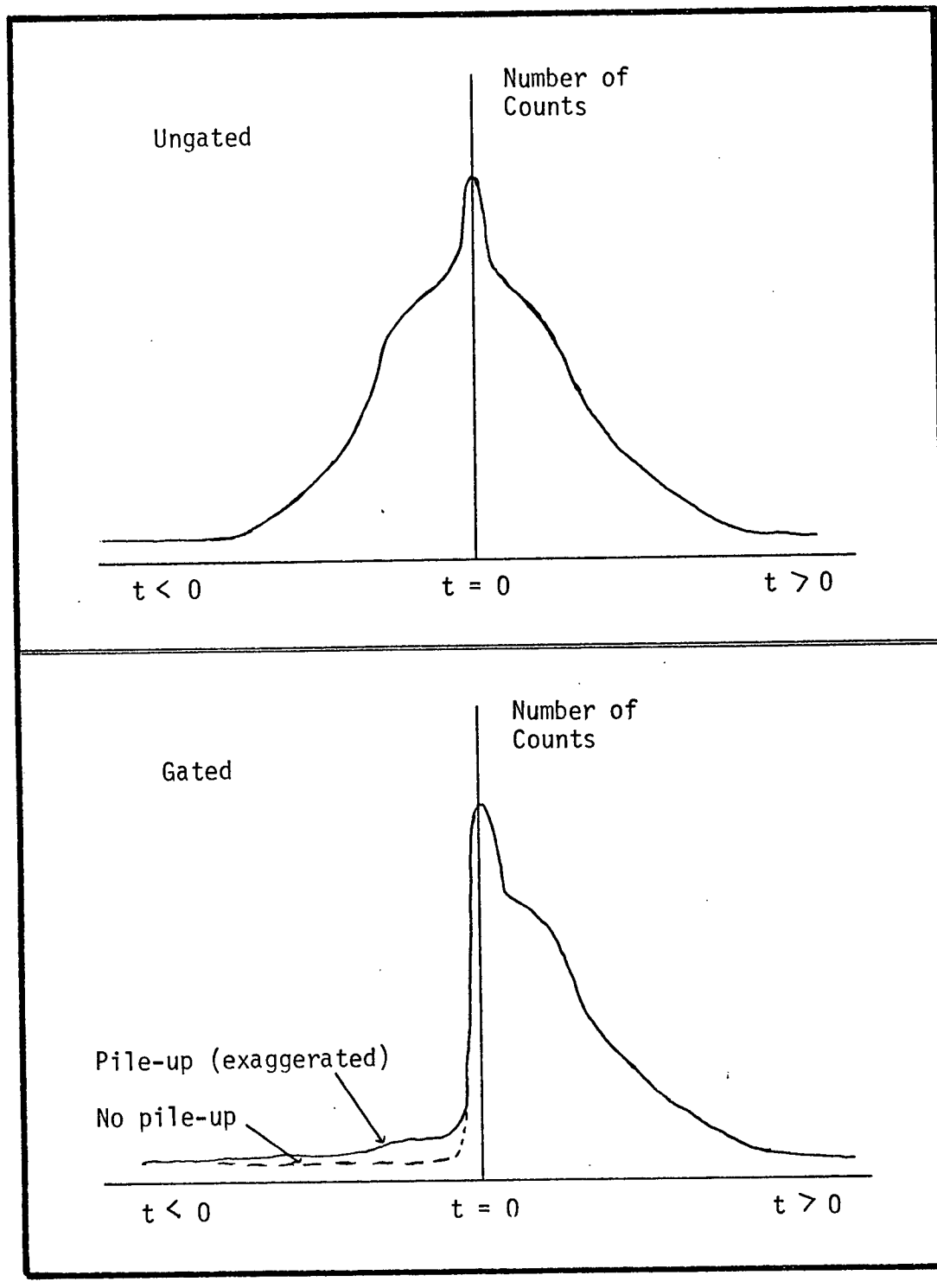

Figure 32 Schematic Diagram of Gated and Ungated Time Spectrum

is generated must, of course, be greater than the slow coincidence resolving time.

These unwanted events occur only on the negative time side, resulting in an apparent asymmetric random coincidence background about $t = 0$. Since the magnitude of the random coincidence background for the $t > 0$ region is inferred from its magnitude on the $t < 0$ region this effect can lead to serious errors.

As a consequence of this problem the pulse width and hence the deadtime of the pile-up gates was shortened by differentiating the photomultiplier output (Section 2.2.3.4). This problem could also arise when encountering excessive count rates such as would occur for discriminator settings which were in the noise region. Because the discriminators were of an updating type their output pulse width and hence the deadtime of the pile-up gates would increase.

The magnitude of such an effect can be estimated by considering the original electronic configuration in which no consideration was given to the effect of such pulse pile-ups in the slow channel. The effective deadtime was then the slow coincidence resolving time of 8 μsec. The count rates from the single-channel analysers were of the order of 5×10^3 from the 0.51 MeV channel. The probability of getting a second energy-correct event in both channels is

$$P = P_{0.51} \times P_{1.28}$$

or

$$P = N_{0.51}dt \times N_{1.28}dt$$

where dt is the effective deadtime.

Hence for this case $P \simeq 3 \times 10^{-4}$.

Since the time-to-amplitude converter ungated output rate was

170 sec^{-1} and about half of this corresponds to negative time events the count rate for "slow pile-up" events was

$$R = P\left(\frac{170}{2}\right) \text{ sec}^{-1}$$

or $$R \simeq .03 \text{ sec}^{-1}.$$

The random background rate is given by (Section A.2)

$$R_{RB} = N_{0.51}N_{1.28}(500 \text{ nsec})$$

or $$R_{RB} = 2.5 \text{ sec}^{-1}.$$

Therefore R_{RB} on negative time was approximately 1/sec. Hence the effect of the "slow pile-up" situation on the random background was

$$\frac{R}{R_{RB}} \simeq \frac{.03}{1} = 3\%.$$

This 3% effect was calculated assuming that the negative time events are uniformly distributed. In fact, since they correspond in shape to an ungated time spectrum the region near t = 0 is emphasized. Since the estimate of background is made within 25 channels of t = 0 (channels 20 to 60 for peak at 85) the effect is somewhat larger. Direct experimental verification of this shape is difficult since statistical significance would require about 1000 counts/channel in the background.

This small increase in the measured random background did manifest itself, however, in causing significant errors in the determination of the long lifetime component in the annihilation spectrum.

APPENDIX B

NUCLEAR INSTRUMENTS AND METHODS 91 (1971) 665–666; © NORTH-HOLLAND PUBLISHING CO.

ON THE FITTING OF DOUBLE EXPONENTIAL LIFETIME SPECTRA USING A MAXIMUM LIKELIHOOD TECHNIQUE

G. F. LEE and G. JONES

Physics Department, University of British Columbia, Vancouver, B.C., Canada

Received 5 October 1970

A modification of a previously presented iterative method for fitting double exponential lifetime spectra is presented. A different choice of parameters is shown to reduce the number of iterations required.

Orth et al.[1]) described an iterative maximum likelihood technique for fitting lifetime spectra consisting of two exponentials with constant background.

Thus

$$\gamma_k = \int^k [I_1 \exp(-t/\tau_1) + I_2 \exp(-t/\tau_2) + B]\mathrm{d}t$$

is the theoretical γ_k (per channel). I_1 and I_2 are the intensities, τ_1 and τ_2 are the lifetimes of the two components respectively and B is the constant background per unit channel. The integration is performed over the kth channel.

In this letter, a modification of this technique is described which reduces the number of iterations needed for convergence and in addition gives the standard deviation of the intensity-lifetime ($I\tau$) product, a quantity equal to the total number of events within one of the exponentials.

Determination of the standard deviation of this quantity normally requires manipulation of the resulting error matrix. In particular the standard deviation $\Delta(I\tau)$ associated with $I\tau$ is given by[2])

$$\Delta(I\tau)_{\mathrm{RMS}} = [I^2(H^{-1})_{\tau\tau} + 2I\tau(H^{-1})_{I\tau} + \tau^2(H^{-1})_{II}]^{\frac{1}{2}}, \quad (1)$$

where H^{-1} is the error matrix[1,2]).

Note that for uncorrelated parameters $(H^{-1})_{ij} = 0$ for $i \neq j$. In this case (1) reduces to the well known special case

$$\Delta(I\tau)_{\mathrm{RMS}} = [I^2(\Delta\tau)^2 + \tau^2(\Delta I)^2]^{\frac{1}{2}}, \quad (2)$$

since $(H^{-1})_{aa} = (\Delta a)^2$.

Since I and τ are correlated it is not sufficient to simply combine the errors in I and τ as in (2) but the full expression (1) must be evaluated.

In the modification described here, the theoretical γ_k (per channel) is of the form

$$\gamma_k = \int^k [(A_1/\tau_1)\exp(-t/\tau_1) + (A_2/\tau_2)\exp(-t/\tau_2) + B]\,\mathrm{d}t,$$

where A_1 and A_2 are the areas under each exponential (the intensity lifetime product). Otherwise the same technique as that of Orth et al.[1]) was used.

The correlation between A and τ was found to be rather less than that between I and τ. This is responsible for the reduction in the number of iterations required. The degree of correlation between two parameters can be easily seen on a contour plot of the likelihood function as shown in fig. 1. This plot is determined by varying I_1 and τ_1 (or A_1 and τ_1) with I_2(or A_2), τ_2 and B set at their optimum values. The value of the likelihood function relative to its peak value is shown. For uncorrelated parameters the contours would be elliptical with minor and major axes parallel to the coordinate axes. It can be seen that in neither case are the parameters uncorrelated, but the degree of correlation is less between A_1 and τ_1 then between I_1 and τ_1. That this results in faster convergence is demonstrated in table 1. The errors are calculated from the error matrix[1]) and convergence is defined to occur when the change in all parameters is less than 0.1% between iterations. W, the logarithmic likelihood function is a maximum at convergence. The number of iterations and hence the amount of computing necessary is re-

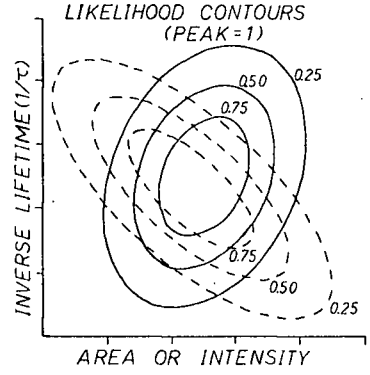

Fig. 1. Maximum likelihood contour plots for A_1 and $1/\tau_1$ (solid line) and I_1 and $1/\tau_1$ (dashed line). The remaining parameters are fixed at their optimum values.

TABLE 1

Iteration number	I_1	I_2	τ_1	τ_2	B	W	
	Analysis of spectrum fitting intensities						
0[a]	852	259	17.9	40.7	6.85	−867.9	
1	926 ± 25	220 ± 25	17.7 ± 0.5	43.6 ± 1.7	6.89 ± 0.29	−861.3	
2	943 ± 32	202 ± 27	18.0 ± 0.6	45.2 ± 2.7	6.85 ± 0.29	−860.0	
3	967 ± 24	174 ± 28	18.5 ± 0.5	47.6 ± 2.5	6.77 ± 0.29	−859.6	
4	970 ± 32	170 ± 35	18.5 ± 0.6	48.3 ± 3.7	6.75 ± 0.30	−859.6	
5	976 ± 30	164 ± 33	18.6 ± 0.6	49.0 ± 3.7	6.73 ± 0.29	−859.6	
6	977 ± 32	163 ± 35	18.7 ± 0.7	49.1 ± 3.9	6.73 ± 0.29	−859.6	C
7	977 ± 32	163 ± 35	18.7 ± 0.7	49.1 ± 3.9	6.73 ± 0.30	−859.6	C
Iteration	A_1 (× 10^2)	A_2	τ_1	τ_2	B	W	
	Analysis of spectrum fitting areas						
0	153	105	17.9	40.7	6.85	−867.9	
1	180 ± 7.0	81 ± 6.8	18.3 ± 0.5	47.2 ± 2.0	6.67 ± 0.28	−862.5	
2	179 ± 11.5	83 ± 11.1	18.5 ± 0.7	48.0 ± 3.7	6.75 ± 0.30	−859.6	
3	182 ± 11.2	80 ± 10.8	18.6 ± 0.6	49.0 ± 3.8	6.73 ± 0.30	−859.6	
4	182 ± 11.4	80 ± 10.9	18.7 ± 0.7	49.1 ± 3.9	6.73 ± 0.30	−859.6	C
5	182 ± 11.4	80 ± 10.9	18.7 ± 0.7	49.1 ± 3.9	6.73 ± 0.30	−859.6	C

[a] Iteration number 0 refers to initial estimates.

duced by the modification described by about one third.

That the correlation between I and τ in fits to lifetime spectra influence the standard deviation in the resulting estimate of the total number of events ($I\tau$) to a considerable degree is readily apparent in the example illustrated in table 1. In this case, the value obtained for the standard deviation in A_1 was 11.4×10^2. This is the same as the value obtained using (1) and the likelihood fit described by Orth et al.[1]). It differs markedly from the value (2×10^2) for the standard deviation obtained if the parameters I_1 and τ_1 are treated as if uncorrelated, and is about 30% larger than the value (8.9×10^2) obtained if the correlated values of ΔI_1 and $\Delta \tau_1$ as determined by Orth et al.[1]) are used in (2), rather than the correct expression (1).

References

[1]) P. H. R. Orth, W. R. Falk and G. Jones, Nucl. Instr. and Meth. **65** (1968) 301.

[2]) J. Orear, Notes on statistics for physicists, UCRL-8417 (1958).

APPENDIX C

DENSITY CORRECTED DATA

The following data was obtained. Where runs were disregarded or not analysed, the run number and the reason (Section 2.3.1) is given.

Run No.	Temp. (K)	Density (amagats)	E/D (V cm^{-1} $amagat^{-1}$)	λ_1 Direct Annihilation Rate (μsec^{-1})	λ_2 Orthopositronium Annihilation Rate (μsec^{-1})
63	296.16	9.94	0.0	51.6 ± 1.4	9.00 ± 0.37
64	296.16	9.68	0.0	53.1 ± 1.9	9.93 ± 0.43
65	296.16	9.25	0.0	49.9 ± 0.7	9.43 ± 0.17
66	295.96	8.91	0.0	48.9 ± 1.3	9.71 ± 0.32
67	296.16	8.78	9.0	46.1 ± 2.1	9.70 ± 0.50
68	296.66	8.65	4.6	45.4 ± 1.8	9.70 ± 0.44
69	297.66	8.51	2.3	44.7 ± 1.8	9.04 ± 0.38
70	298.56	8.44	0.0	45.4 ± 1.8	9.44 ± 0.47
71	298.46	8.36	7.1	44.5 ± 1.7	9.49 ± 0.46
72	297.16	8.15	12.0	42.7 ± 1.8	9.28 ± 0.48
73	297.16	7.93	2.5	41.1 ± 1.2	8.99 ± 0.36
74	296.86	7.84	1.3	42.8 ± 1.2	9.60 ± 0.38
75	297.26	7.75	8.1	38.9 ± 1.4	9.24 ± 0.44
76	297.46	7.64	0.0	42.0 ± 1.8	9.31 ± 0.44
77	297.16	7.49	3.0	40.7 ± 0.9	9.18 ± 0.25
78	296.36	7.34	1.1	38.8 ± 1.3	9.26 ± 0.42
79	295.76	7.13	2.9	38.2 ± 1.3	9.15 ± 0.47
80	295.16	6.76	0.0	37.8 ± 0.9	9.78 ± 0.32
81	295.46	6.20	2.6	32.5 ± 0.5	8.76 ± 0.27
82	295.56	5.76	0.0	30.7 ± 1.2	8.57 ± 0.59
83	background				
84	468.16	5.00	7.9	24.8 ± 1.9	7.81 ± 1.58
85	466.16	5.01	15.9	23.8 ± 1.2	7.40 ± 1.72

Run No.	Temp. (K)	Density (amagats)	E/D (V cm^{-1} $amagat^{-1}$)	λ_1 Direct Annihilation Rate (μsec^{-1})	λ_2 Orthopositronium Annihilation Rate (μsec^{-1})
86	464.16	5.01	3.9	24.4 ± 1.5	8.85 ± 2.47
87	464.16	5.01	11.8	23.7 ± 3.9	9.67 ± 3.48
88	463.16	4.99	19.7	21.7 ± 2.5	7.07 ± 2.84
89	463.66	4.97	0.0	25.2 ± 1.9	7.79 ± 1.65
90	462.16	4.97	23.8	19.1 ± 1.3	5.04 ± 2.70
91	459.16	4.97	31.7	19.6 ± 4.1	10.21 ± 4.20
92	chi-squared bad				
93	464.16	4.95	0.0	27.0 ± 3.2	9.33 ± 1.38
94	574.66	4.68	0.0	25.4 ± 2.0	9.41 ± 1.26
95	579.16	4.64	8.5	24.6 ± 3.1	10.31 ± 1.35
96	579.16	4.63	17.0	23.8 ± 3.1	9.56 ± 1.38
97	568.16	4.66	25.4	19.2 ± 2.5	8.56 ± 1.58
98	570.66	4.63	4.2	24.5 ± 3.7	9.61 ± 1.81
99	570.16	4.63	0.0	25.2 ± 5.4	9.88 ± 1.12
100	571.16	4.60	21.4	21.1 ± 3.0	9.38 ± 1.73
101	573.16	4.58	12.9	21.5 ± 2.1	8.26 ± 1.50
102	569.16	4.60	0.0	26.3 ± 3.8	10.97 ± 1.20
103	567.16	4.59	0.0	21.2 ± 3.9	8.18 ± 1.44
104	367.16	5.01	0.0	26.0 ± 2.2	6.90 ± 1.43
105	364.66	5.03	31.2	18.2 ± 1.3	4.02 ± 1.27
106	did not converge				
107	368.16	4.97	7.9	23.6 ± 1.7	5.67 ± 1.26
108	368.16	4.98	15.8	20.8 ± 1.5	4.78 ± 1.92
109	background				
110	364.66	5.00	19.7	20.5 ± 1.5	6.57 ± 1.40
111	did not converge				
112	electronics failure				
113	366.16	5.00	23.6	20.7 ± 2.0	8.12 ± 1.52
114	367.16	4.97	26.1	20.9 ± 1.2	8.91 ± 1.48
115	368.16	4.96	3.9	25.9 ± 3.2	9.22 ± 1.34

Run No.	Temp. (K)	Density (amagats)	E/D (V cm^{-1} $amagat^{-1}$)	λ_1 Direct Annihilation Rate (μsec^{-1})	λ_2 Orthopositronium Annihilation Rate (μsec^{-1})
116	367.16	4.92	0.0	27.8 ± 1.5	9.47 ± 0.73
117	294.16	5.16	0.0	26.5 ± 2.7	8.31 ± 1.39
118	did not converge				
119	294.16	5.10	23.2	19.0 ± 1.5	6.19 ± 2.50
120	chi-squared bad				
121	291.91	4.91	16.0	22.1 ± 2.1	8.19 ± 1.48
122	294.66	4.68	0.0	25.8 ± 4.3	8.79 ± 0.67
123	295.66	4.58	0.0	25.2 ± 2.3	8.92 ± 1.41
124	295.66	4.55	0.0	27.2 ± 3.3	10.05 ± 1.79
125	large temperature variation				
126	211.66	3.52	0.0	19.4 ± 2.9	6.19 ± 6.13
127	did not converge				
128	211.16	3.45	11.4	17.4 ± 1.5	9.54 ± 4.89
129	did not converge				
130	did not converge				
131	did not converge				
132	did not converge				
133	did not converge				
134	did not converge				
135	did not converge				
136	293.66	10.05	0.0	53.2 ± 1.3	11.07 ± 1.04
137	213.16	9.96	0.0	57.4 ± 1.9	9.69 ± 0.40
138	206.16	9.88	0.0	57.5 ± 2.9	9.83 ± 0.51
139	209.66	9.32	0.0	53.0 ± 2.6	9.06 ± 0.54
140	background				
141	background				
142	background				
143	background				
144	background				
145	background				

Run No.	Temp. (K)	Density (amagats)	E/D (V cm^{-1} $amagat^{-1}$)	λ_1 Direct Annihilation Rate (μsec^{-1})	λ_2 Orthopositronium Annihilation Rate (μsec^{-1})
146	background				
147	background				
148	background				
149	background				
150	background				
151	background				
152	background				
153	136.16	5.86	33.6	23.8 ± 1.3	5.95 ± 1.40
154	136.16	5.62	0.0	39.9 ± 2.4	9.09 ± 0.83
155	140.16	5.17	15.2	29.9 ± 1.6	8.39 ± 0.99
156	138.16	4.98	7.9	31.9 ± 1.6	8.29 ± 1.18
157	137.16	4.80	0.0	34.9 ± 1.8	9.22 ± 0.87
158	139.16	4.52	26.1	19.8 ± 2.9	8.78 ± 1.80
159	132.16	4.52	34.8	16.9 ± 1.3	5.74 ± 2.77
160	135.16	4.24	0.0	25.6 ± 1.8	7.68 ± 1.58
161	166.16	3.83	0.0	22.6 ± 1.7	7.33 ± 1.68
162	did not converge				
163	188.16	3.56	0.0	22.5 ± 3.3	8.14 ± 2.20
164	did not converge				
165	212.16	14.77	0.0	86.3 ± 1.9	11.07 ± 0.39
166	159.66	14.23	0.0	99.7 ± 3.3	11.25 ± 0.33
167	180.16	13.01	0.0	84.4 ± 1.3	11.14 ± 0.41
168	229.16	10.64	0.0	61.3 ± 2.4	9.58 ± 0.46
169	250.66	9.46	0.0	51.1 ± 1.4	9.09 ± 0.40
170	240.16	9.25	0.0	51.4 ± 1.1	10.09 ± 0.32
171	208.16	8.97	0.0	51.7 ± 1.9	10.02 ± 0.49
172	209.16	8.77	9.0	45.5 ± 1.8	9.12 ± 0.60
173	209.16	8.70	22.6	37.4 ± 1.4	8.34 ± 0.74
174	209.66	8.70	18.1	39.7 ± 1.4	8.33 ± 0.65
175	212.16	8.60	13.7	43.7 ± 1.5	8.67 ± 0.55

Run No.	Temp. (K)	Density (amagats)	E/D (V cm^{-1} $amagat^{-1}$)	λ_1 Direct Annihilation Rate (μsec^{-1})	λ_2 Orthopositronium Annihilation Rate (μsec^{-1})
176	209.66	8.72	4.5	50.3 ± 1.7	9.37 ± 0.48
177	207.16	8.80	0.0	53.4 ± 1.8	9.85 ± 0.46
178	206.16	8.82	15.6	42.8 ± 1.4	8.16 ± 0.46
179	208.66	8.77	20.2	39.2 ± 1.4	8.82 ± 0.85
180	equipment failure				
181	299.16	7.13	0.0	38.6 ± 1.5	9.43 ± 0.42
182	background				
183	421.16	6.36	0.0	31.8 ± 3.6	9.34 ± 1.10
184	472.16	6.24	0.0	34.4 ± 1.9	9.36 ± 0.61
185	background				
186	586.66	5.91	0.0	32.3 ± 2.5	9.35 ± 0.55
187	298.16	6.90	0.0	36.7 ± 1.7	9.45 ± 0.61
188	298.16	6.82	5.8	38.0 ± 2.9	9.00 ± 0.50
189	298.16	6.79	23.2	28.2 ± 1.1	7.88 ± 0.61
190	298.16	6.76	17.5	29.9 ± 1.2	8.31 ± 0.59
191	298.16	6.73	11.7	32.7 ± 1.3	9.47 ± 0.62
192	298.16	6.65	14.8	31.9 ± 1.2	8.61 ± 0.48
193	297.66	6.61	20.8	29.1 ± 1.4	8.76 ± 0.72
194	298.16	6.67	0.0	33.6 ± 2.0	8.08 ± 0.62
195	298.16	6.52	0.0	34.9 ± 1.1	8.94 ± 0.38
196	373.66	6.08	19.5	27.9 ± 0.8	8.51 ± 0.41
197	373.66	6.08	13.0	30.2 ± 1.3	8.49 ± 0.65
198	369.66	6.04	6.5	33.1 ± 2.3	9.47 ± 0.65
199	373.16	6.02	9.8	31.2 ± 1.8	8.90 ± 0.56
200	298.16	6.33	24.9	26.2 ± 1.3	8.21 ± 0.84
201	298.16	6.28	50.1	20.5 ± 2.1	8.40 ± 1.27
202	298.16	6.25	63.1	17.3 ± 1.9	7.72 ± 2.28
203	298.16	6.21	38.0	20.7 ± 1.1	6.98 ± 1.19
204	298.16	6.15	57.6	18.0 ± 2.1	8.77 ± 1.78
205	298.16	6.10	0.0	33.7 ± 1.8	8.91 ± 0.57

Run No.	Temp. (K)	Density (amagats)	E/D (V cm^{-1} $amagat^{-1}$)	λ_1 Direct Annihilation Rate (μsec^{-1})	λ_2 Orthopositronium Annihilation Rate (μsec^{-1})
206	298.16	6.09	32.3	22.6 ± 1.1	7.94 ± 0.95
207	298.16	6.09	34.9	21.4 ± 1.2	7.36 ± 1.10
208	298.16	6.07	0.0	30.9 ± 1.3	8.55 ± 0.63
209	298.16	6.02	29.4	22.3 ± 1.2	7.78 ± 1.08
210	298.16	5.97	27.7	23.7 ± 1.3	7.88 ± 0.99
211	298.16	5.95	30.5	20.7 ± 1.3	7.50 ± 1.52
212	331.66	5.67	0.0	30.9 ± 1.4	8.78 ± 0.59
213	571.16	5.10	0.0	26.1 ± 1.3	7.95 ± 0.82
214	571.16	5.08	31.0	17.9 ± 1.1	5.45 ± 2.41
215	572.66	5.06	15.6	21.0 ± 1.1	6.59 ± 1.38
216	572.66	5.06	7.8	23.4 ± 1.4	8.20 ± 1.45
217	571.66	5.07	0.0	24.0 ± 1.2	7.47 ± 1.00
218	572.66	5.05	5.0	23.5 ± 1.3	8.02 ± 1.07
219	571.16	5.06	6.4	24.0 ± 1.2	7.90 ± 0.97
220	521.16	5.14	0.0	26.8 ± 1.8	9.33 ± 0.99
221	430.16	5.32	0.0	27.2 ± 1.4	7.70 ± 0.96
222	410.16	5.38	0.0	29.7 ± 2.7	10.89 ± 1.36

APPENDIX D

CALCULATION OF DERIVATIVES

D.1 Determination of $\partial(\lambda/D)/\partial(E/D)^2$ at E = 0

The total positron annihilation rate is from 1-2

$$\frac{\lambda}{D} = \frac{1}{D} \frac{\int_o^\infty \nu_a'(v) v^2 f(v) dv}{\int_o^\infty v^2 f(v) dv} \quad \text{sec}^{-1} \text{ amagat}^{-1}$$

where $\nu_a'(v)$ is in sec^{-1}.

Therefore

$$\frac{\partial\left(\frac{\lambda}{D}\right)}{\partial\left(\frac{E}{D}\right)^2} = \frac{\partial\left(\frac{\lambda}{D}\right)}{\partial \mathcal{E}^2}$$

$$= \frac{\int_o^\infty v^2 f dv \frac{\partial}{\partial \mathcal{E}^2}\left(\int_o^\infty \nu_a v^2 f dv\right) - \int_o^\infty \nu_a v^2 f dv \frac{\partial}{\partial \mathcal{E}^2}\left(\int_o^\infty v^2 f dv\right)}{\left(\int_o^\infty v^2 f dv\right)^2}$$

where $\mathcal{E} = \frac{E}{D}$

and $\nu_a(v)$ is density independent annihilation rate in units of sec^{-1} amagat^{-1}.

Taking $\partial(\lambda/D)/\mathcal{E}^2$ into integral

$$\frac{\partial\left(\frac{\lambda}{D}\right)}{\partial \mathcal{E}^2} = \frac{\int_o^\infty v^2 f dv \int_o^\infty \nu_a v^2 \frac{\partial}{\partial \mathcal{E}^2} f dv - \int_o^\infty \nu_a v^2 f dv \int_o^\infty v^2 \frac{\partial}{\partial \mathcal{E}^2} f dv}{\left(\int_o^\infty v^2 f dv\right)^2}.$$

Using the approximation (Section 1.3.2.2)

$$f(v) = C \exp\left(-\int_o^v \frac{v' dv'}{\left(\frac{e^2 E^2}{m^2 3\mu \nu_d'(v)^2} + \frac{kT}{m}\right)}\right)$$

where $\nu_d'(v)$ is in sec^{-1}.

Therefore $$\frac{\partial f}{\partial \mathcal{E}^2} = fg(v)$$

where $$g(v) = \frac{\partial}{\partial \mathcal{E}^2}\left(- \int_0^v \frac{v'dv'}{\left(\frac{e^2E^2}{m^2 3\pi \nu_d^2 D^2} + \frac{kT}{m}\right)} \right)$$

where $\nu_d(v)$ is density independent momentum-transfer rate in units of $\sec^{-1}$ amagat^{-1}.

Hence $$\frac{\partial\left(\frac{\Delta}{D}\right)}{\partial \mathcal{E}^2} = \frac{\int_0^\infty v^2 f dv \int_0^\infty \nu_a v^2 f g dv - \int_0^\infty \nu_a v^2 f dv \int_0^\infty v^2 f g dv}{\left(\int_0^\infty v^2 f dv\right)^2}.$$

Specifically $$g(v) = -\int_0^v \frac{\partial}{\partial \mathcal{E}^2}\left(\frac{v'}{\left(\frac{e^2\mathcal{E}^2}{m^2 3\pi \nu_d^2} + \frac{kT}{m}\right)}\right) dv'$$

$$= \int_0^v \frac{v'}{\left(\frac{e^2\mathcal{E}^2}{m^2 3\pi \nu_d^2} + \frac{kT}{m}\right)^2}\left(\frac{e^2}{m^2 3\pi \nu_d^2}\right) dv'.$$

For the special case E = 0

$$g(v)\Big|_{E=0} = \frac{e^2}{m^2 3\pi}\int_0^v \frac{v'}{\left(\frac{kT}{m}\right)^2}\frac{1}{\nu_d^2} dv'$$

$$= \frac{e^2}{3\pi k^2 T^2}\int_0^v \frac{v'}{\nu_d^2} dv'.$$

If $$h(v) - h(A) = \int_A^v \frac{x}{\nu_d(x)^2} dx$$

then $$g(v)\Big|_{E=0} = \frac{e^2}{3\pi k^2 T^2}\Big(h(v) - h(0)\Big).$$

Then $$\frac{\partial\left(\frac{\Delta}{D}\right)}{\partial \mathcal{E}^2} = \frac{e^2}{3\pi k^2 T^2}\left(\int_0^\infty v^2 f dv \int_0^\infty \nu_a v^2 f(h(v) - h(0)) dv \right.$$

$$\left. - \int_0^\infty \nu_a v^2 f dv \int_0^\infty v^2 f(h(v) - h(0)) dv \right)\left(\int_0^\infty v^2 f dv \right)^{-2}.$$

Since h(0) is independent of v

$$\frac{\partial\left(\frac{\lambda}{D}\right)}{\partial \mathcal{E}^2} = \frac{e^2}{3\pi k^2 T^2} \frac{\int_0^\infty v^2 f dv \int_0^\infty \nu_a v^2 f h dv - \int_0^\infty \nu_a v^2 f dv \int_0^\infty v^2 f h dv}{\left(\int_0^\infty v^2 f dv\right)^2}.$$

For the special case

$$\nu_d(v) = A v^B \sec^{-1} \text{ amagat}^{-1}$$

$$h(v) - h(0) = \int_0^v \frac{v'}{\nu_d^2} dv' = \frac{1}{A^2} \int_0^v v^{1-2B} = \frac{v^{2-2B}}{2A^2(1 - B)} \Bigg|_0^v.$$

Therefore

$$h(v) = \frac{v^{2-2B}}{2A^2(1 - B)}$$

valid for $B \neq 1$.

For B = 1

$$h(v) = \frac{1}{A^2} \int \frac{1}{v'} dv' = \frac{1}{A^2} \ln v.$$

If one uses $\nu_a(v) = S v^{-R} \sec^{-1} \text{ amagat}^{-1}$ (Section 3.2.2)

and

$$f \Big|_{E = 0} = C \exp^{-\frac{mv^2}{2kT}}$$

then all the integrals (from above) that must be calculated are of the type

$$\int_0^\infty v^p e^{-qv^2} dv = \frac{\Gamma\left(\frac{p}{2} + \frac{1}{2}\right)}{q^{\frac{p}{2} + \frac{1}{2}}}.$$

Using this integral result and simplifying (for $B \neq 1$)

$$\frac{\partial\left(\frac{\lambda}{D}\right)}{\partial \mathcal{E}^2}\Bigg|_{E = 0} = \frac{2e^2}{3\pi k^2 T^2} \frac{S}{\pi A^2 (1 - B)} \left(\frac{2kT}{m}\right)^{1 - B - \frac{R}{2}}$$

$$\times \left(\frac{\sqrt{\pi}}{2} \Gamma\left(\frac{5}{2} - B - \frac{R}{2}\right) - \Gamma\left(\frac{3}{2} - \frac{R}{2}\right) \Gamma\left(\frac{5}{2} - B\right)\right).$$

For B = 1

$$\frac{\partial\left(\frac{\lambda}{D}\right)}{\partial \mathcal{E}^2}\Bigg|_{E = 0} = \frac{e^2}{3\pi k^2 T^2} \frac{S}{\sqrt{\pi} A^2} \left(\frac{2kT}{m}\right)^{-\frac{R}{2}} \Gamma\left(\frac{3}{2} - \frac{R}{2}\right) \left(\psi\left(\frac{3}{2} - \frac{R}{2}\right) - \psi\left(\frac{3}{2}\right)\right)$$

where $$\psi(x) = \frac{\Gamma'(x)}{\Gamma(x)}.$$

In fact, since the limit as $B \to 1$ of the expression derived from $\nu_d = Av^B$ $(B \neq 1)$ is identical to the second expression, fitting $\partial(\lambda/D)/\partial\mathcal{E}^2$ at $E = 0$ using the first expression only does not discriminate against the value $B = 1$.

D.2 Derivatives for Maximum Likelihood Program

In order to use the expression obtained for $\partial(\lambda/D)/\partial\mathcal{E}^2$ at $E = 0$ in a maximum likelihood fitting program the first and second partial derivatives with respect to the variables A and B must be determined. Such calculations are straightforward but clumsy. For completeness the results are included in this section.

$$\frac{\partial}{\partial A}\left(\frac{\partial\left(\frac{\lambda}{D}\right)}{\partial\mathcal{E}^2}\bigg|_{E=0}\right) = \frac{-2K}{A^3(1-B)}\left(\frac{2kT}{m}\right)^{-B} X$$

$$\frac{\partial}{\partial B}\left(\frac{\partial\left(\frac{\lambda}{D}\right)}{\partial\mathcal{E}^2}\bigg|_{E=0}\right) = \frac{K}{A^2(1-B)}\left(\frac{2kT}{m}\right)^{-B}\left(-\left(\ln\left(\frac{2kT}{m}\right) + \frac{1}{(1-B)}\right)X - Y\right)$$

$$\frac{\partial^2}{\partial A^2}\left(\frac{\partial\left(\frac{\lambda}{D}\right)}{\partial\mathcal{E}^2}\bigg|_{E=0}\right) = \frac{6K}{A^4(1-B)}\left(\frac{2kT}{m}\right)^{-B} X$$

$$\frac{\partial^2}{\partial B^2}\left(\frac{\partial\left(\frac{\lambda}{D}\right)}{\partial\mathcal{E}^2}\bigg|_{E=0}\right) = \frac{K}{A^2(1-B)}\left(\frac{2kT}{m}\right)^{-B}\left(\left(\left(-\ln\left(\frac{2kT}{m}\right) + \frac{1}{(1-B)}\right)^2 + \frac{1}{(1-B)^2}\right)X + \left(-\ln\left(\frac{2kT}{m}\right) + \frac{1}{(1-B)}\right)Y + Z\right)$$

$$\frac{\partial^2}{\partial A\partial B}\left(\frac{\partial\left(\frac{\lambda}{D}\right)}{\partial\mathcal{E}^2}\bigg|_{E=0}\right) = \frac{-2K}{A^3(1-B)}\left(\frac{2kT}{m}\right)^{-B}\left(\left(-\ln\left(\frac{2kT}{m}\right) + \frac{1}{(1-B)}\right)X - Y\right)$$

where

$$K = \frac{2e^2}{3\pi k^2T^2}\frac{S}{\pi}\left(\frac{2kT}{m}\right)^{1-\frac{R}{2}}$$

$$X = \frac{\sqrt{\pi}}{2}\Gamma\left(\frac{5}{2} - B - \frac{R}{2}\right) - \Gamma\left(\frac{3}{2} - \frac{R}{2}\right)\Gamma\left(\frac{5}{2} - B\right)$$

$$Y = \frac{-\sqrt{\pi}}{2}\Gamma\left(\frac{5}{2} - B - \frac{R}{2}\right)\Psi\left(\frac{5}{2} - B - \frac{R}{2}\right)$$

$$+ \Gamma\left(\frac{3}{2} - \frac{R}{2}\right)\Gamma\left(\frac{5}{2} - B\right)\Psi\left(\frac{5}{2} - B\right)$$

$$Z = \frac{\sqrt{\pi}}{2}\left(\Gamma\left(\frac{5}{2} - B - \frac{R}{2}\right)\left(\Psi'\left(\frac{5}{2} - B - \frac{R}{2}\right) + \Psi^2\left(\frac{5}{2} - B - \frac{R}{2}\right)\right)\right)$$

$$- \Gamma\left(\frac{3}{2} - \frac{R}{2}\right)\left(\Gamma\left(\frac{5}{2} - B\right)\left(\Psi'\left(\frac{5}{2} - B\right) + \Psi^2\left(\frac{5}{2} - B\right)\right)\right)$$

and $\Psi(x) = \frac{1}{\Gamma(x)}\frac{d}{dx}\Gamma(x)$ = digamma function

$\Psi'(x) = \frac{d}{dx}\Psi(x)$ = trigamma function

$\Psi^2(x) = \Psi(x)\Psi(x)$.

D.3 Calculation of Higher Order Terms

If λ/D is expanded as a power series in $(E/D)^2$, that is

$$\frac{\lambda}{D} = A + B\left(\frac{E}{D}\right)^2 + C\left(\frac{E}{D}\right)^4 + \ldots,$$

then $$\left.\frac{\partial\left(\frac{\lambda}{D}\right)}{\partial\left(\frac{E}{D}\right)^2}\right|_{E=0} = \left. B + 2C\left(\frac{E}{D}\right)^2\right|_{E=0} = B$$

and $$\left.\frac{\partial}{\partial\left(\frac{E}{D}\right)^2}\left(\frac{\partial\left(\frac{\lambda}{D}\right)}{\partial\left(\frac{E}{D}\right)^2}\right)\right|_{E=0} = 2C.$$

Therefore an estimate of the temperature dependence of the higher order term can be obtained by calculating

$$\left.\frac{\partial}{\partial\left(\frac{E}{D}\right)^2}\left(\frac{\partial\left(\frac{\lambda}{D}\right)}{\partial\left(\frac{E}{D}\right)^2}\right)\right|_{E=0}.$$

This laborious task will not be described in detail here. However,

the result of such a calculation shows that this derivative and hence the value of C is related to T by

$$C \propto \frac{1}{T^{2 + 2B + \frac{R}{2}}}.$$

The effect of the higher order term is thus expected to increase at lower temperatures and therefore the range of values of E/D over which the approximation $\lambda/D = A + B(E/D)^2$ is valid is reduced.

APPENDIX E

CALCULATION OF ANNIHILATION RATE FROM TEMPERATURE RESULTS

From Section 1.3.2.2

$$\frac{\lambda(T)}{D} = \frac{1}{D}\frac{\int_o^\infty v^2 \nu_a'(v) f dv}{v^2 f dv} \text{ ⁄sec}^{-1} \text{ amagat}^{-1}$$

where $\nu_a'(v)$ is in ⁄sec^{-1}.

For the case of E = 0, f can be approximated by

$$f = C\exp^{-\frac{mv^2}{2kT}}.$$

Hence

$$\frac{\lambda(T)}{D} = \frac{\int_o^\infty v^2 \nu_a(v) e^{-\frac{mv^2}{2kT}} dv}{v^2 e^{-\frac{mv^2}{2kT}} dv} \text{ ⁄sec}^{-1} \text{ amagat}^{-1}$$

where $\nu_a(v)$ is density independent in units of ⁄sec^{-1} amagats^{-1}.

Therefore

$$\frac{\lambda(T)}{D} = \frac{\int_o^\infty v^2 \nu_a(v) e^{-\frac{mv^2}{2kT}} dv}{\left(\frac{k}{m}\right)^{\frac{3}{2}} \sqrt{\frac{\pi}{2}}\, T^{\frac{3}{2}}}.$$

If $\frac{\lambda(T)}{D} = aT^b$ (Section 2.3.3.1)

then $$K_1 aT^{\frac{3}{2}+b} = \int_o^\infty v^2 \nu_a(v) e^{-\frac{mv^2}{2kT}} dv$$

where $$K_1 = \left(\frac{k}{m}\right)^{\frac{3}{2}} \sqrt{\frac{\pi}{2}}.$$

Making the substitutions

$$s = \frac{1}{T} \quad \text{and} \quad t = \frac{mv^2}{2k}$$

$$s^{-\left(\frac{3}{2}+b\right)} = \int_0^\infty \left(\frac{\mathcal{V}_a''(t)}{aK_1} \left(\frac{2kt}{m}\right)^{\frac{1}{2}} \left(\frac{k}{m}\right) \right) e^{-st} dt$$

$$= \int_0^\infty \left(\frac{2\mathcal{V}_a''(t)t^{\frac{1}{2}}}{a\sqrt{\pi}} \right) e^{-st} dt.$$

Therefore

$$\frac{\Gamma\left(\frac{3}{2}+b\right)}{s^{\frac{3}{2}+b}} = \int_0^\infty \left(\frac{2\Gamma\left(\frac{3}{2}+b\right)\mathcal{V}_a''(t)t^{\frac{1}{2}}}{a\sqrt{\pi}} \right) e^{-st} dt.$$

Using the Laplace transform of

$$\frac{\Gamma\left(\frac{3}{2}+b\right)}{s^{\frac{3}{2}+b}} \quad \text{for} \quad \left(\frac{3}{2}+b > 0\right)$$

$$t^{\frac{3}{2}+b-1} = \left(\frac{2\Gamma\left(\frac{3}{2}+b\right)\mathcal{V}_a''(t)t^{\frac{1}{2}}}{a\sqrt{\pi}} \right)$$

and

$$\mathcal{V}_a''(t) = \frac{a\sqrt{\pi}t^b}{2\Gamma\left(\frac{3}{2}+b\right)}.$$

Therefore

$$\mathcal{V}_a(v) = \frac{a\sqrt{\pi}}{2\Gamma\left(\frac{3}{2}+b\right)} \left(\frac{mv^2}{2k}\right)^b$$

or

$$\mathcal{V}_a(v) = \frac{a\sqrt{\pi}}{2\Gamma\left(\frac{3}{2}+b\right)} \left(\frac{m}{2k}\right)^b v^{2b} \text{ sec}^{-1} \text{ amagat}^{-1}.$$